AUTÓNOMA UNIVERSITY

DEPARTMENT OF BIOCHEMESTRY

PROTECTION AGAINST PARACETAMOL-INDUCED ADVERSE EFFECTS IN THE LIVER BY THE INHIBITION OF THE PROTEIN TYROSINE PHOSPHATASE 1B

DOCTORAL THESIS

BY

MAYSA AHMED ABD EL-HAMID MOBASHER

Madrid, 2013

DEPARTMENT OF BIOCHEMISTRY

FACULTY OF MEDICINE

AUTÓNOMA UNIVERSITY

PROTECTION AGAINST PARACETAMOL-INDUCED ADVERSE EFFECTS IN THE LIVER BY THE INHIBITION OF THE PROTEIN TYROSINE PHOSPHATASE 1B

Submitted in Partial Fulfillment of the Requirements
For The Degree of Doctoral

MAYSA AHMED ABD EL-HAMID MOBASHER

Medical Bachelor Degree and Bachelor of Surgery, Zagazig University, Egypt, 2005
Master Degree of Molecular Biomedicine, Autónoma University, Spain, 2010

Supervised by

Dra. ÁNGELA MARTINEZ VALVERDE

Senior Research Scientist

***Ángela María Martinez Valverde**, Doctora en Farmacia e Investigadora Científica del Consejo Superior de Investigaciones Científicas, adscrito al Instituto de Investigaciones Biomédicas "Alberto Sols" de Madrid,*

***CERTIFICA**:*

*Que Dña. **Maysa Ahmed Abd El-hamid Mobsher**, Licenciada en Medicina por la Universitdad, de Zagazig, ha realizado bajo su dirección el trabajo titulado:*

*"**Protection against paracetamol-induced adverse effects in the liver by the inhibition of the Protein Tyrosine Phosphatase 1B**".*

El que suscribe considera el trabajo realizado satisfactorio y AUTORIZA su presentación como Tesis Doctoral en el de Departamento de Bioquímica de la Facultad de Medicina de la Universidad Autónoma de Madrid

Y para que conste donde proceda, expido el presente certificado en Madrid, a 4 de Junio de2013,

Fdo: Ángela María Martinez Valverde

VºBº

El Tutor de la Tesis Doctoral

Fdo.: Paloma Martín Sanz

This work has been performed in the Institute of Biomedicine Alberto Sols (Joint Center CSIC/UAM) founded by a predoctoral fellowship of the JAE program (CSIC). The experimental research was founded by projects SAF2009-01615 and SAF2012-33283 (to AMV) from MINECO.

Ningún número de experimentos, por muchos que sean, Podrán demostrar que tenga razón. Tan solo un Experimento puede demostrar que estoy equivocado

Albert Einstein

TO THE SOUL OF MY MOTHER
TO MY FATHER
TO MY HUSBAND AND MY
BEAUTIFUL GIRLS

ACKNOWLEDGEMENTS

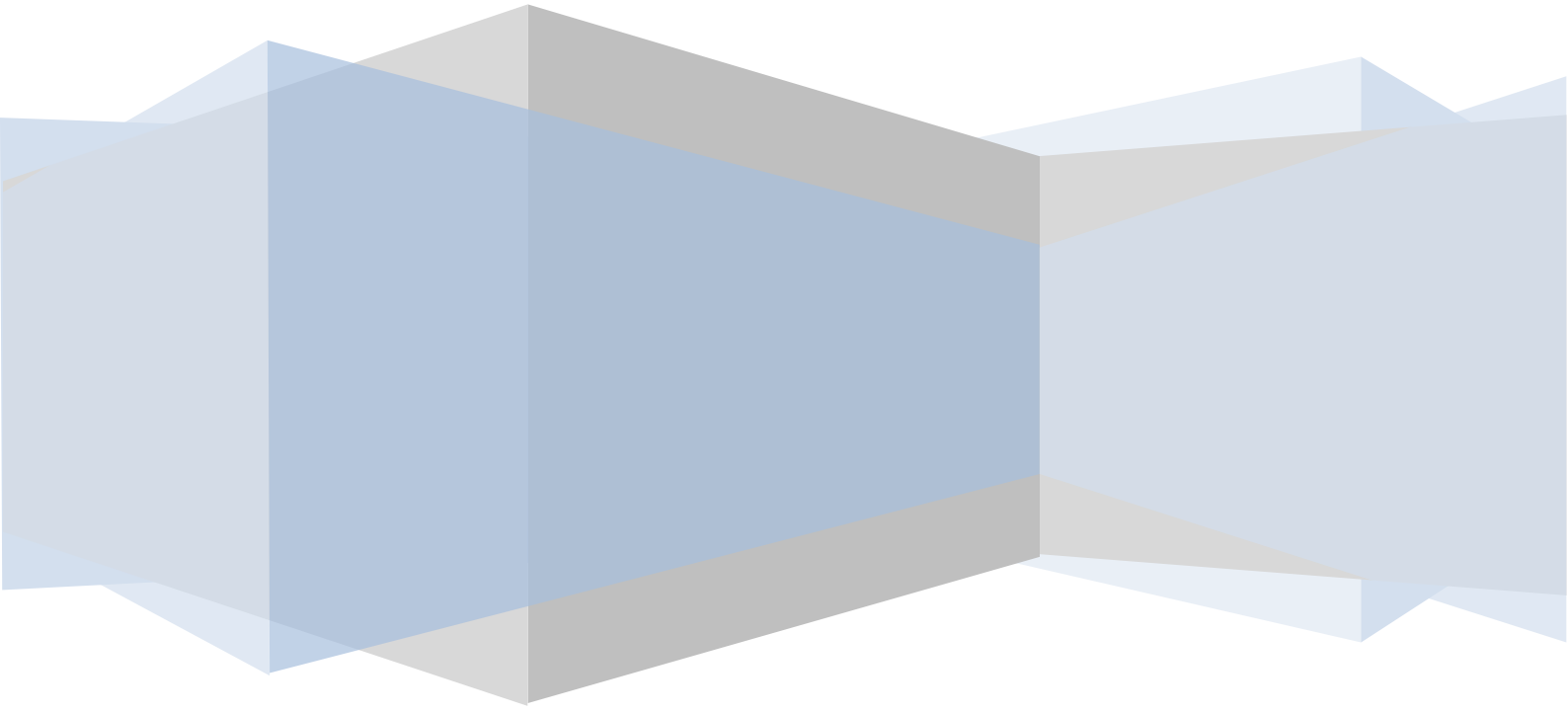

This has been a long journey. I have been fortunate to have had the possibility to gain professional experience and training from several institutes and meet many wonderful people. I would like to express my gratitude to all the people who have supported, encouraged and helped me on the road. To all who are remembered, unintentionally forgotten or here not mentioned – Thank You.

First of all I want to thank Al-mighty god for giving me tremendous courage and power to complete this research and Thesis work.

With a high sense of veneration my deep thanks goes to my supervisor Dra. Ángela Maria Martinez Valverde for her continuous involvement, supervision, encouragements, patience, devotion, and advices. Not only she provided professional guidance but extended my horizon to integrate multi-disciplinary approach in research. I would like to thank her again for her strong support, friendship, and for giving me the opportunity to conduct my research and work in her group.

Also, with a high sense of veneration my deep thanks go to Dr. Luis Goya, Dra. Sonia Ramos and Dra. M Ángeles Martin, My work could not be possible without their incomparable contribution

Farther more, a profound gratitude and esteem should be expressed with respect to the teaching and administrative staff of institute of Biomedical investigations - Alberto Sols (CSIC). I set Dr. Jorge Martín-Pérez, Dra. Carmela Calés Bourdet, Dr. Luis del Peso Ovalle, Dr. Carlos Gancedo Rodríguez For their engagement and assistance, during the four years.

I would like also to express my gratitude to Dr. Jordi Muntané and Dr. Kenneth J. Simpson for their precious helps.

Sincere appreciations and thanks are extended to my colleagues and friends in my lab Ana Isabel Arroba Espinosa, Beatriz Santamaria Pérez, Agueda Gonzáles Rodrigez, Virginia Pardo Marqués, Pilar Valdecantos Jiménez de Andrade, Ester Garcia-Casarrubios Pimente, for their help, friendship, and pleasant way of working in a team, kindness, encouragements, constructive criticism, helps. Their welcoming was always warm, cordial, and friendly. It was a great opportunity to get to know Spain and Spanish people.

Also I want to expresses my deepest gratitude to my brother and my sisters, and all my relatives, and friends for their continued affection and encouragement during my stay in Spain, far away from them.

I am deeply grateful for the financial grant received that have allowed me to finish my PhD. It was funded by (Higher institute for scientific investigations- CSIC)

My deepest thankful for my small family. My daughters SHAZA and HANA and my kind husband DIAA for teaching me patience, persistence and perseverance; and for support me in extraordinary times of need.

I cannot close this note without expressing my sincere thanks to my father for his great help that he provided me during critical moments of my thesis.
Finally, I let her for the end because I really cannot find the right words to thank her, to praise her and to admire her. I learned from her the sense of work and I found behind her serious visage all qualities of amiable women. Who can be other than my dear mother. ***I MISS YOU***

SUMMARY/ RESUMÉN

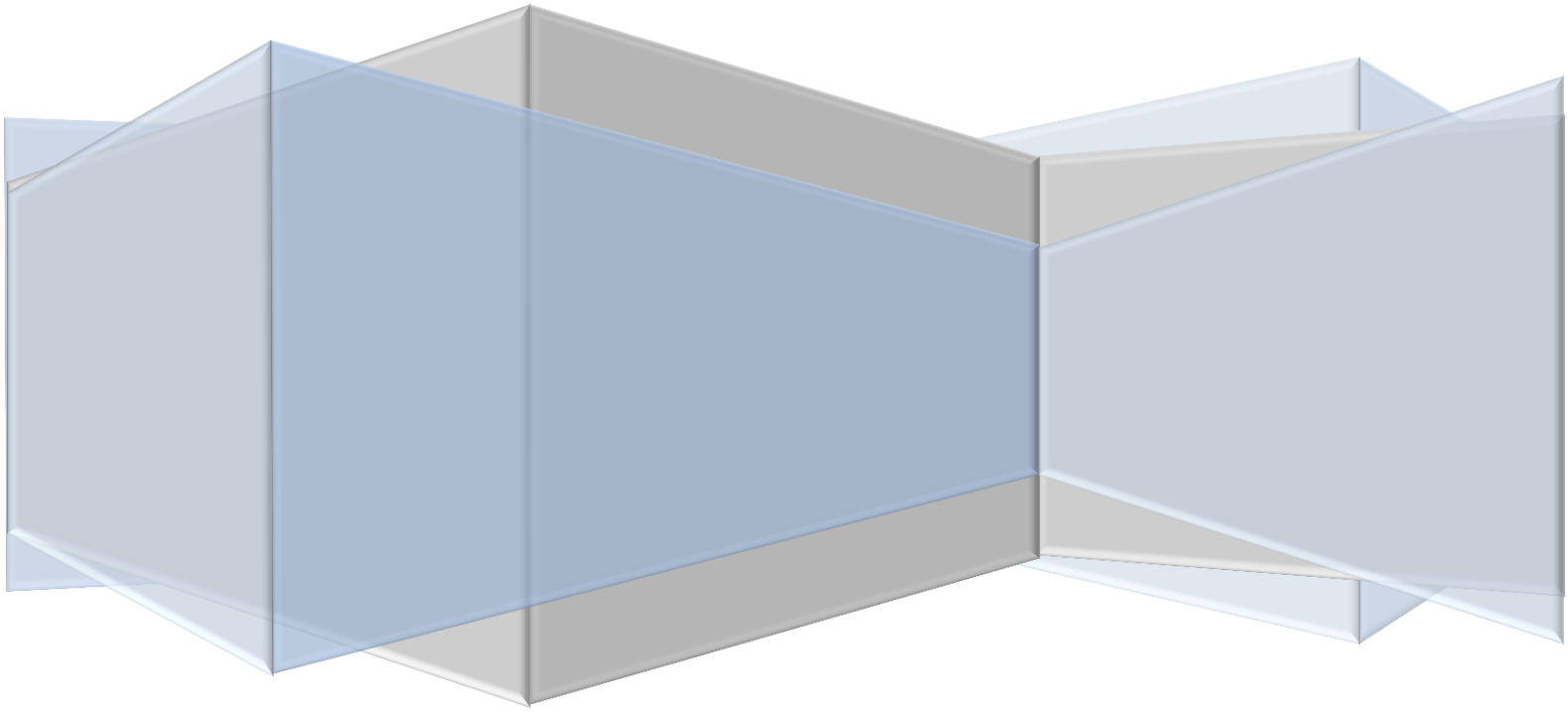

Summary

Acute hepatic failure secondary to acetaminophen (APAP) poisoning is associated with high mortality. PTP1B is a negative regulator of tyrosine kinase growth factor signaling. In the liver, this pathway confers protection against injury. However, the involvement of PTP1B in the intracellular networks activated by APAP is unknown. We have assessed PTP1B expression in APAP-induced liver failure in humans and its role in the molecular mechanisms that regulate the balance between cell death and survival in human and mouse hepatocytes as well as in a mouse model of APAP-induced hepatotoxicity. PTP1B expression was increased in human liver tissue removed during liver transplant from patients for APAP overdose. PTP1B was up-regulated by APAP in primary human and mouse hepatocytes together with activation of JNK and p38 MAPK, resulting in cell death. Conversely, Akt phosphorylation and the anti-apoptotic Bcl2 family members BclxL and Mcl1 were decreased. PTP1B deficiency in mouse hepatocytes protected against APAP-induced cell death preventing GSH depletion, ROS generation and activation of JNK and p38 MAPK. APAP-treated PTP1B$^{-/-}$ hepatocytes showed enhanced anti-oxidant defense through the glycogen synthase kinase GSK3β/SKF axis, delaying tyrosine phosphorylation of Nrf2 and its nuclear exclusion, ubiquitination and degradation. IGFIR-mediated signaling decreased in APAP-treated wild-type hepatocytes, but was maintained in PTP1B$^{-/-}$ cells or in wild-type hepatocytes with reduced PTP1B levels by RNA interference. Likewise, both signaling cascades were modulated in mice resulting in less severe APAP hepatotoxicity in PTP1B$^{-/-}$ mice. Our results demonstrated that PTP1B is a central player of the mechanisms triggered by APAP in hepatotoxicity suggesting a novel therapeutic target against APAP-induced liver failure.In the initial experiments of APAP-mediated toxicity in hepatocytes we found that APAP also increased PTP1B and activated JNK at subtoxic doses. These data prompted us to evaluate the cross-talk between subtoxic doses of APAP and insulin signaling in hepatocytes. Insulin signaling was decreased in hepatocytes stimulated with subtoxic doses of APAP through decreasing IR and IRS1 tyrosine phosphorylation. However, PTP1B deficiency protected against these effects. In an *in vivo* chronic treatment with APAP, wild-type mice showed a trend towards a decrease in whole body glucose homeostasis whereas in mice lacking PTP1B no deleterious effects were observed.

Resumén

El fallo hepático agudo debido a una sobredosis de paracetamol está asociado con una elevada mortalidad. La PTP1B modula negativamente la señalización mediada por los receptores de factores de crecimiento de la súper familia tirosina quinasa. En el hígado, estas rutas confieren protección frente al daño. En esta Tesis Doctoral hemos investigado la expresión de PTP1B en el daño agudo inducido por sobredosis de paracetamol en humanos, así como su papel en la regulación de los mecanismos moleculares responsables del balance supervivencia/muerte celular en el hígado. Hemos encontrado un aumento en la expresión de PTP1B en el tejido hepático procedente de individuos que necesitaron trasplante tras una sobredosis de paracetamol. Así mismo, los niveles de PTP1B aumentaron en hepatocitos humanos y murinos tratados con paracetamol en paralelo con la activación de las quinasas de estrés JNK y P38 MAPK y la inducción de muerte celular. Por el contrario, la activación de Akt y los niveles de proteínas anti-apoptóticas de la familia Bcl2 se encontraron disminuidos. La deficiencia en PTP1B protegía a los hepatocitos frente a la muerte inducida por paracetamol ya que preveía la depleción de GSH, la generación de ROS y la activación de las quinasas de estrés. Además, los hepatocitos PTP1B$^{-/-}$ tratados con APAP presentaron una mayor respuesta antioxidante modulando las quinasas GSK3β/SKF lo que retrasaba la fosforilación en tirosina del Nrf2 responsable de su salida del núcleo y posterior ubiquitinación y degradación. La inhibición de PTP1B también evitaba la disminución de la fosforilación del IGF-IR y Akt. Estos dos mecanismos se modulaban de igual manera en ratones sometidos a una sobredosis de paracetamol, presentando los ratones PTP1B$^{-/-}$ una menor hepatotoxicidad. Estos resultados demostraban que la PTP1B regula los mecanismos moleculares desencadenados por dosis tóxicas paracetamol, lo que sugiere que la PTP1B podría ser una diana terapéutica frente a este daño hepatocelular. La expresión de PTP1B y la activación de las quinasas de estrés también aumentaban en hepatocitos estimulados con dosis subtóxicas de paracetamol, de manera similar a lo que ocurre en situaciones de resistencia a la insulina. Hemos encontrado que dosis subtóxicas de paracetamol disminuyen la señalización de la insulina en los hepatocitos y este efecto se atenúa en ausencia de PTP1B. Por último, presentamos evidencias de que la administración crónica de paracetamol podría alterar la homeostasis glucídica del organismo y esto se evitaría mediante la inhibición de la PTP1B.

INDEX OF CONTENTS

ABBREVIATIONS

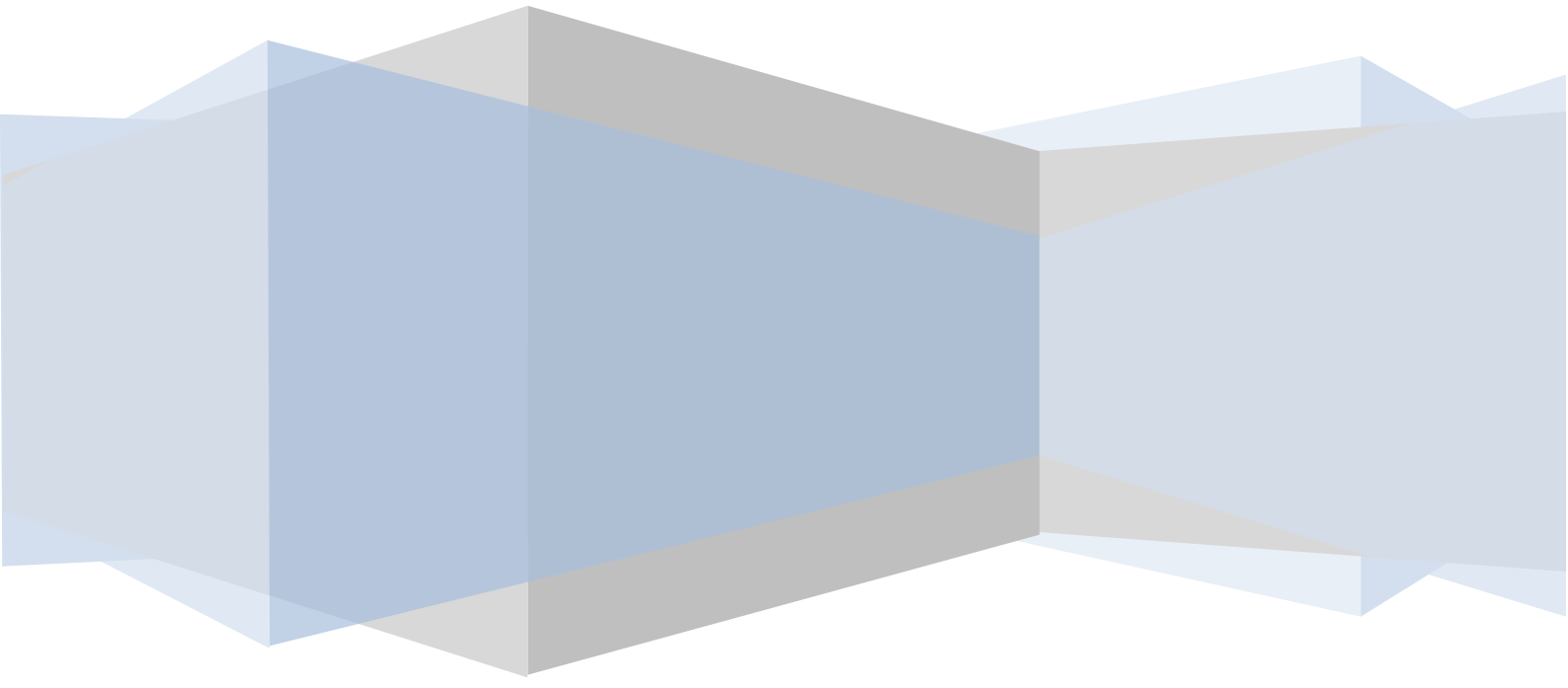

AKT: Protein kinase B.

ALT: Alanine amino transaminase.

APAP: Aacetaminophen .paracetamol.

APAP–NAC: APAP–N-acetylcysteine.

APAP–GSH: APAP-glutathione.

AREs: Antioxidant response elements.

ASK-1: Apoptosis signaling-regulating kinase 1.

bFGF: Basic fibroblast growth factor.

BMDC: Bone marrow-derived cells.

BSA: Bovine serum albumin.

BTB/POZ: Bric-a-brac, tramtrack, broad-complex/poxvirus zinc finger.

bZIP: Basic leucine zipper.

CDK: Dual-specific kinases.

CHL: Human Chang Liver Cells.

CLK1: Dual-specific kinases linase 1.

CLK2: Dual-specific kinases linase 2.

CNC: Cap 'n' collar.

CTR: C-terminal region.

Cul3: Cullin 3.

Cyp2e1: Cytochrome P450.

DAPI: Diamidino-2-phenylindole.

DGR: Double glycine repeat.

DILI: Drug-induced liver injury.

DMEM: Dulbecco's Modified Eagle Medium.

DMSO: Dimethyl sulfoxide.

DTT: 1,4-dithiothreitol.

ECL: Enhanced chemioluminiscence.

EDTA: Ethylenediaminetetracetic acid.

EGF: Epidermal growth factor.

ER: Endoplasmic reticulum.

FBS: Fetal bovine serum.

GCL-C: γ-glutamyl cysteine ligase catalytic subunit.

GCL-M: γ-glutamyl cysteine ligase modulatory subunit.

GPx: Glutathione peroxidase.

GR: Glutathione reductase.

GSH: Glutathione (in its reduced form).

GSK-3β: Glycogen synthase kinase 3 beta.

Gss: GSH synthase.

GTT: Glucose Tolerance Test.

HCV: Hepatitis C virus.

H&E: Hematoxilin and eosin.

HEPES: N-2-hydroxyethylpiperazine-N'-2'-etanesulfónico.

HFD: High-fat diet.

HGP: Hepatic glucose production.

HIF: Hypoxia-inducible factor.

HO·: Hydroxyl radical.

H_2O_2: Hydrogen peroxide.

HO-1: Heme oxigenase-1.

Huh7: Hepatoma human cell line.

IGFIR: Insulin-like growth factor I receptor.

i.p: Intraperitoneally.

IR: Insulin receptor.

IRS1: Insulin receptor substrate 1.

IRS2: Insulin receptor substrate 2.

ITT: Insulin Tolerance Test.

IVR: Intervening region.

JNK: C-jun (NH2) terminal kinase.

Keap1: Kelch-like ECH-associated protein1.

LDH: Lactate dehydrogenase.

Mcl1: Myeloid cell leukemia sequence 1.

MEFs: Mouse embryonic fibroblasts

MKK4/7: MAPK kinase 4/7.

MPT: Mitochondria permeability transition.

mRNA: messenger ribonucleic acid.

NAFLD: Nonalcoholic fatty liver disease.

NAPQI: N-acetyl-p-benzoquinone imine.

Neh: Nrf2-ECH<chicken Nrf2>homologous domain.

NFκB: Nuclear Factor Kappa B.

NOX: NADPH oxidase.

NQO1: NAD(P)H quinone oxidoreductase.

Nrf2: Nuclear factor erythroid-2-related factor 2.

NTR: N-terminal region.

OPT: O-phthalaldehyde.

p38 MAPK: p38 mitogen-activated protein kinase.

PBS: Phosphate-buffered saline.

PERK: PKR-like endoplasmic reticulum kinase.

PKC: Protein kinase C.

PLCγ: Phospholipase C gamma.

PMSF: Phenylmethylsulfonyl fluoride.

PPAR: Peroxisome proliferator-activated-γ receptors.

PTMα: Prothymosin-α.

PTP1B: Protein tyrosine phosphatase 1B.

PTT: Pyruvate tolerance tests.

QTL: Quantitative trait locus.

Rbx1: Ring Box Protein 1.

RNA: Ribonucleic acid.

ROS: Reactive oxygen species.

SDS: Sodium dodecyl sulfate.

shRNA: Short hairpin RNA.

siRNA: Small interfering RNA

SKF: Src kinase family.

sMafs: Small Mafs.

SPB: Sodium phosphate buffer.

SUMO: Small ubiquitin-related modifier.

tBHQ: Tertiary butylhydroquinone.

TBS: Tris buffered saline.

TCA 5%, EDTA: trichloroacetic acid containing 2 mM EDTA.

T2DM: Type 2 diabetes mellitus.

TEMED: N, N, N, N'-tetramethylenediamine.

TNFα: Tumour necrosis Factor α.

TTBS: Tween-20-Tris buffered saline.

TGFβ: Transforming Growth Factor β.

INTRODUCTION

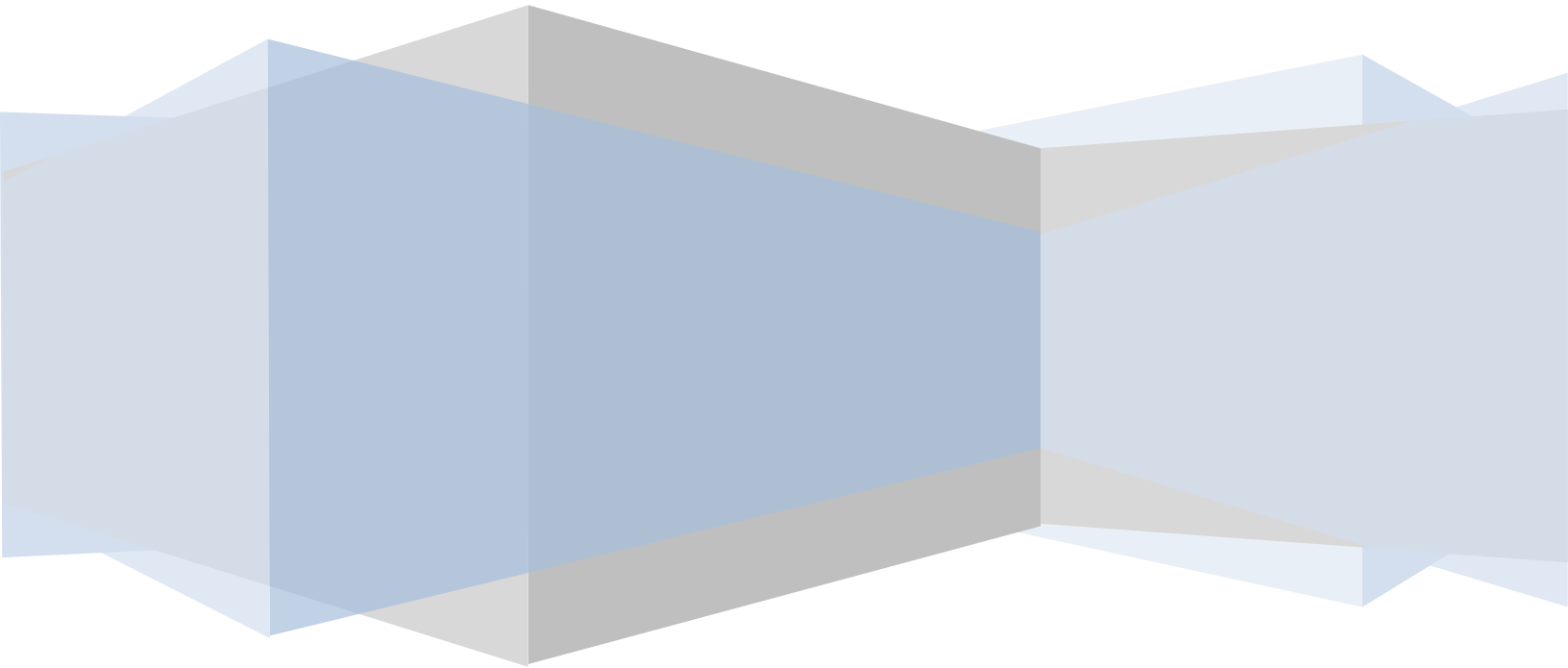

1. General Characteristics Of The Liver.

The liver is the largest gland in the human body, weighting approximately 1.500 grams (about 2.5% of adult's body weight) and occupying a large region mostly on the right side of the body, below the diaphragm and behind ribs five through ten (Figure 1). The liver is closely associated with the small intestine, processing the nutrient-enriched venous blood that leaves the digestive tract. The liver is also considered the most complex and important internal organ in the human body. It performs over five hundred metabolic functions, resulting in the synthesis of the products that are released into the blood stream (e.g. glucose derived from gluconeogenesis, plasma proteins, clotting factors and urea), or that are excreted to the intestinal tract (bile). Also, several products are stored in the liver parenchyma (e.g. glycogen, fat and fat soluble vitamins). A total loss of liver function leads to death within minutes (Marieb 2001; Arias 1994; Netter 2006), demonstrating the physiological liver's importance.

1.1. Microscopic Anatomy Of The Liver.

The basic functional unit of the liver is the liver lobule. The primary structure of a lobule is shown in (Figure 2) and includes:

- Hepatocytes form the bulk of the lobule and arranged as interconnected plates.
- Portal triads at each corner of the lobule.
- Central vein.
- Liver sinusoids that run from the central vein to the portal triads are the canals formed by the plates of hepatocytes. They are approximately 8-10 μm in diameter and are comparable with the diameter of normal capillaries.
- Hepatic macrophages (Kupffer cells).
- Bile canaliculi. They are little canals of 1μm in diameter formed among the walls of adjacent hepatocytes.
- Space of Disse that is a small space between the sinusoids and the hepatocytes.

The portal triads consist of three vessels: a hepatic portal arteriole, a hepatic portal venule and a bile duct. The blood from the arteriole and the venule flows in the same direction through the sinusoids towards the central vein which eventually leads to the hepatic vein and the inferior vena cava. Secreted bile flows in the opposite direction through the bile canaliculi away from the central vein towards the portal triad and exiting via the bile duct. As blood flows through the sinusoids and

the space of Disse towards the central vein, nutrients are processed and stored by the hepatocytes and blood cells and bacteria are engulfed by the Kupffer cells.

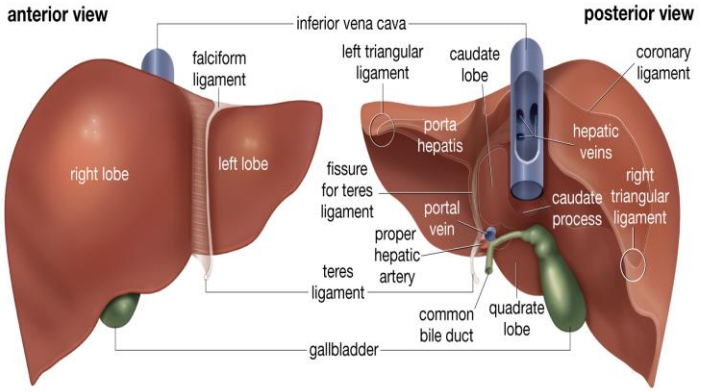

Figure 1. Normal gross anatomy of the liver.

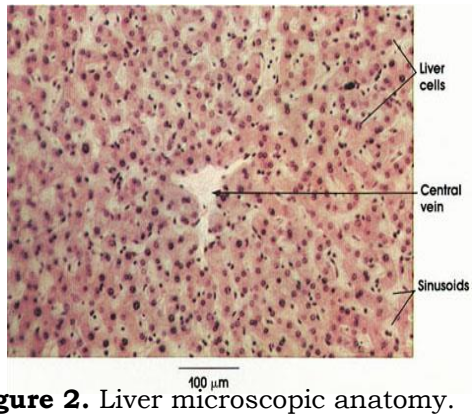

Figure 2. Liver microscopic anatomy.

1.2. The Liver Cell Types.

The liver has five cell types: hepatocytes, Kupffer cells, sinusoidal endothelial cells, bile duct epithelial cells and Ito cells.

1-Hepatocytes:- represent 60% of the liver's cells and about 80% of the liver's total cell mass (Kuntz, 2008b). Most of the liver's synthetic and metabolic capabilities stem from the work of hepatocytes.

2-Kupffer cells:- are macrophages that reside in the sinusoids. The liver has a large number of these macrophage lineage cells which make up 80% of the total body macrophages (Bouwens et al., 1986; Seki et al., 2000; Doherty et al., 2000). These cells help to clear out the old red blood cells and bacteria. They also break down the heme (the iron-containing pigment in hemoglobin) into bilirubin which then becomes one of the chief pigments of bile.

3-Sinusoidal endothelial cells:- are fenestrated (latin for "windows"), meaning that they have large pores that allow most proteins to pass freely through the sinusoidal endothelium into the space of Disse where they can make direct contact with hepatocytes. The pores are also bi-directional, meaning that proteins created by the liver and the other substances stored or processed by the liver can also be passed back into the blood.

4-Bile duct epithelial cells:- line the interlobular bile ducts within the portal triads.

5-Ito cells:- are found in the space of Disse. They are also known as stellate cells, lipocytes or perisinusoidal cells. They comprise approximately 15% of all liver cells (Bauer et al., 2001; Friedman 2000; Rockey 2001). These cells store Vitamin A and

manufacture and secrete a number of important hepatic growth factors such as Hepatocyte Growth Factor (HGF) and Transforming Growth Factor β (TGFβ) and matrix components (collagen) and, therefore, they play a prominent role in liver regeneration and in the development of liver fibrosis, respectively. When stimulated by micro-environmental changes, these cells can transform into facultative fibroblasts or myofibroblasts.

1.3. Functions Of The Liver.

The liver has many functions, acting as a gatekeeper between the digestive system and the circulatory system. The four essential liver functions are:

-Synthesis of many proteins that circulate in the blood. This include albumin, coagulation factors, alpha1-antitrypsin, very low density lipoproteins etc..

-Storage of nutrients for later use. The liver balances the supply of nutrients with the demand. For example, the liver stores glucose as glycogen and converts it back into glucose when needed (Nordlie et al., 1999; Pilkis et al., 1992; Saltiel et al., 2001). If the supply of glycogen is depleted, the liver can also synthesize glucose from amino acids, lactate, and glycerol. Additionally, the liver metabolizes fatty acids, cholesterol and amino acids (Xiao et al., 2010). When there is a surplus of glucose in the bloodstream, the liver can convert the excess glucose and amino acids into fatty acids for storage. The liver synthesizes cholesterol and removes it from circulation. Finally, the liver can synthesize non-essential amino acids when needed by the body.

-Detoxification and elimination of toxic substances. Toxins are detoxified by the liver's ability to metabolize lipophillic compounds. These compounds (bound to albumin) enter the liver sinusoids and then into the area of Disse. Enzymes in the hepatocytes are involved in the metabolism of the lipophillic compounds, which include toxins and many drugs.

-Production of bile. Bile acts as a detergent that breaks fats down into smaller components, so they can be digested in the small intestine. Bile also provides the liver a way to remove wastes including bilirubin, cholesterol and toxins. Bile is formed in the biliary canaliculi and then drains into the interlobular bile ducts.

2. Drug-Induced Liver Injury.

The liver, as the major site of drug metabolism, is also the major site of drug injury. Drug-induced liver injury (DILI) continues to be a problem for many commonly used drugs and represents a major challenge in designing potential therapies (Kaplowitz 2005; Thames 2004). Paracetamol (APAP, an analgesic), valproic acid (an anti-convulsant drug) and zafirlukast (a drug used for asthma) are examples of the commonly used drugs that are associated with liver injury. The development of strategies to reduce DILI has important implications in liver injury. It may also increase the availability of many drugs involved in the treatment of a wide range of diseases.

Hepatocyte injury and death is the critical initiating event leading to the clinical manifestations of DILI. Hepatocyte injury can be triggered directly by some drugs (parent compound), but in most cases involves the formation of reactive metabolites generated during metabolism (Kaplowitz 2005; Uetrecht 2008). Since most drugs are lipophilic, drug clearance involves biotransformation by cytochrome P450 (CYP) or other phase I enzymes to reactive metabolites for conjugation with hydrophilic carriers (e.g. glucuronide, GSH) and excretion into urine or bile. However, as the name suggests, reactive metabolites are highly reactive molecules that not only covalently bind to hydrophilic carriers, but also covalently bind to proteins (Jollow et al., 1973; Kaplowitz 2005). Reactive metabolites can also directly, through redox cycling, or indirectly, through glutathione (GSH) depletion, increase the generation of reactive oxygen species (ROS) (superoxide O_2, hydrogen peroxide H_2O_2, hydroxyl radical HO·) in hepatocytes (Hanawa et al., 2008).

Covalent binding and ROS production caused by reactive metabolites can modify proteins and other macromolecules to cause hepatocyte stress and injury that can activate and/or inhibit a wide range of signaling pathways. Whether the hepatocyte survives or undergoes cell death following injury by reactive metabolites is determined, in great part, by the balance between pro-death and pro-survival signaling pathways. If pro-death pathways are primarily activated, these signaling pathways will initiate hepatocyte death following hepatocyte injury. Even in necrotic death, pro-death pathways such as the activation of the c-Jun N-terminal kinase (JNK) can trigger cell death to occur (Hanawa et al., 2008). Consequently, pharmacological inhibition of these pro-death pathways can often prevent cell death, even in the presence of extensive cell injury. On the other hand, the

activation of pro-survival pathways (e.g., protein kinase B/Akt, DNA repairing enzymes) may inhibit cell death by directly inhibiting pro-death signaling, or indirectly by increasing cell repair or metabolism (Saberi et al., 2008). The modulation of these pro-death and pro- survival signaling pathways in hepatocytes may decrease the extent of liver injury caused by drugs and, therefore, represent a potential therapeutic strategy for the treatment of DILI.

2.1. APAP-Induced Liver Injury.

Studying the intrinsic signaling pathways involved in DILI, as well as other steps involved in DILI, has been hampered by the availability of good animal models (Dixit and Boelsterli 2007; Kaplowitz 2005). Very few drugs that cause liver injury in humans can be studied in animals and, consequently, a mechanistic understanding of how drugs cause liver injury is lacking. The noted exception is APAP, which causes liver injury in animals in a dose-dependent manner. Accordingly, most of the knowledge about DILI has come from work with APAP at high doses that cause liver injury in both humans and experimental animals (Kaplowitz 2005). In addition, since APAP-induced liver injury exhibits idiosyncratic features in animals, a number of recent metabolomic and genomic studies have focused on understanding the underlying mechanism(s) responsible for the idiosyncratic nature of APAP-mediated hepatotoxicity (Welch et al., 2005, 2006).

APAP, called acetaminophen in North America, is a widely used over the-counter analgesic and antipyretic drug (Bessems et al., 2001; James et al., 2003; Prescott et al., 1983). APAP was originally introduced as an analgesic by Von Mering in 1893, but was not widely used until the 1960s, following the recognition that the structural analogue phenacetin was nephrotoxic in chronic abusers (Hinson 1980). According to the US Food and Drug Administration, each week approximately 50 million adults in the United States take APAP-containing products. At therapeutic doses, it is believed to be safe, having analgesic and antipyretic effects similar to those of aspirin or ibuprofen. Unlike these other drugs, APAP has only weak anti-inflammatory properties. Because APAP is well tolerated, available without a prescription, and lacks the gastric side effects of aspirin (gastrointestinal bleeding and Rye's syndrome), it has become in the recent years a common household drug. Although considered safe at therapeutic doses, at higher doses APAP produces a centrilobular hepatic necrosis that can be fatal. APAP poisoning has been recognized as a public health problem (Lee 2007; Kaplowitz 2004; Prescott 1980) because approximately one-half of all cases of acute liver failure in the US and Great Britain

today (Larson et al., 2005; Ostapowicz et al., 2002) are due to APAP toxicity. APAP, in these countries, is also the second leading cause of liver transplantation which accounts for considerable levels of morbidity and mortality (Lee 2004). Therefore, APAP-induced acute toxicity has become an essential model for studying drug-induced liver and kidney failure. In the liver, APAP overdose produces a centrilobular hepatic necrosis that can be fatal as it progresses to fulminant liver failure (Ramachandran et al., 2009). However, despite of substantial progress in understanding APAP-induced hepatotoxicity (James et al., 2003; Jaeschke et al., 2006; Han et al., 2010), additional injurious mechanisms responsible for the cellular damage induced by this drug remain unknown.

2.2. Metabolism Of APAP-Mediated Hepatotoxicity.

In a series of four publications it has been shown that APAP was converted by drug metabolizing enzymes to a reactive metabolite that covalently bind to proteins (Jollow et al., 1973; Mitchell et al., 1973a, b; Potter et al., 1973). Subsequently, the reactive metabolite of APAP was identified to be N-acetyl-p-benzoquinone imine (NAPQI). It was found to be formed by cytochrome P-450 (CYP) by a direct two electron oxidation of APAP, a previously unrecognized mechanism of CYP (Dahlin et al., 1984; Gillette et al., 1981; Potter et al., 1987). The CYP isoforms important in APAP metabolism are CYP2E1, CYP1A2, CYP3A4 and CYP2D6 (Dong et al. 2000; Raucy et al., 1989; Snawder et al., 1994; Thummel et al., 1993).

At nontoxic doses, the metabolite was efficiently detoxified by GSH forming an APAP-GSH conjugate (Jollow et al., 1974) and eliminated in urine or bile as APAP–cysteine, APAP–N-acetylcysteine (APAP–NAC) and APAP-glutathione (APAP–GSH) (Ghosh et al., 2009) (Figure 3). However, at toxic doses, glucuronidation and sulfation routes become saturated and more extensive bioactivation of the drug occurs, leading to a rapid depletion of the hepatic GSH pool as much as 80–90% (Jollow et al., 1974; Mitchell et al., 1973a, b) and, subsequently, NAPQ1 covalently binds to proteins. The amount of covalent binding correlated with the relative hepatotoxicity (Jollow et al., 1973). Thus, detoxification of NAPQI is extremely rapid, and the rapid rate may explain why covalent binding to proteins was not observed in hepatocytes until GSH was almost completely depleted (Mitchell et al., 1973a, b). NAPQI binds to cysteine groups on cellular proteins forming APAP-protein adducts. NAPQI also binds to mitochondrial proteins, which, in turn, causes oxidative stress that may trigger signaling pathways through mitochondrial toxicity, ultimately leading to lethal cell injury. Moreover, generation of ROS and nitrogen species, lipid

peroxidation, mitochondrial dysfunction, disruption of calcium homeostasis and induction of apoptosis and necrosis are also involved in APAP-induced hepatotoxicity (Ghosh et al., 2009; Reid et al., 2005). Therefore, tight control of ROS levels by antioxidant molecules and detoxifying enzymes is important to restore the balance between oxidants and antioxidants in cells challenged with oxidative insults. In this regard, nuclear factor erythroid-2-related factor 2 (Nrf2) activates detoxifying enzymes by binding to antioxidant response elements (AREs) in promoters of several genes. Animals deficient in Nrf2 are highly susceptible to APAP-induced liver injury (Enomoto et al., 2001). Thus, Nrf2 may serve as an endogenous regulator by which cells combat oxidative stress.

In initial work describing the importance of hepatic GSH in APAP-induced hepatotoxicity in mice, Mitchell et al. (1973a, b) showed that administration of cysteine prevented hepatotoxicity. This finding led to the development of N-acetylcysteine as the preferred antidote for the treatment of APAP hepatotoxicity (Peterson et al., 1977; Piperno et al., 1976; Prescott et al., 1977). Rumack and coworkers analyzed the toxicity data from a large number of APAP overdose patients treated with N-acetylcysteine (Rumack et al. 1981) and noticed that treatment of APAP-poisoned patients during the first 10 hours after the overdose was effective at decreasing the toxicity (Prescott et al., 1977; Rumack et al., 1981), but those patients who were treated with N-acetylcysteine after 10 hours were most susceptible to the development of hepatotoxixity. The mechanisms by which N-acetylcysteine inhibits APAP toxicity have been postulated to be an increase in detoxification of NAPQI by a direct conjugation and also an increase in GSH synthesis (Corcoran et al., 1985).

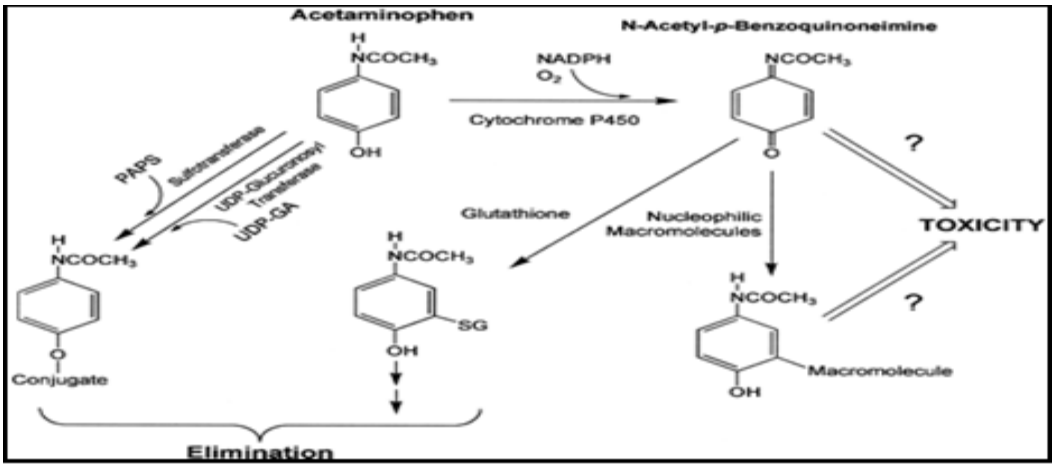

Figure 3. Schematic representation depicting the role of metabolismin APAP Toxicity.

ROS (reactive oxigen species) have important roles in diverse physiological and pathological processes. Low levels of ROS play important roles in regulating vascular tone (Gutterman et al., 2005), cell adhesion (Chiarugi et al., 2003; Huo et al., 2009) immune responses (Grisham 2004) and growth factor actions (Hensley et al., 2000). Intermediate levels of oxidative stress induce an adaptive protective signal pathway (i.e. Keap1-Nrf2 signal pathway) to induce the antioxidant response. Likewise, higher amounts of ROS can trigger an inflammatory response through activation of Nuclear Factor Kappa B (NFκB) and Activating Protein 1 (AP-1 transcription factors).

Cells have evolved adaptive mechanisms to endure oxidative stress. In general, there are three cellular antioxidant defence systems to fight against oxidative stress: low-molecular-weight antioxidants, enzymatic antioxidant pathways and free-ion sequestration. One of the major endogenous low molecular weight antioxidant is GSH because it serves as the most abundant cellular thiol resource and provides a buffer system to maintain cellular redox status. GSH can be either synthesized from glutamate-cysteine ligase (GCL) or from GSH synthase (Gss.) GSH reduces H_2O_2 through glutathione peroxidase (Gpx) and it is also oxidized to its disulfide form (GSSG). GSSG is returned to GSH through glutathione reductase (GR) using NADPH as a co-factor. Multiple studies have shown that the Gpx-GSH pathway is also a major intracellular antioxidant mechanism that repairs lipid peroxidation (Imai et al., 2003), DNA fragmentation (Higuchi 2003) and protein adduction (Filippin et al., 2008).

3. Signaling Pathways Involved In APAP Hepatotoxicity.

3.1. The JNK-Mitochondrial Signaling Loop in APAP-Induced Liver Injury.

The first signaling pathway identified to modulate APAP-induced liver injury was mediated by JNKs (Gunawan et al., 2006; Henderson et al., 2007; Latchoumycandane et al., 2007). JNKs are a family of serine/threonine kinases belonging to the MAPK family that mediate the cellular responses to environmental stresses, growth factors, as well as to proinflammatory cytokines (Johnson et al., 2007). JNK is activated through phosphorylation by MKK4/7 (MAPK kinase 4/7), which is in turn activated upstream by ASK1 (apoptosis signal-regulating kinase 1) and other MAP3Ks. In most cells, including hepatocytes, two JNK isoforms (JNK1 and JNK2) are expressed (Johnson et al., 2007). JNK plays an important role in stress response and is activated by stressors such as ROS (Czaja 2007), UV light and proinflammatory cytokines such as Tumour Necrosis Factor α (TNF-α) (Czaja

2007; Han et al., 2009). Once activated, JNK regulates many metabolic and survival pathways, but also mediates cell death (Johnson et al., 2007; Weston et al., 2002). The ability of JNK to mediate both cell survival and cell death pathways is often determined by the duration of its activation (Han et al 2009; Liu et al., 2002). Transient JNK activation is associated with cell stress responses such as JunD phosphorylation that can protect cells, whereas sustained JNK activation promotes both apoptotic and necrotic cell death pathways (Czaja 2007; Han et al., 2009; Lamb et al., 2003). In this regard, sustained JNK is important in mediating apoptosis and necrosis caused by a wide range of agents, including ROS, TNFα, UV light and various drugs and toxins (Johnson et al., 2007; Weston et al., 2002). In the liver, prolonged JNK activation has been shown to mediate injury caused by APAP, ischemia and TNFα (Gunawan et al., 2006; Hanawa et al., 2008; Han et al., 2010; Bradham et al., 1997). JNK-dependent cell death is accompanied in many cases by its translocation to mitochondria (Hanawa et al., 2008; Aoki et al. 2002; Chauhan et al., 2003) and cell death is preceded by loss of the mitochondrial function, suggesting that the direct interaction of JNK with mitochondria is important. JNK binding to isolated brain mitochondria has also been shown to shut down mitochondrial metabolism by leading to down-regulation of pyruvate dehydrogenase activity (Zhou et al., 2008). It has been reported that during APAP-induced liver injury, NAPQI induced sustained JNK activation at least partially due to activation of the extra-mitochondrial MAPK cascade initiated by ASK1 activation (Nakagawa et al., 2008) and translocation to mitochondria (Hanawa et al., 2008; Shinohara et al., 2008). This, in turn, induces mitochondrial permeability pore transition leading to hepatocyte death. JNK translocation to mitochondria may also promote mitochondrial ROS generation, which is important in sustaining JNK activation in a self-amplifying loop, particularly when mitochondria are rendered susceptible by toxins such as APAP and anisomycin. Several studies have demonstrated that treatment of mice with a JNK inhibitor or knocking down JNK (using antisense or knockout mice) was able to markedly protect against APAP-induced liver injury without affecting APAP metabolism (i.e., GSH depletion and covalent binding) (Gunawan et al., 2006; Hanawa et al., 2008). Thus, even in the presence of significant cytoplasmic and mitochondrial GSH depletion and covalent binding, hepatocyte death did not occur without JNK. This finding represents a paradigm shift from the notion that hepatocyte necrosis was a passive death due to mitochondrial GSH depletion and covalent binding and demonstrated that APAP-induced hepatotoxicity requires the active participation of JNK (Kaplowitz et al.,

2008). The mechanism by which JNK induces hepatocyte death following APAP involves a complex JNK-mitochondria signaling loop with several steps: (a) mitochondrial GSH depletion and ROS generation (b) redox changes and ASK-1 activation of JNK (c) JNK modulation of Bcl-2 family members (d) JNK translocation to mitochondria and inhibition of mitochondrial bioenergetics.

Two isoforms of JNK, JNK1 and JNK2, are expressed in the liver (Bogoyevitch 2006). JNK1 has been suggested to play an important role in insulin resistance and fatty liver disease (Schattenberg et al., 2006), while JNK2 has been shown to be involved in TNFα-induced apoptosis and ischemia reperfusion (Theruvath et al., 2008; Wang et al., 2006). In the APAP model, both JNK1 and JNK2 appear to be involved in hepatotoxicity, although JNK2 may play a slightly more preferential role. Remarkably, knocking down either JNK1 or JNK2 alone in mice could not protect against APAP-induced liver injury. Only when both isoforms of JNK were simultaneously knocked down protection against APAP was observed (Hanawa et al., 2008).

3.2. The Nrf2-Keap1-ARE Transcription Pathway.

Nrf2:INrf2 (Keap1, Kelch-like ECH-associating protein1) are cellular sensors of oxidative and electrophilic stress. Nrf2 is a nuclear factor that controls the expression and coordinated induction of a battery of genes which encode detoxifying enzymes, drug transporters (MRPs), anti-apoptotic proteins and proteasomes.

3.2.1. Nrf2.

Nrf2 is a leucine zipper/CNC protein which when present in the nucleus functions as transcription factor that regulates coordinated activation of a battery of cytoprotective genes that include biotransformation enzymes, antioxidant proteins, drug transporters, anti-apoptotic proteins and proteasomes. It contains various domains; a N-terminal hydrophobic domain followed by Keap1 binding domain, transcriptional activation domain, CNC domain and basic and leucine zipper domain. Nrf2 through its leucine zipper domain heterodimerizes with small Maf or Jun proteins and bind to antioxidant response elements (ARE) in target genes (Kaspar et al., 2009; Zhang 2006; Aleksunes et al., 2007; Hayes et al., 2009; Kwak et al., 2003). Coordinated induction of cytoprotective gene transcription through the ARE is essential for cellular protection against oxidative stress and related disorders. This induction is controlled by cap 'n' collar (CNC) family of factors. This regulatory region contains a tandem AP1-NFE2 motif, originally termed as the

DNase hypersensitive site 2, which has a strong enhancer activity (Moi et al., 1990; Ikuta et al., 1991). Subsequent work to clone the transcription factors that bind to this AP1-NFE2 site have identified several members belonging to the CNC subfamily of the basic leucine zipper (bZIP) transcription factors; among the first identified were p45-NFE2 (Chan et al., 1993), Nrf1 (Chan et al., 1993) and Nrf2 (Moi et al., 1994). Nrf3 (Kobayashi et al., 1999) and two distantly related proteins, i.e., Bach1 (Oyake et al., 1996) and Bach2 (Muto et al., 1998) are other CNC family proteins discovered and characterized later. These proteins function as heterodimeric transcription factors by dimerizing with other bZIP proteins such as small Mafs (sMafs) (Igarashi et al., 1994).

The Nrf1 gene is essential for embryonic development and targeted gene disruption of Nrf1 in mice resulted in embryonic lethality with severe anemia and liver abnormalities such as non-alcoholic steatohepatitis (Chan et al., 1998; Xu et al., 2005). By contrast, Nrf2-disrupted mice were normal, fertile, and did not show a phenotype of developmental deficits (Chan et al., 1996; Itoh et al., 1997), suggesting that Nrf2 is not essential for murine development and survival. However, these mice were hypersensitive to oxidative stress (Chan et al., 1996, 2000; Kwak et al., 2001). Evidence from the past 10 years points to Nrf2 as a key regulator of the cellular responses to oxidative stress in multiple tissues and cell types. Therefore, the Nrf2 signaling pathway could be a therapeutic target for preventing oxidative stress-related diseases.

3.2.2. Keap1.

Detailed analysis of Nrf2 activity and structure across various species has identified six evolutionarily conserved domains named Neh (Nrf2-ECH<chicken Nrf2>homologous domain) (Itoh et al., 1997). The domain in the N terminus, Neh2, was discovered as having a negative regulatory role for the transactivating activity of Nrf2 (Itoh et al., 1999). Deletion of Neh2 was found to remarkably increase Nrf2's transactivation activity, which hinted that the Neh2 may contain a critical interaction site to which the negative regulator of Nrf2 binds. Using a yeast two-hybridization system and Neh2 as a bait, Keap1 (Kelch-like ECH-associating protein1), a zinc metalloprotein, was identified to be the major protein-interacting with the Neh2 domain. Based on Keap1 cDNA sequences, the primary structure of murine Keap1 was predicted to be composed of 624 amino acids and there is ~95% homology between human and mouse (Itoh et al., 1999). Molecular dissecting analysis suggests that Keap1 consists of five domains: the N terminal region (NTR),

the BTB/POZ (Bric-a-brac, tramtrack, broad-complex/poxvirus zinc finger), the intervening region (IVR), the double glycine repeat (DGR) or Kelch domain and the C-terminal region (CTR) (Itoh et al., 2004A). The BTB/POZ domain is involved in protein homodimerization and heterodimerization making homomeric and heteromeric multimers of Keap1 (Yoshida et al., 1999). In addition, both BTB and IVR domains are involved in proteasome-dependent Nrf2 degradation (Kobayashi, et al., 2004). The DGR or Kelch domain binds to the Neh2 domain of Nrf2, anchoring Nrf2 into actin cytoskeleton (Itoh et al., 1999; Kang et al., 2004). From crystal structure analysis of the Kelch domain of human Keap1, it was revealed to have six structurally similar β-propeller blades (Li et al., 2004B). These inter- and intra-blades, which are tied firmly by hydrogen bonds, are believed to construct the complex structure of Keap1-Nrf2 and its anchorage to actin. The C-terminal region of Keap1 was also shown to bind to the Neh2 domain of Nrf2 (Tong et al. 2006A). A "two-site molecular recognition model" has thus been proposed for Keap1-Nrf2 complex whereby the two motifs, namely DLG and ETGE, in the Neh2 domain of Nrf2 independently associate with the Keap1-DC (DGR and CTR) (Tong et al., 2006B). This double tethering of Nrf2 with Keap1 is thought to contribute to the overall stability of the Keap1-Nrf2 complex.

3.2.3. The Nrf2 Signaling Pathway.

Under physiological/basal conditions, Keap1/Cul3-RBX1 complex is present in the cytosol constantly degrading Nrf2 (Kobayashi et al., 2004; Dhakshinamoorthy et al., 2004). In the absence of cellular stress, Nrf2 is tethered within the cytoplasmic Keap1 (Itoh et al., 1999; Dhakshinamoorthy et al., 2001), which interacts with the actin cytoskeleton (Kang et al. 2004). This interaction occurs between a single Nrf2 protein and Keap1 dimer (Tong et al., 2006). Keap1 serves as a substrate linker protein for interactions with the Cullin 3 (Cul3)-based E3 ubiquitin ligase to regulate the stability of Nrf2 (Cullinan et al., 2004). Covalent conjugation of proteins by ubiquitin usually involves three enzymatic activities for activating (E1), conjugating (E2) and ligating (E3) ubiquitin to a substrate (Furukawa et al., 2005). In this case, Nrf2 serves as the substrate, while Cul3 serves as a scaffold protein that forms the E3 ligase complex Ring Box Protein 1 (Rbx1) that recruits a cognate E2 enzyme (Kobayashi et al., 2006).

Keap1, via its N-terminal BTB/POZ domain, binds to Cul3 (Geyer et al., 2003) and via its C-terminal Kelch domain binds to Nrf2, leading to the ubiquitination and proteasomal degradation of Nrf2 through the 26S proteasome (Stewart et al., 2003;

Nguyen et al., 2003). While the Keap1-mediated ubiquitination and degradation occurs primarily in the cytosol, Keap1/Cul3-RBX1 complex is also present in the nucleus and degrades Nrf2 under basal conditions (Niture et al., 2009). Exposure to a number of stressors (such as APAP) and inducing agents leads to redox modulation of cysteines in Keap1, which lead to its dissociation of Nrf2, thereby rescuing Nrf2 from proteasomal degradation(Figure 4) and allowing for the entry into the nucleus (Jain et al., 2005). Another mechanism for the activation of Nrf2 involves secondary sensor proteins and the activation of kinase-mediated signaling pathways, resulting in phosphorylation of Nrf2 (Figure 4). Experiments revealed that phosphorylation of Nrf2 by protein kinase C (PKC) promotes its dissociation from Keap1 and that a serine to alanine mutation at amino acid 40 (S40A) in Nrf2, which is the target site for PKC, decreased this PKC-dependent dissociation (Bloom et al., 2003; Huang et al., 2002). PKR-like endoplasmic reticulum kinase (PERK)-dependent phosphorylation of Nrf2 also triggers dissociation of the Nrf2-Keap1 complex (Cullinan et al., 2003). It also seems possible that PKC and/or PERK or their upstream signaling molecules may act as sensors for oxidative stress (Kobayashi et al., 2006). Therefore, it appears that both Keap1 modification and PKC/PERK phosphorylation of Nrf2 are required for its activation (Niture et al., 2009). Upon interruption of Keap1-Nrf2 binding, Nrf2 translocates to the nucleus where, in association with small Maf proteins modulates transcription of the ARE-containing genes (Itoh et al., 1997) and coordinates the transcription of genes involved in phase II detoxification and antioxidant defence (Kaspar et al.,2009; Shelton et al 2013).

Chronic Nrf2 activation within the nucleus has been shown to be harmful and in mouse models results in postnatal death from malnutrition and hyperkeratosis and increased risk for tumorigenesis (Wakabayashi et al., 2003). Because of this potentially pathogenic role, mechanisms exist within the cell to degrade Nrf2 shortly following its activation. After translocation and accumulation of Nrf2, nuclear degradation occurs to prevent constitutive activation. The DGR region of Keap1 and prothymosin-α (PTMα), a chromatin remodeling nuclear protein, import Keap1 into the nucleus in a complex with CuI3 and Rbx1. Upon entering the nucleus, Keap1 releases PTMα, binds to Nrf2, and triggers degradation to shut off downstream gene expression. This autoregulatory loop between Nrf2 and Keap1 controls the abundance of each protein within the cytosol and nucleus, thus allowing for induction of phase II enzymes while preventing chronic constitutive expression of these genes (Zhang et al ., 2005).

Along with Keap1/Cul3-RBX1 complex, additional negative regulators of Nrf2 are present in the nucleus. In this regard, a delayed mechanism involving GSK3β and Src kinases family (SKF) that controls switching off of Nrf2 activation of gene expression has been recently demonstrated (Niture et al., 2011; Rada et al., 2011). GSK3β is a multifunctional serine/threonine kinase, which plays a major role in various signaling pathways (Kannoji et al., 2008). SKF are frequently overexpressed and/or activated in human cancers and play key roles in cancer cell invasion, metastasis, proliferation, survival, and angiogenesis (Ingley 2008). The SKF contains two major subfamilies, including the Src subfamily and the Lyn subfamily (Ingley 2008). Src subfamily has four members including Src, Yes, Fyn, and Fgr (Ingley 2008).

Recently, it has been demonstrated that activation of GSK3β by its tyrosine phosphorylation at 216 by an unknown tyrosine kinase phosphorylates SKF at unknown threonine residue(s), leading to nuclear import/accumulation of these kinases that, in turn, phosphorylate Nrf2 at tyrosine 568. This was followed by Nrf2 nuclear export and binding with Keap1 leading to its degradation (Figure 4).

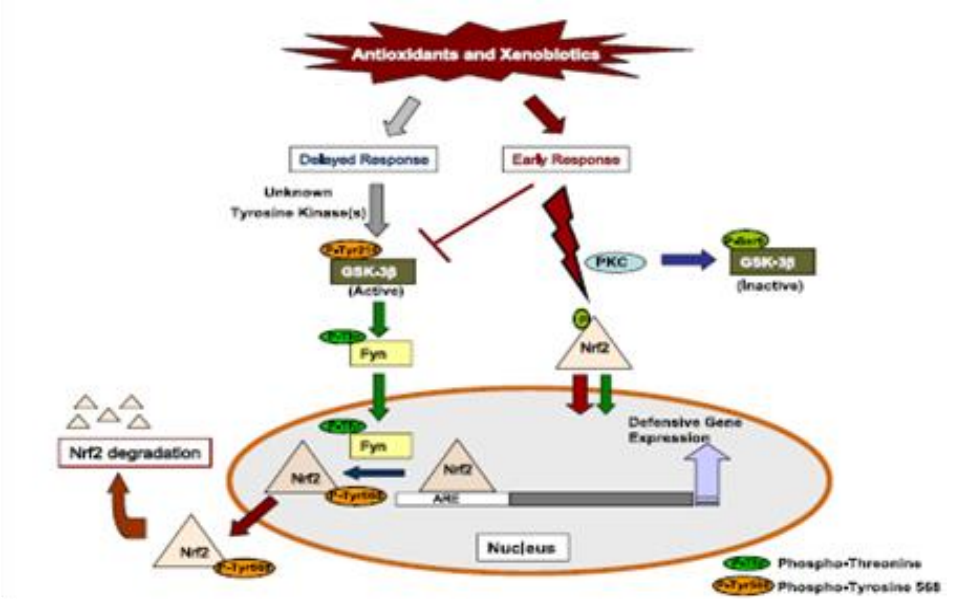

Figure4. Model depicting the role of GSK-3β in regulating nuclear export of Nrf2 via Fyn phosphorylation.

4. Molecular Mechanism Involved In Hepatocyte Survival Against Apoptotic Triggers: Role Of Protein Tyrosine Phosphatase 1B.

4.1. Role Of PTP1B In The Balance Between Cell Death And Survival.

Cell survival and cell death are governed by stimulatory and inhibitory signals. Whereas trophic factors simultaneously stimulate mitosis and inhibit cell death, negative growth signals regulate the opposite of these biological effects. Deregulation of apoptosis represents an underlying cause or contributor to many diseases. In the liver, a balance between apoptotic and anti-apoptotic signals must be tightly controlled to prevent alterations during hepatic development and pathological conditions such as liver disease (Bursch et al., 2005) (Canbay et al., 2004). Activation of death receptors such as Fas/CD95 and TNFα, mitochondrial damage and oxidative stress of the ER are the major triggers of apoptosis that ultimately produce liver damage (Ockner 2001). On the other hand, in the liver, trophic factors include endogenous growth factors such as EGF, basic fibroblast growth factor (bFGF), TGF-β and IGFs that act through receptors belonging to the tyrosine kinase superfamily (Schulte-Hermann et al., 1995). Consistent with this notion, inhibitors of tyrosine kinases and protein tyrosine phosphatases can also modulate apoptosis in the liver.

Protein tyrosine phosphatase 1B (PTP1B) was the first mammalian protein tyrosine phosphatase identified and purified to homogeneity (Tonks et al., 1988). This phosphatase is widely expressed and localizes predominantly to the ER through a cleavable proline-rich C-terminal segment. Cleavage of this segment appears to release the enzyme from the ER and increase its specific activity (Frangioni et al., 1993). The mechanism by which ER-bound PTP1B spatially and temporally interacts with plasma membrane or cytosolic substrates is not completely understood. In this regard, Haj et al. (Haj et al., 2002) demonstrated that dephosphorylation can occur at the ER membrane after endocytosis of activated receptors. On the other hand, time-lapse imaging analysis suggests that ER-bound PTP1B accesses its substrates by extending to immature focal adhesion sites or axonal growth cones in a microtubule-dependent manner and it is required for proper cellular matrix attachment and motility (Hernandez et al., 2006). Finally, some proteins may act as linkers to facilitate the binding of PTP1B to its substrates. In this model, phospholipase C gamma (PLCγ) binds simultaneously to PTP1B and its substrate JAK2 by forming a ternary complex and facilitates its inactivation

(Choi et al., 2006). Similarly, the binding of PTP1B to the cytoplasmic domain of N-cadherin facilitates the dephosphorylation of β-catenin and promotes the assembly of the cell-cell adhesion N-cadherin-β-catenin complex (Balsamo et al., 1996).

In addition to its location at the ER surface, four mechanisms sometimes working in tandem are known to regulate PTP1B activity: oxidation, phosphorylation, sumoylation and proteolysis. PTP1B activity is regulated in vivo by reversible oxidation involving cysteine 215 at its active site, which temporarily abrogates its enzymatic activity. Such redox modification is an important mechanism in determining the extent and duration of phosphotyrosil-dependent signaling responses. In this regard, a transient burst of ROS with the subsequent inactivation of PTP1B has been reported in response to EGF (endogenous growth factors) or insulin stimulation (Meng et al., 2003). Very recently, it has been reported that expression of conformation-sensor scFvs as intracellular antibodies (intrabodies) stabilized oxidized inactive form of PTP1B and enhanced insulin-induced tyrosyl phosphorylation of IR and its substrate IRS1 and increased insulin-induced phosphorylation of protein kinase B (AKT). These data suggest that stabilization of this conformation of PTP1B with appropriate therapeutic molecules may offer a paradigm for phosphatase drug development (Haque et al., 2011). Regarding phosphorylation, PTP1B is regulated by both serine and tyrosine phosphorylation although this effect is still controversial. For instance, phosphorylation of PTP1B at Ser 50 by Akt can decrease its enzymatic activity towards the activated insulin receptor (IR), perhaps as a part of a positive feed-back loop to regulate insulin signaling (Ravichandran et al., 2001). By contrast, the dual-specific kinases CDK-like linase 1 and 2 (CLK1 and CLK2) are also able to phosphorylate PTP1B at the same residue resulting in two-fold stimulation of its activity. The reason for these discrepant results is not known. Similar controversial results have been reported by tyrosine phosphorylation of PTP1B at tyrosines 66, 152 and 153 in response to insulin stimulation (Bandyopadhyay et al., 1997; Dadke et al., 2001). Regarding sumoylation, a recent report showed that PTP1B interacts with small ubiquitin-related modifier (SUMO) E3 ligase on lysines 335 and 347 resulting in reduction of its capacity to dephosphorylate the IR (Dadke et al., 2001). Finally, in vivo experiments have revealed that calpain-1 proteolyzes PTP1B into inactive fragments in platelets (Kuchay et al., 2007).

The fact that PTP1B has been related with the sensitivity of tumour cells to apoptosis induced by TNFα (Perez et al., 1999) prompted several groups to

investigate the involvement of this phosphatase in the susceptibility of hepatocytes to undergo apoptosis induced by different stimuli in cellular systems and in models of hepatotoxicity in mice. In immortalized hepatocytes, PTP1B deficiency concurs with the attenuation of the cellular apoptotic machinery in response to growth factor withdrawal, whereas PTP1B over-expression accelerates cell death (Gonzalez-Rodriguez et al., 2007b). Early activation of caspase-3 occurred in hepatocytes that overexpress PTP1B, but was nearly abolished in PTP1B$^{-/-}$ cells. At the molecular level, PTP1B overexpression/deficiency altered the balance of pro-(Bim) and anti-(Bcl-xL) apoptotic members of the Bcl-2 family upon serum withdrawal. Likewise, cytosolic cytochrome C increased rapidly in hepatocytes with increased PTP1B expression whereas it was retained in the mitochondria of PTP1B$^{-/-}$ cells. Similar modulation was observed in the analysis of DNA laddering and hypodiploid cells.

TGF-β plays a dual role in hepatocytes, mediating both tumour suppressor and promoter effects (Fabregat et al., 2007). The suppressor effects of this cytokine can be negatively regulated by activation of survival signals, mostly dependent on tyrosine kinase activity. Using immortalized hepatocytes, Ortiz et al. (Ortiz et al., 2012) have found that PTP1B deficiency conferred resistance against TGF-β mediated apoptosis and growth inhibition. At the molecular level, this effect correlated with lower Smad2/Smad3 phosphorylation and nuclear translocation, the lack of up-regulation of the inhibitory Smad7 and sustained activation of Akt and ERK1/2. Interestingly, in the presence of the general tyrosine kinase inhibitor genistein both responses were recovered. Moreover, PTP1B$^{-/-}$ hepatocytes stimulated with TGF-β showed elevated NF-κB activation. In the light of these results, knockdown of the NF-κB p65 subunit increased the response to TGF-β of PTP1B$^{-/-}$ hepatocytes in terms of Smad2/3 phosphorylation and apoptosis. The lack of PTP1B also promoted an altered NADPH oxidase (NOX) expression pattern induced by TGF-β ,strongly increasing the NOX1/NOX4 ratio, which was reverted by genistein and NF-κB p65 subunit knock-down. Alternatively, NOX1 knock-down in PTP1B$^{-/-}$ hepatocytes recovered the apoptotic response to TGF-β through the inhibition of nuclear translocation of NF-κB p65 subunit, increase of Smad2 phosphorylation and decrease of levels of the inhibitory Smad7. Altogether, these results highlight the role of PTP1B in the signaling cascades activated by TGF-β that involve Smads2/3, Smad7, NF-κB and NOX1/4 family members. Further work will be necessary to study the potential role of this novel pathway in pathological conditions characterized by kinase hyperactivation, such as liver cancer.

The role of PTP1B in response to liver damage has been studied in vivo in mice injected with a lethal dose of the Fas/CD95 agonist antibody Jo2, a model of fulminant hepatitis (Sangwan et al., 2006). In agreement with the in vitro studies in hepatocytes, PTP1B$^{-/-}$ mice are resistant to Fas-induced liver damage and lethality. This is due to reduced hepatic apoptosis and reduced levels of circulating liver enzymes compared to the lethal effects in the wild-type mice including tachypnea, shallow breathing, and prostration indicative of severe liver failure. Histological analysis of livers from the Jo-2-injected wild-type mice that showed distress revealed parenchymal necrosis, haemorrhage, and hepatocyte apoptosis assayed by TUNEL, whereas livers from the majority of PTP1B$^{-/-}$ mice showed no significant histologic pathological features. Consistent with the histological data, cleavage of caspases-8, -9, -3, and -6, normally activated following Fas receptor oligomerization, was detected in liver extracts from wild-type mice 6 hours post-Jo-2 treatment but was significantly abrogated in PTP1B$^{-/-}$ mice. Because activation of caspase-8 is one of the first events following activation of Fas/CD95, these data demonstrate that one of the earliest events in Fas-induced apoptosis is abrogated in PTP1B$^{-/-}$ mice. Protection against Fas-mediated apoptosis in the liver of PTP1B$^{-/-}$ mice correlated with an elevation and/or activation of numerous anti-apoptotic signaling proteins including FLIPL, ERK1/2 and NF-κB. In addition, the resistance of PTPIB$^{-/-}$ hepatocytes to Fas-mediated apoptosis also required tyrosine kinase activity, because as occurred with TGF-β (Ortiz et al., 2012), PTP1B$^{-/-}$ hepatocytes were rendered susceptible to Fas-mediated apoptosis by pretreatment with genistein. Upon analysis of different PTP1B substrates, it was found that HGFR/Met showed sustained tyrosine phosphorylation and increased activation of its downstream mediator ERK1/2 in both livers and primary hepatocytes lacking PTP1B after Jo-2 treatment. The observation that the majority of PTP1B$^{-/-}$ mice are protected against Fas-mediated liver damage suggests that pharmacological manipulation of PTP1B activity may constitute a viable therapeutic modality for treatment against hepatotoxins and liver damage. A similar inhibition of caspase induction and death receptor-induced liver damage was demonstrated for the compound suramin (Eichhorst et al., 2004). Notably, suramin is an inhibitor of PTP1B at concentrations shown to provide protection to death receptor-mediated liver damage. This effect is promising since the efficacy of PTP1B inhibitors in hepatoprotection remains unexplored.

4.2. Metabolic Functions Of PTP1B.

In mammalian cells, insulin is the principal hormone controlling glucose homeostasis, as it suppresses hepatic gluconeogenesis and promotes glycogen synthesis and storage in liver and muscle, triglyceride synthesis in liver and storage in adipose tissue, and amino acid storage in muscle (DeFronzo 2004). Insulin resistance in major insulin target tissues such as liver, adipose tissues and skeletal muscle is a key pathogenic feature of type 2 diabetes mellitus (T2DM). Among them, the liver plays a major role in controlling blood glucose homeostasis through the balance between glucose utilization and storage (Klover et al., 2004; Radziuk et al., 2001). The molecular mechanism underlying hepatic insulin resistance is not completely understood, however, it is believed to involve impairment of the IR signaling network. A number of epidemiologic and clinical studies have shown a close association between nonalcoholic fatty liver disease (NAFLD) and chronic hepatitis C virus (HCV) infection and insulin resistance (Angulo 2002; Bugianesi et al., 2005; Larter et al., 2006; Lauer et al., 2001). Therefore, one of the challenges facing researchers in the field is the selection of therapeutic targets against hepatic insulin resistance among components of the insulin signaling cascade.

PTP1B locus maps to human chromosome 20 in the region q13.1-q13.2 (Brown-Shimer et al., 1990) and its mouse orthologous to the H2-H3 region of chromosome 2 has been identified as a quantitative trait locus (QTL) linked to diabetes and obesity (Lembertas et al., 1997). Consistent with a role of PTP1B in human insulin resistance, single nucleotide polymorphisms associate with diabetes have been found within the coding and 3´UTR regions. PTP1B directly interacts with and dephosphorylates the activated IR (Salmeen et al., 2000) (Seely et al., 1996) and also exhibits high specific activity for IRS1 (Goldstein et al., 2001) (Figure 5). It has been reported that overexpression of PTP1B in hepatic cellular models such as Fao hepatoma cells impairs insulin-stimulated glucose metabolism and reduction of PTP1B in these cells increased insulin signaling (Egawa et al., 2001) (Clampit et al., 2003). In vivo experiments have demonstrated that reduction of PTP1B expression by 60% in the liver of ob/ob mice increased IRS1/2 tyrosine phosphorylation and Akt activation in response to insulin (Gum et al., 2003). Mice lacking PTP1B exhibited increased insulin sensitivity at 10–14 week of age owing to enhanced phosphorylation of IR in liver and skeletal muscle, resistance to weight gain on a high-fat diet (HFD), and an increased basal metabolic rate (Elchebly et al., 1999) (Klaman et al., 2000). More recent studies have demonstrated that PTP1B re-

expression in the liver of PTP1B null mice leads to a marked attenuation of their enhanced insulin sensitivity (Haj et al., 2005). Moreover, liver-specific deletion of PTP1B improves glucose tolerance (Delibegovic et al., 2009). Interestingly, elevated PTP1B expression in the liver is induced by a high fat diet and coincides with increased levels of TNF-α and CD68, two markers of hepatic inflammation associated to steatosis (Zabolotny et al., 2008). Altogether, these results reinforce the complexity of PTP1B actions in hepatic metabolism and underline the importance of the clinical trials that are actually being carried out with small molecular inhibitors of PTP1B that can be promising drugs for the treatment of hepatic insulin resistance and T2DM (Kasibhatla et al., 2007).

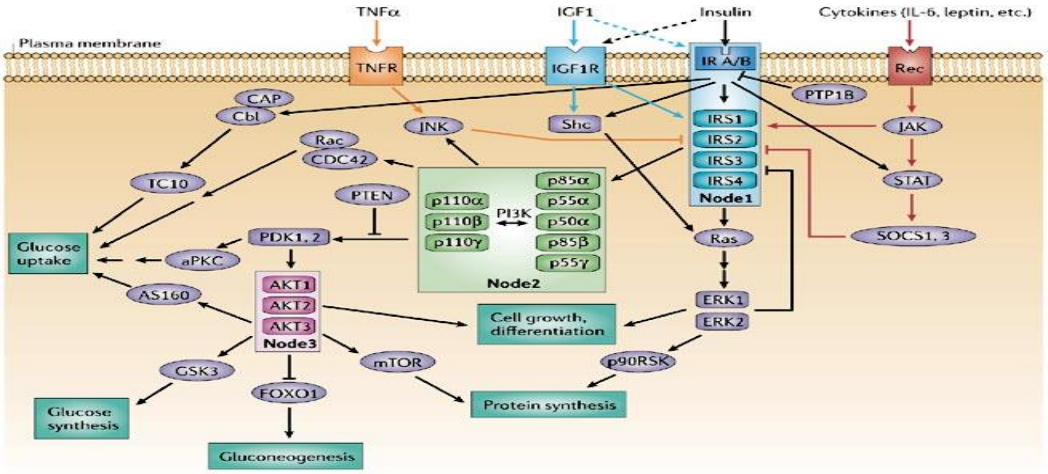

Figure 5. Critical nodes form an important part of the signalling network that functions downstream of the insulin receptor (IR) (black arrows) and the growth factor-1 receptor (IGF1R) (blue arrows).

OBJECTIVES

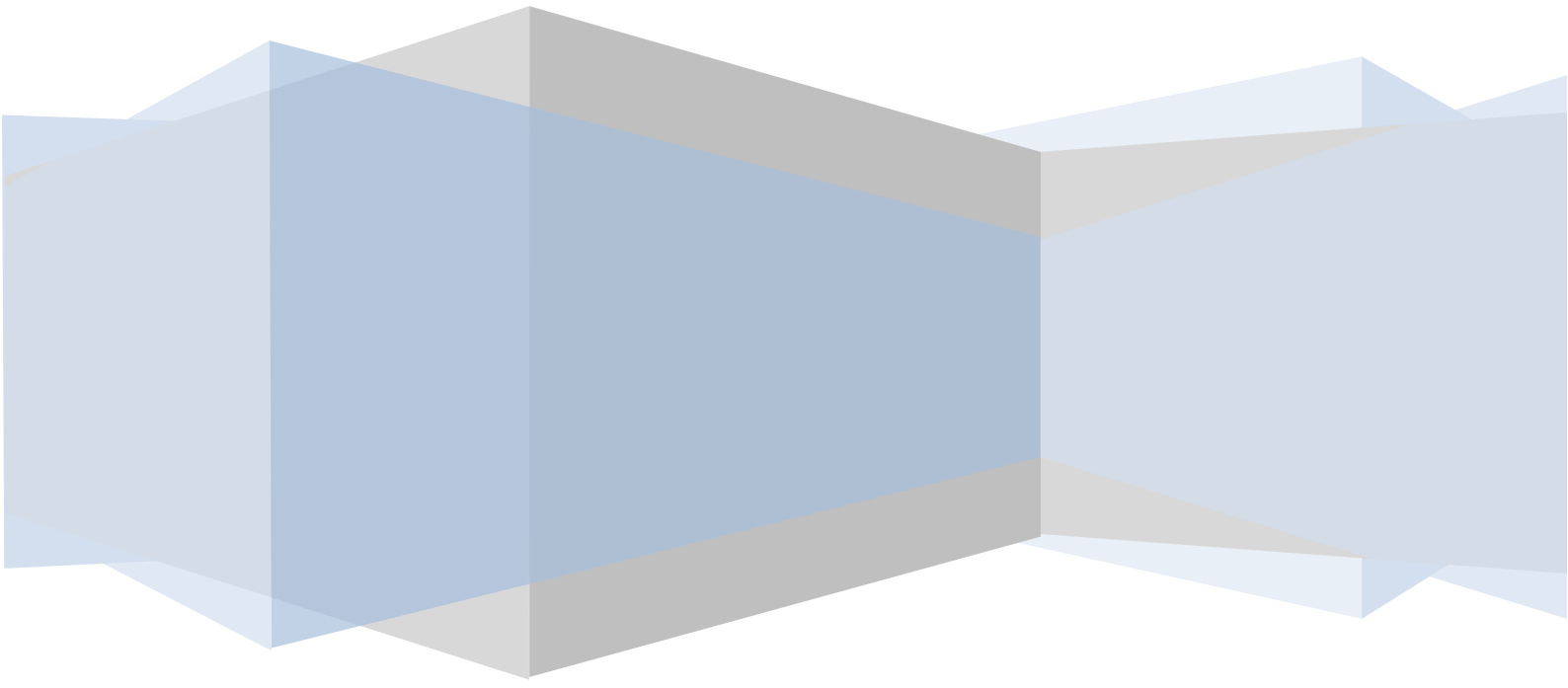

Protein Tyrosine Phosphatase 1B negatively modulates the signaling pathways activated by receptors of the tyrosine kinase superfamily which are involved in hepatocyte survival. In fact, previous studies of the laboratory have assessed the role of PTP1B in mediating hepatocyte survival and liver regeneration. However, PTP1B functions in physiological responses such as hepatocellular survival during drug injury are poorly understood. Our hypothesis is that PTP1B might modulate signaling pathways triggered in response to alterations in liver homeostasis induced by APAP. On this basis, the objectives of this study are:

1- Assess PTP1B expression in APAP-induced acute liver failure in humans and hepatocytes.

2- Analyze the effect of PTP1B deficiency on the activation of stress and survival-mediated signaling pathways in mouse hepatocytes.

3- Study the effect of PTP1B deficiency on APAP-induced oxidative stress.

4- Study APAP-mediated hepatotoxicity in wild-type and PTP1B-deficient mice.

5- Investigate the cross-talk between subtoxic doses of APAP and insulin signaling in hepatocytes with or without PTP1B.

6- Analyze the effect of chronic administration of APAP in whole body glucose homeostasis in wild-type and PTP1B-deficient mice.

MATERIALS AND METHODS

1. Materials

1.1. Reagents.

- Fetal bovine serum (FBS), Medium 199, Dulbecco's Modified Eagle Medium (DMEM), 0.25% Trypsin-0.02% EDTA, and Trizol® were from Gibco Life Technologies, Gaithersburg, MD, USA (www.invitrogen.com).
- Insulin, Paracetamol (APAP), MG132, penicillin, streptomycin, Trichloroacetic Acid, Ethylenediaminetetraacetic acid (EDTA), o-phthalaldehyde (OPT), Tris, Sucrose, 1,4-Dithiothreitol (DTT), Dinitrophenyl hydrazine, Guanidine and Crystal Violet were from Sigma-Aldrich, St Louis, MO, USA (www.sigma-aldrich.com).
- Protein A-agarose, leupeptin, and aprotinin were from Roche Molecular Biochemicals, Barcelona, Spain (www.roche-applied-science.com).
- PP2 was purchased from Tocris Bioscience, Ellsville, MO, USA (www.tocris.com).
- Reagents for protein electrophoresis were from BioRad, Hercules, CA, USA (www.bio-rad.com).
- RNA spin kit was from HealthCare (www.gehealthcare.com).
- Caspase-3 substrate (Ac-DEVD-AMC) was from Enzo Life Sciences (Lausen, Switzerland).
- Renilla was from Promega (Madison, CA).
- siRNA oligos targeted for mouse PTP1B and GSK3β were synthesized by Dharmacon (www.thermoscientific.com).
- Immunofluorescence mounting medium, ABC reagent and DAB (peroxidase substrate kit were from Vector Laboratories (Burlingame, CA), (www.vectorlabs.com).

1.2. Antibodies.

Antibody	Provenance	Reference
Anti-Akt	Cell Signaling Technology (MA, USA)	#9272
Anti-cleaved (Asp175) caspase-3	Cell Signaling	#9661
Anti-phospho JNK (Thr183/Tyr185)	Cell Signaling	#4668
Anti-phospho p38 MAPK (Thr180/Tyr182)	Cell Signaling	#9211
Anti-p38 MAPK	Cell Signaling	#9212
Anti-ubiquitin	Cell Signaling	#3936
Anti-Bclx	BD Biosciences (San Diego, CA).	610211
Anti-phospho GSK3β (pY216)	BD Biosciences	612312
Anti-cytochrome C	Santa Cruz Biotechnology (Palo Alto, CA).	556433
Anti-GSK3β	Santa Cruz	6102019
Anti-JNK	Santa Cruz	sc-571
Anti-phospho-Akt1/2/3 (Ser473)	Santa Cruz	sc-7985-R
Anti-phospho-Akt1/2/3 (Thr 308)	Santa Cruz	Sc-16646-R
Anti-phospho IGF-IR (Tyr1165/1166)	Santa Cruz	sc-01704
Anti-phospho IRβ (Tyr1162/1163)	Santa Cruz	sc-25203
Anti-Nrf2	Santa Cruz	sc-722
Anti-Mcl1	Santa Cruz	sc-819

Anti-Fyn	Santa Cruz	sc-16
Anti-Keap1	Santa Cruz	sc-33569
Anti-human PTP1B	Santa Cruz	sc-14021
Anti-IRS-1	Upstate (Millipore)	06-248
Anti-IRS2	Upstate (Millipore)	06-506
Anti-p85α	Upstate (Millipore)	06-195
Anti-mouse PTP1B	Upstate (Millipore)	07-088
Anti-HO1	Upstate (Millipore)	AB1284
Anti-phospho Ser (clone 4A4)	Upstate (Millipore)	05-1000X
Anti-phospho Tyr (clone 4G10)	Upstate (Millipore)	05-321
Anti-phospho Tyr IRS1 (1179)	Upstate (Millipore)	07-844
Anti-Lamin B	Abcam, Cambridge, UK	aB16048
Anti-Cyp2E1	Abcam	aB19140
Anti-Cytochrome C oxidase subunit I	Molecular Probes (Eugene, OR).	A-6403
Anti-β actin	Sigma Chemical CO. (St. Louis, MO, USA)	A-5441
Anti-c-Src	Calbiochem (Merck Biosciences)	MAb-327
Anti-GCLc and GCLm	gift from T Kavanagh	University of Washington,USA
Anti-IGF-IR	a gift of S. Pons	CSIC, Spain

Table 1 Primary Antibodies.

2. Methods

2.1. *In Vitro* Experiments:-

2.1.1. Cell Culture:-

2.1.1.1. Primary Human Hepatocytes:-

Human hepatocytes were isolated from liver biopsies obtained from twelve patients (eight male and four female aged 58 ± 4.0 years) at Hospital Santa Sofía (Córdoba, Spain) submitted to a surgical resection for liver tumours after obtaining patients' written consent.

- Hepatocytes isolation was based on the two-step collagenase procedure (Pichard et al., 2006). Cell viability was consistently >85%, as determined by trypan blue exclusion.

- Hepatocytes (8×10^6 cells; 150.000 cells/cm^2) were seeded at confluence on type I collagen-coated dishes (Iwaki, Gyouda, Japan) and maintained in DMEM-Ham-F12:William's E (1:1) medium supplemented with 26 mmol/L $NaHCO_3$, 15 mmol/L HEPES, 0.29 g/L glutamine, 50 mg/L vitamin C, 2 mg/L insulin, 200 µg/L glucagon, 50 mg/L transferrin and 4 ng/L ethanolamine containing 5% heat-inactivated fetal bovine serum (FBS) for 12 h.

- The medium was removed, replaced with a fresh culture serum-free medium and hepatocytes were stimulated with various doses of APAP for different time periods.

2.1.1.2. Human Chang Liver Cells (CHL):-

CHL cells, purchased to the American Type Culture Collection (ATCC), were a gift from Dr P. Martín-Sanz (CSIC, Spain). These cells were grown in DMEM with 10% heat-inactivated FBS and stimulated with different doses and different time-periods.

2.1.1.3. Primary Mouse Hepatocytes:-

Mouse hepatocytes were isolated from male wild-type ($PTP1B^{+/+}$) and PTP1B-deficient ($PTP1B^{-/-}$) mice, maintained on the same mixed C57/BL6 x 129 sv genetic background, at 10-12 weeks by perfusion with collagenase and cultured as previously described (González-Rodríguez et al., 2010). Isolated

hepatocytes were cultured in DMEM supplemented with 10% FBS for 24 h. Then, the medium was removed and replaced with DMEM plus 1% FBS and hepatocytes were stimulated with APAP for different time periods and different doses.

2.1.1.4. Immortalized Neonatal Hepatocytes:-

The generation and characterization of immortalized hepatocyte cell lines from wild-type and PTP1B$^{-/-}$ mice was previously performed in the laboratory (González-Rodríguez et al., 2007). Cells were grown in DMEM with 10% heat-inactivated FBS and stimulated with various doses of APAP for various time periods.

2.1.1.5. Maintenance Of Cell Lines:-

The obtained cell lines were grown at 37ºC in 5% CO_2 in DMEM supplemented with:

- 10% heat-inactivated FBS.
- 20 mmol/L Hepes pH 7.4.
- Antibiotics: penicillin-G (0.12 mg/mL) and streptomycin (0.1 mg/mL).

When the cells had reached confluence, they were trypsinized according to the following procedure:

- The culture medium was aspirated.
- The cells were washed two times with phosphate buffered saline (PBS), pH 7.4.
- Trypsin (0.25%)-EDTA was added for 1 minute, then removed.
- The culture plates were maintained in the incubator for 2-3 minutes.
- Then, the plates were removed from the incubator and carefully shacked.
- Trypsin action was stopped by adding culture medium supplemented with 10% FBS.
- The cell suspension was distributed between several plates. Cell density was adjusted to the requirements of each experiment.

2.1.1.6. Freezing And Thawing The Cell Lines:-

When cells reached 80% confluence, they were washed twice with warm PBS and trypsinized as indicated above. Trypsinization was stopped with medium containing FBS-12% dimetylsulfoxide (DMSO). The cell suspension was introduced into a cryopreservation vial. Then, the vials were frozen according with the following steps:

1: -20°C for 1-2 hours.
2: -80°C for 15-24 hours.
3: -170°C in liquid nitrogen containers.

Conservation: The cells were stored frozen in liquid nitrogen.

When required, cells were thawed by removing the vials from the liquid nitrogen container and incubating them at 37°C for 5 minutes. Once thawed, the cell suspension was seeded in culture dishes.

2.1.2. Evaluation Of Cellular Viability:-

Cell viability was determined by two alternative methods: gross detection of cell viability by using the crystal violet assay (Granado-Serrano et al., 2007) and analysis of cytotoxicity by measuring lactate dehydrogenase (LDH) leakage into the extracellular medium (Alia et al., 2005).

2.1.2.1. Analysis Of Cellular Viability By Crystal Violet:-

Measurement of cellular viability by crystal violet is also based on the integrity of the cell plasma membrane since when it is altered the dye can enter into the cell. Then, the dye enters into both the living and the dead cells and only remains inside the living cells. Thus, the amount of dye is proportional to the number of living cells.

- Cells were seeded at low density (10^4 cells per well) in 12-well multiwall plates and they were grown for 20 hours.
- Once cells were cultured under the experimental conditions required, the culture medium was discarded.
- Cells were washed once with PBS.

- Cells were fixed with a suitable fixer (1% glutaraldehiyde) at least 10 minutes at room temperature or overnight at 4°C.
- Cells were washed three times with PBS.
- The remaining viable adherent cells were stained with crystal violet (0.2% w/v in 2% ethanol) for 20 minutes at room temperature.
- Excess of crystal violet was discarded and plates were rinsed with tap water three times.
- 1% sodium dodecyl sulfate (SDS) was added to solubilize membranes.
- The absorbance of each plate was read in a spectrophotometer at 560 nm.
- Plates without cells were processed in parallel to correct the non-specific adhesion of crystal violet to the plastic.
- Remaining viable cells were calculated as the percentage of absorbance with respect to control cells (incubated in the absence of APAP).

2.1.2.2. LDH Leakage Assay:-

Cellular damage was evaluated by LDH leakage assay. An LDH assay was performed by assessing LDH released into the media as a marker of necrotic cell death.

- Cells (2×10^5 per well) were treated with APAP for different conditions.
- Briefly, after the different treatments the cell culture medium was collected in a new tube.
- Cells were scraped in PBS.
- Cells were first sonicated to ensure the breakdown of the cell membrane to release the total amount of LDH.
- Then, cells were centrifuged at 1.000 x g for 15 minutes at 4°C to clear up the cellular debris.
- LDH assay mixture (1.35 mol/L Tris pH 7.4, 0.4 mmol/L NADH and 0.08 mol/L pyruvate; pH 7) was prepared fresh for each experiment and was added to the sample.

- 10 µL of each sample was placed in duplicate to a 96 well plate. In the same manner, 10 µL of each culture medium were also placed in a 96-well multiwell plate for the assay.
  - 200 µL of the buffer mentioned above were added to each well.
  - Absorbance was measured at time zero (t=0) and after 5 minutes (t=5) in the spectrophotometer at an emission wavelength of 460 nm and an excitation wavelength of 340 nm.
  - The LDH leakage was estimated by the ratio between the LDH activity in the culture medium to the total LDH activity in the medium plus in the cells, as previously described (Welder et al., 1994; Alia et al., 2006).

2.1.3. Quantification of Apoptosis:-

2.1.3.1. Quantification Of Apoptotic Cells By Flow Cytometry:-

This method is based on the staining of DNA with propidium iodide. Propidium iodide intercalates between DNA bases, emitting fluorescence which intensity is proportional to the amount of cellular DNA. Staining with propidium iodide allows analyzing the percentage of cells in different cell cycle phases and also the percentage of apoptotic (hypodiploid) cells (Darzynckiewicz et al., 1992).

- After induction of apoptosis by APAP at different doses, the supernatant was collected. Attached cells were washed once with PBS.
- Cells were trypsinized as described above.
- Adherent and non-adherent cells were collected by centrifugation at 2.500 x g for 5 minutes at 4°C.
- Cells were washed once with PBS followed by centrifugation at 2.500 x g for 5 minutes at 4°C.
- Cells were fixed with cold ethanol (80% v/v) for 1 minute.
- Cells were centrifuged at 2.500 x g for 5 minutes at 4°C. The cell pellet was resuspended in 2 ml of cold PBS.
- Cells were centrifuged at 2.500 x g for 5 minutes at 4°C.

- The cells were then washed, resuspended in 500 µL of PBS and incubated with RNAse A (10 µg) for 30 minutes at 37°C.
- After addition of 0.05% (w/v) propidium iodide, cells were analyzed by flow cytometry.

2.1.3.2. Analysis Of Caspase-3 Activity:-

The enzymatic activity of caspase-3 was measured by a fluorometric method. We define a unit of caspase-3 activity as the amount of active enzyme necessary to produce an increase in 1 fluorimetric arbitrary unit after 2-hour incubation with the reaction mixture. Briefly,

- After treatment, cells were scraped off and then collected by centrifugation at 600 x g for 5 minutes at 4°C.
- Cells were lysed in 5 mmol/L Tris/HCl pH 8, 20 mmol/L EDTA and 0.5% (v/v) Triton X-100.
- Lysates were clarified by centrifugation at 15.700 x g for 10 minutes at 4°C.
- Lysates were incubated with reaction mixture for 2 hours at 37°C in the dark.
- Reaction mixture contained :

  -25 µL of cell lysate.

  -325 µL of assay buffer (20 mmol/L HEPES pH 7.5, 10% (v/v) glycerol, 2mmol/L DTT).

  -20 µM (final concentration) caspase-3 substrate.

- Enzymatic activity was measured in a luminescence spectrophotometer (Perkin Elmer LS-50, Norwalk, CT) (λ excitation, 380 nm; λ emission, 440 nm).
- Then, protein concentration of cell lysates was determined and the results were expressed as caspase-3 activity/micrograms of total protein.

2.1.4. Determination Of Cellular Oxidative Stress:-

2.1.4.1. Determination Of GSH:-

The content of GSH was quantified by the fluorometric assay of Hissin and Hilf (1976). The method takes advantage of the reaction of GSH with o-phthalaldehyde (OPT) at pH 8.0. Briefly,

- After the different treatments, the culture medium was removed.
- Cells were scraped off then collected by centrifugation at 2.000 x g for 5 minutes at 4°C in PBS.
- Cells were then resuspended in 5% (w/v) trichloroacetic acid containing 2 mmol/L EDTA.
- The cells were homogenized by sonication for 10 minutes.
- Homogenates were centrifuged at 1.000 x g for 30 minutes at 4°C.
- 50 µL of the clear supernatant was transferred to a 96 multiwell plate for the assay.
- Then, 15 µL of 1 mol/L NaOH, 175 µL of 0.1 mol/L sodium phosphate buffer (SPB) pH 8 containing 5 mmol/L EDTA and 10 µL of 74 mmol/L OPT were added per well.
- A standard curve with increasing concentrations of GSH was prepared and similar amounts were added as before.
- The plate was covered with aluminium paper and was kept at room temperature for 15-20 minutes.
- Fluorescence was measured at an excitation wavelength of 340 nm and emission wavelength of 460 nm. The results of the samples were referred to a standard curve of GSH as described (Alia et al., 2006)

2.1.4.2. Measurement Of Intracellular Reactive Oxygen Species (ROS):-

For visualization and analysis of intracellular ROS by flow cytometry, the oxidation-sensitive DCFH-DA probe was used.

- For the assay, cells were plated in 6 well-multiwell plate at a rate of 2 $\times 10^5$ cells per well.
- Then the APAP was added for 6 h.
- Later, cells were detached by trypsinization.
- The cells were incubated with 5 µmol/L DCFH-DA for 30 minutes at 37°C.
- Cellular fluorescence intensity was measured by using a FACScan flow cytometer (BD, San José, CA). For each analysis, 10.000 events were recorded.

2.1.4.3. Determination Of Glutathione peroxidase (GPx) And Glutathione reductase (GR) Enzymatic Activities:-

The determination of GPx activity is based on the oxidation of GSH by GPx, using t-BOOH as a substrate, coupled to the disappearance of NADPH by GR. GR activity was determined by following the decrease in absorbance due to the oxidation of NADPH utilized in the reduction of oxidized glutathione (G-S-S-G) (Rodríguez-Ramiro et al., 2011).

- For the assay of the GPx and GR activities, 1.5 × 10^6 cells per well were treated with APAP for 16 h.
- Cells were collected in PBS and centrifuged at 1.000 x g for 5 minutes at 4°C.
- Cell pellets were resuspended in 20 mmol/L Tris containing 5 mmol/L EDTA and 0.5 mmol/L 2-mercaptoethanol.
- Cells were sonicated for 10 minutes.
- Homogenates were centrifuged at 3.000 x g for 15 minutes at 4°C.
- Enzyme activities were measured with a mixture of (50 mmol/L potassium phosphate buffer pH 7.5 mmol/L GSH and Glutathione Reductase 50 U/mL, 9.6 mmol/L NADPH) for the blank.

- Enzyme activities were measured with the same mix with adding samples instead of the buffer.

2.1.5. Transfection:-

2.1.5.1. Transient Transfection With siRNA:-

RNA silencing (siRNA) has become a major application in research to perform "knock-down" experiments. The limitations of the silencing approach rely on the toxicity of the transfection procedure for cells as well as the off-target effects on the expression of other genes or proteins. Immortalized hepatocytes were seeded in 6 well-multiwell dishes and incubated overnight at 37°C with 5% CO2.

- When 40-50% confluence was reached, cells were transfected with10 nmol/L of PTP1B or 25 nmol/L GSK3β siRNAs or with similar concentrations of scrambled control siRNA following DharmaFECT General Transfection Protocol.
- 48 hours after the transfection, cells were used for experiments and treated with APAP for different time periods.

2.1.5.2. Luciferase Assays:-

Transient transfections of HEK293T cells were performed with the expression vectors for pcDNA3.1mNrf2-V5/HisB (a gift from Dr. J.D. Hayes, Biomedical Research Institute, Ninewells Hospital and Medical School, University of Dundee, Dundee, Scotland, United Kingdom), Renilla, and 3xARE-Luc (a gift of Dr J. Alam, Department of Molecular Genetics, Ochsner Clinic Foundation, USA) combined with myc-PTP1B (a gift of Dr M. Tremblay, Mc Graw Hill University, CA) only in the indicated cases.

- HEK293T cells were seeded on 24-well plates (10^5 cells per well) and cultured in DMEM with 10% heat-inactivated FBS for 16 hours.
- Then, the cells were transfected using calcium phosphate protocol.
- After transfection, cells were treated with vehicle (PBS), APAP (10 and 20 mmol/L) or tBHQ (15 µmol/L) for 16 hours.

- Cells were lysed and assayed for luciferase activity with the dual luciferase assay system (Promega), according to the manufacturer's instructions.
- Relative light units were measured in a GloMax 96 microplate luminometer with dual injectors (Promega).

2.1.6. Immunoflorescencee:-

Cells were grown in glass coverslips until 80% confluence was reached. Then, cells were treated directly in 6 well-multiwell plates with APAP as indicated in the Results section. Cells were washed twice with PBS, fixed in 100% (v/v) methanol at -20°C for 2 minutes and then processed to immunofluorescence.

2.1.6.1. Nrf2 Immunofluorescence:-

- Cells were blocked in Blocking Buffer (1% BSA in PBS) for 30 minutes at room temperature.
- While blocking, primary antibody was prepared by diluting as 1/50 in 1% BSA in PBS. Primary anti-Nrf2 antibody was applied for 1 hour at 37°C or overnight at 4°C.
- Cells were washed four times (5 minutes each) with PBS.
- Then, cells were incubated for 45 minutes at 37°C with fluorescence-conjugated secondary antibody (Alexa 488 goat anti-rabbit) followed by four final washes of 5 minutes each in PBS.
- Immunofluorescence was examined in a Nikon Eclipse 90i microscope (camera Nikon DS-Qi1Mc at plan Apo 20x, N.A 0, 75 or at plan Apo 40x, N.A 0, 95).

2.1.6.2. 4′,6′-diamidino-2-phenylindole (DAPI) Staining:-

To examine the apoptotic changes in nuclei, DAPI (4′,6′-Diamidino-2-phenylindole) staining assay was performed.

- Cells were grown in glass cover slips and fixed as described above.

- After 80–90% confluence was reached, the cells were treated with different concentrations of APAP.
- Cells were fixed with methanol for 3 minutes at -20°C in the dark.
- Fixed cells were washed twice with PBS.
- Then, cells were stained with 1 µmol/L DAPI for 15 minutes in the dark.
- Then, cells were washed four times (5 minutes each time) with PBS to remove the excess of DAPI.
- Cover slips were placed in a glass slide with immunofluorescence mounting medium (Vector, Burlingame, CA).
- Nuclear morphology was analyzed by fluorescence microscopy in a Nikon Eclipse 90i microscope.
- Then, the incidence of condensed and/or fragmented nuclei was calculated.

2.1.7. Analysis Of Protein Expression:-

2.1.7.1. Protein Extracts:-

A- Preparation of total cell lysates.

- Detached cells were collected by centrifugation at 600 x g for 5 minutes at 4ºC.
- Attached cells were scraped off in ice-cold PBS and pelleted by centrifugation at 600 x g for 5 minutes at 4ºC.
- Then, cells were resuspended in lysis buffer (25 mmol/L HEPES pH 7.4, 2.5 nmol/L EDTA, 0.1% (v/v) Triton X-100, 1 mmol/L phenylmethylsulfonyl fluoride (PMSF), 5 µg/ml leupeptin and 2.5µg/ml aprotinin).
- Cellular lysates were clarified by centrifugation at 15.700 x g for 10 minutes at 4ºC.

- The supernatants were transferred to fresh tubes for immediate use or frozen at -80°C.

B- Extraction Of Nuclear And Cytosolic Proteins.

We followed the methods of Andrews-Faller (1991) and Schreiber-Schaffner (1989). Briefly,

- Cells were resuspended at 4°C in Buffer A (10 mmol/L HEPES-KOH, pH 7.9, 1.5 mmol/L MgCl2, 10 mmol/L KCl, 0.5 mmol/L DTT, 0.2 mmol/L PMSF, 0.75 µg/mL leupeptin, 0.75 µg/mL aprotinin).
- Cells were allowed to swell on ice for 10 minutes.
- Then, cells were vortexed for 10 seconds.
- Samples were centrifuged at 400 x g for 2 minutes or at 15.700 x g for 10 seconds at 4°C.
- The supernatant containing the cytosolic fraction was stored at -80°C.
- The pellet was resuspended in cold buffer C (20 mmol/L HEPES-KOH, pH 7.9, 25% glycerol, 420 mmol/L NaCl, 1.5 mmol/L MgCl2, 0.2 mmol/L EDTA, 0.5 mmol/L DTT, 0.2 mmol/L PMSF, 0.75 µg/mL leupeptin, 0.75 µg/mL aprotinin) and incubated on ice for 20 minutes for high salt extraction.
- Cellular debris was removed by centrifugation at 15.700 x g for 2 minutes at 4°C and the supernatant nuclear fraction was stored at –80°C.

C- Preparation Of Mitochondrial And Cytosolic Extracts.

For the preparation of mitochondrial and cytosolic extracts we followed the following protocol:

- Cells were scrapped off in the culture media and then centrifuged at 600 x g for 5 minutes at 4°C.
- The precipitates were resuspended in 3 ml of isotonic isolation buffer and collected by centrifugation at 600 x g for 5 minutes at 4°C.

- Then, the isotonic isolation buffer was removed and the cells pellets were resuspended in 750 µl of hypotonic isolation buffer and incubated at 37ºC for 5 minutes.
- Samples were homogenized using a teflon pestle Potter (Wheaton Instruments, Milville, cat. 903,475).
- 250 µl of hypertonic isolation buffer was added to balance the buffer´s osmolarity.
- Samples were centrifuged at 400 x g for 5 minutes at 4ºC, the supernatants contained the cytosolic protein fraction and the pellets containing the mitochondrial fraction were resuspended in lysis buffer and kept on ice for 30 minutes.
- Samples were centrifuged at 15.700 x g for 5 minutes at 4ºC.
- The supernatants contained the mitochondrial protein fraction were kept at -80ºC until being used.

Isotonic Buffer	Hypotonic Buffer	Hypertonic Buffer
10 mmol/L Hepes pH 7.6	10 mmol/L Hepes pH 7.6	10 mmol/L Hepes pH 7.6
1 mmol/L EDTA	1 mmol/L EDTA	1 mmol/L EDTA
250 mmol/L sucrose	50 mmol/L sucrose	450 mmol/L sucrose

Table 2. Mitochondrial isolation buffer

2.1.7.2. Protein Determination:-

Protein determination was performed by the Bradford dye method in duplicate, using the Bio-Rad reagent and BSA to prepare the standard curve.

2.1.7.3. Immounoprecipitations:-

Immunoprecipitations were performed to separate a specific protein from a total protein extract.

- Protein A/G beads were prepared by washing the beads in Lysis Buffer 3 times. Then, they were resuspended in Lysis Buffer at 1/1 proportion.

- Then 20 µL of Protein A/G beads were added to the total protein lysate.
- Tubes were rotated for at least 2 hours at 4°C. Then, beads were collected by centrifugation at 15.700 x g for 5 seconds at 4°C. Beads were washed 4 times with 500 µL of cold Lysis Buffer.
- 40 µL of sample buffer were added to the beads. Samples were incubated 5 minutes at 95°C and loaded into a gel as it will be described in the next section.

2.1.7.4. Western Blot:-

The western blot is a widely accepted analytical technique used to detect specific proteins in a sample of protein homogenate or extract. It uses gel electrophoresis to separate native or denatured proteins by their molecular weight. The proteins are then transferred to a membrane and further stained with antibodies specific to the target protein.

Polyacrilamyde Gel Electrophoresis (SDS-PAGE):-

- Sample Preparation: the protein extracts containing equals amount of protein (20-100 µg) were mixed with 4x loading buffer (for a final concentration of 1x) and heated at 95°C for 5 minutes. A molecular weight marker was loaded in one lane (Bio-Rad).
- Samples were stored at -20°C until they were used.
- The preparation of gels and buffers for SDS-PAGE was performed as described in Antibodies: A Laboratory Manual (Ed Harlow, David P Lane).

Loading Buffer	Electrophoresis Buffer
100 mmol/L Tris pH 7.6	25 mmol/L Tris pH 8.3
10% Glycerol (v/v)	250 mmol/L Glycine
4% SDS (p/v)	0.1% SDS (p/v)
0.2% Bromophenol blue (p/v)	
2 mmol/L β-mercaptoethanol	

Table 3. Composition of the loading and electrophoresis buffer

B. Protein Transfer:-

After the proteins were separated by SDS-PAGE, they were transferred to a nylon membrane (Immobilon P, Millipore). Membranes were activated for 1 minute in methanol and then washed twice with distilled water. Membranes were maintained wet in transfer buffer. Two types of transfer were used:

1-Semi-dry Transfer: We used the Trans-blot SD Semi-Dry (Bio-Rad). The conditions used were: voltage 15V and time 30-45 minutes depending on the size of the gel, the percentage of acrylamide and the size of the protein to study.

SEMI-DRY Transfer buffer	WET Transfer buffer
48 mmol/L Tris pH 8.3	66 mmol/L Tris pH 8.5
40 mmol/L Glycine	383 mmol/L Glycine
20% (v/v) Methanol	20% (v/v) Methanol
	0.1% (p/v) SDS

Table 4. Composition of Transfer buffer.

2-Wet Transfer: Wet transfer equipment Trans-Blot (Bio-Rad). The conditions used were: voltage: 70V and time 2 hours.

C. Antibody staining:-

- The membranes were blocked for 1 hour at room temperature or overnight at 4°C using blocking solution (5% non-fat dried milk or 3% bovine serum albumin(BSA)).
- The membranes were washed with TBS supplemented with 0.05% (v/v) Tween 20 (TTBS) for four times (10 minutes each).
- Then, the membranes were incubated with appropriate dilutions of primary antibody in TTBS overnight at 4°C or for 2 hours at room temperature.
- The membranes were washed four times with TTBS (10 minutes each).

- Then, the membranes were incubated with the recommended dilution of labelled secondary antibody in TTBS at room temperature for 1 hour.
- The membranes were washed three times with TTBS (10 minutes each) and we performed a final wash with TBS without Tween for another 10 minutes.
- For signal development immunoreactive bands were visualized using the ECL western blotting protocol (Millipore) and Agfa radiographic films.

2.2. *In Vivo* Experiments:-

2.2.1. Animal Models:-

2.2.1.1 Acute APAP Treatment:-

3 month-old wild type ($PTP1B^{+/+}$) mice and PTP1B-deficient ($PTP1B^{-/-}$) mice were used throughout the study. Mice were obtained from Abbot Laboratories as previously described (González-Rodríguez et al., 2010) and maintained on the same mixed genetic background (C57Bl/6J x 129 Sv/J). All Animal experimentation was conducted accordingly to the accepted guidelines for animal care of the Comunidad de Madrid (Spain). Mice were fed a standard chow diet ad libitum and had free access to drinking water. Overnight fasted mice were intraperitoneally (i.p.) injected with 300 mg/kg APAP dissolved in physiological saline. Control mice received an equivalent volume of saline. Mice were sacrificed at 1, 3, 6 and 24 h and livers were collected and kept at -80ºC.

2.2.1.2. Chronic APAP Treatment:-

3 month-old wild type ($PTP1B^{+/+)}$ mice and $PTP1B^{-/-}$ mice were used throughout the study. Mice were fed a standard chow diet ad libitum. Mice were treated with APAP in the drinking water for 6 months. APAP dose was 90 mg/kg/day during the first 3 months of the treatment. Then, the APAP dose was increased to 120 mg/kg/day during the last 3 months of the treatment. Control mice had free access to drinking normal water. Mice were sacrificed after 6 months.

2.2.2. Analysis Of Alanine Amino Transaminase (ALT) Activity:-

Blood was collected in tubes containing heparin and diluted 1/30 with saline (0.9% NaCl). ALT activity was determined by direct measurement with the Reflotron test (Ref. 10745120, Roche Diagnostics).

2.2.3. Glucose, Pyruvate And Insulin Tolerance Tests:-

Briefly, after chronic APAP treatment mice were fasted overnight and given an i.p. injection of 2 g D-glucose/kg for glucose tolerance tests (GTT) or sodium pyruvate (1.5 g/kg) for the pyruvate tolerance test (PTT) both dissolved in sterile saline.

For measuring fasted glucose levels, blood was obtained from the tail vein and glucose concentrations were measured with an Accu-Check Aviva glucometer (Roche). Blood glucose was measured at time zero (t=0) before starting the experiment. Then, glucose or pyruvate were injected and glucose measurements were taken at 30, 60 and 90 minutes after injection. The area under the curve (AUC) was calculated as AUC_{Ground} (AUC_G mmol/Lol/L * minutes) and represented in graph (Pruessner et al., 2003).

Intraperitoneal insulin tolerance tests (ITT) were performed on 4 h fasted mice injected with 0.75 U/kg human regular insulin. Blood glucose was measured at time zero, 30 and 60 minutes after injection.

2.2.4 Measurment of the Insulin Levels:-

The blood was collected from mice that had been fasted for 24 h and the serum insulin was determined by RIA (Fernández-Millán et al., 2013).

2.2.5. Liver histology:-

Liver histology was performed according to the following steps:

1-Chemical fixation of the tissue: after sacrifice, liver samples were fixed in 4% paraformaldehyde for 48 hours. Subsequently, fixation was continued for a further 24 hours in 70% ethanol.

2- Liver specimens were embedded in paraffin. Then, liver specimens were cut in 10 µm thickness slices and placed on glass slides (this step was performed at the histology service at IIB).

3- Hematoxilin and Eosin (H&E) staining was performed for the analysis of liver structures.

4- Histological changes were analyzed and histological grading of hepatic necrosis was performed by two blinded observers as indicated.

Necrosis in 30% of the total area (1 point).

Necrosis in 30–60% of the total area (2 points).

Necrosis in 60% of the total area (3 points).

2.2.6. PTP1B immunohistochemistry:-

We analysed PTP1B by immunohistochemistry in human liver samples. We obtained samples from 8 patients, some individuals intoxicated with APAP (five patients) and some healthy subjects (3persones). These samples were kindly donated from Dr Kenneth J. Simpson in the division of Clinical and Surgical Sciences, University of Edinburgh, Edinburgh EH164TJ, United Kingdom. Informed written consent was obtained from each patient. We also analysed mouse liver samples that were fixed as described above (section 2.2.5).

2.2.6.1- Deparafinize/hydrate sections:-

Tissue sections were embedded in paraffin and deparaffinised and dehydrated accordingly the following steps.

- Sections were incubated twice in xylene for 5 minutes each.
- Sections were incubated once in100% ethanol for 3minutes each.
- Sections were incubated twice in 90% ethanol for 3 minutes each.
- Sections were incubated once in 70% ethanol for 3 minutes each.
- Sections were washed twice in distilled H_2O for 5 minutes each.

2.2.6.2 -Antigen Unmasking:-

Antigen retrieval was performed by boiling the slides in 10 mmol/L sodium citrate buffer pH 6.0 for 2 minutes.

2.2.6.3-Staining:-

- Sections were washed in PBS three times for 5 minutes each.

- Then, sections were incubated in hydrogen peroxide 3% in PBS for 10 minutes to block the endogenous peroxidase.
- Sections were blocked with 6% BSA in PBS for 45 minutes at room temperature.
- Blocking solution was removed and then slides were incubated with the primary antibody anti-PTP1B (1/250 dilutions in 1% BSA in PBS) overnight at 4°C.
- Antibody solution was removed and sections were washed three times in PBS for 5 minutes each.
- Samples were incubated with a secondary antibody for 1 h at room temperature (biotinylated goat anti-rabbit antiserum 1/500 dilutions in 1% BSA in PBS).
- Secondary antibody solution was removed and sections were washed for four times with PBS for 5 minutes each.
- Then, the slides were incubated with streptavidin/peroxidase for 30 minutes at room temperature.
- 75-100 µl of DAB reagent (Vector Laboratories) was added to each section.
- As soon as the sections develop stain, slides were washed in PBS for 5 minutes followed by two washes with distilled H_2O for 5 minutes each.
- Sections were counterstained in Hematoxylin.
- Sections were washed in distilled H_2O two times for 5 minutes each to remove the excess of the dye.
- Sections were dehydrated and mounted:
    - Sections were incubated in 70% ethanol twice for 10 seconds each.
    - Sections were incubated in 90% ethanol twice for 10 seconds each.
    - Sections were incubated in 100% ethanol twice for 10 seconds each.

- Sections were incubated in xylene twice for 10 seconds each.
- The sections were mounted using DePeX (SERVA electrophoresis) as a mounting medium

- Sections were examined in a Nikon Eclipse 90i microscope and light-microphotographs were taken with an associated Leitz digital camera (Leitz DFC300 FXC).

2.2.7. Analysis of Oxidative Stress:-

2.2.7.1. Determination of GSH:-

For the analysis in liver samples, 50 mg of tissue were homogenized as described in section (2.1.4.1) Fluorescence was measured at an excitation wavelength of 340 nm and an emission wavelength of 460 nm. The results of the samples were referred to a standard curve of GSH.

2.2.7.2. Determination Of Protein Carbonyl Content:-

Liver tissue (100-200 mg) was homogenized (1:5 w/v) in 0.25 mol/L Tris, 0.2 mol/L sucrose and 5 mmol/L 1,4-dithiothreitol cold buffer, pH 7.4.

- Then, samples were centrifuged at 10.000 x g for 30 minutes at 4ºC.
- Liver homogenates were incubated with 4 volumes of 10 mmol/L DNPH for 1 hour in dark at room temperature. The samples were vortexed every 15 minutes.
- In parallel, the corresponding blank was prepared for each sample in the same order but the liver homogenates were incubated with 4 volumes of 2 mol/L HCL.
- Both samples and blanks were precipitated with the same volume of 20% TCA (final TCA concentration 10%).
- Samples were incubated 10 minutes on ice
- Samples were centrifuged at 10.500 x g for 1 minute at 4ºC.
- The pellets were washed three times in 1 mL of a mix of ethyl acetate and 96% ethanol (1:1).
- Pellets were resuspended in 500 µL of 6 M guanidine, pH 2.5.

- Protein oxidation of liver homogenates was measured as carbonyl groups content according to the method of Richert (Richert etal., 2002).
- Absorbance was measured at 360 nm and carbonyl content was expressed as nmol/mg protein using the extinction coefficient 22.000 nmol/L/cm. Protein content in liver homogenates was measured with the Bradford reagent.

2.2.8. Determination Of APAP-Protein Adducts:-

Analysis of APAP covalently bound to proteins in liver was measured by initial protease treatment of liver homogenates.

- 100 mg of liver tissue were placed into 1 mL of ice cold PBS containing 8.0 g/L NaCl, 0.2 g/L KCl, 1.44 g/L Na_2PO_4 and 0.24 g/L KH_2PO_4 and adjusted to pH 7.2.
- Samples were homogenized and the homogenates were centrifuged at 10.000 x g for 30 minutes at 4ºC.
- The supernatants were removed and stored at -80°C.

Samples were sent to Drs Lynda Letzig and Laura P. James in the Section of Clinical Pharmacology and Toxicology, Arkansas Children´s Hospital, Little Rock, USA for analysis of APAP-cysteine adducts by high performance liquid chromatography-electrochemical (HPLC-EC) as described in Kenneth et al., 2002.

2.2.9. Analysis of Protein Expression:-

2.2.9.1. Preparation of Protein extracts:-

- Frozen livers were homogenized in 16 volumes (w/v) of ice-cold lysis buffer containing 50 mmol/L Tris-HCl, 1% Triton X-100, 2 mmol/L EGTA, 10 mmol/L EDTA acid, 100 mmol/L NaF, 1 mmol/L Na_4P_2O7, 2 mmol/L Na_3VO_4, 100 µg/ml PMSF, 1 µg/ml aprotinin, 1 µg/ml pepstatin A and 1 µg/ml leupeptin.
- Liver was homogenized in the same lysis buffer using the Brinkman PT 10/35 Polytron.
- Extracts were kept ice-cold at all times.

- Liver extracts were cleared by microcentrifugation at 40.000 x g for 20 minutes at 4ºC. The supernatant was aliquoted and stored at -80ºC.

2.2.9.2 - Extraction of nuclear and cytosolic proteins:-

- Livers were resuspended at 4ºC in 10 mmol/L HEPES-KOH, pH 7.9, 1.5 mmol/L $MgCl_2$, 10 mmol/L KCl, 0.5 mmol/L DTT, 0.2 mmol/L PMSF, 0.75 µg/ml leupeptin and 0.75 µg/ml aprotinin (Buffer A).
- Then, samples were allowed to swell on ice for 10 minutes.
- Samples were vortexed for 10 seconds at maximum speed.
- Samples were centrifuged at 1.500 x g for 3 minutes at 4ºC.
- The supernatant containing the cytosolic fraction was stored at -80ºC.
- Pellet was re-suspended in cold buffer B (20 mmol/L HEPES-KOH, pH 7.9, 25% glycerol, 420 mmol/L NaCl, 1.5 mmol/L MgCl2, 0.2 mmol/L EDTA, 0.5 mmol/L DTT, 0.2 mmol/L PMSF, 0.75 µg/ml leupeptin and 0.75 µg/ml aprotinin) and rotate at 4ºC in the cold room for 20 minutes.
- Cellular debris was removed by centrifugation at 15.700 x g for 10 minutes at 4ºC and the nuclear supernatant fraction was stored at – 80ºC.

The analysis of protein expression was performed by western blot as described in 2.2.7.4 section.

2.2.10. Analysis of gene expression by Quantitative Real-time PCR.

Total RNA extraction from liver samples was performed with Trizol. Total RNA was reverse transcribed using the SuperScriptTM III First-Strand Synthesis System for qPCR following manufacturer¨s indications (Invitrogen). qPCR was performed with an ABI 7900 sequence detector using the SyBr Green method and d(N)6 random hexamer with the primers indicated in Table 2. Primer-probe sets for mouse PTP1B, TNFα, IL6 and IL1β were purchased as predesigned TaqMan gene expression assays (Applied Biosystems).

Gene Product	Forward Primer	Reverse Primer
NQO1	5'-GGTAGCGGCTCCATGTACTC-3'	5'-CATCCTTCCAGGATCTGCAT-3'
GPx	5'-GGACTACACCGAGATGAACG-3'	5'-GATGTACTTGGGGTCGGTCA-3'
HO-1	5'-CACAGATGGCGTCACTTCGTC-3'	5'-GTGAGGACCCACTGGAGGAG-3'
GCLM	5'-TTACCGAGGCTACGTGTCAGAC-3'	5'-TATCGATGGTCAGGTCGATGTC-3'
GCLC	5'-AATCAGCCCCGATTTAGTCAGG-3'	5'-CCAGCTGTGCAACTCCAAGGAC-3'
B-actin	5'-TCCTTCCTGGGCATGGAG-3'	5'-AGGAGGAGCAATGATCTTGATCTT-3'

Table 5. Primers used in qPCR reactions.

2.2.11. Data Analysis.

Data are expressed as mean ± SEM. Comparisons between groups were made using one-way ANOVA. For qRT-PCR a two way ANOVA test followed by a Bonferroni's post-test has been used. Differences were considered to be statistically significant at $P<0.05$. The data were analyzed by the SPSS for Windows statistical package, version 9.0.1.

RESULTS

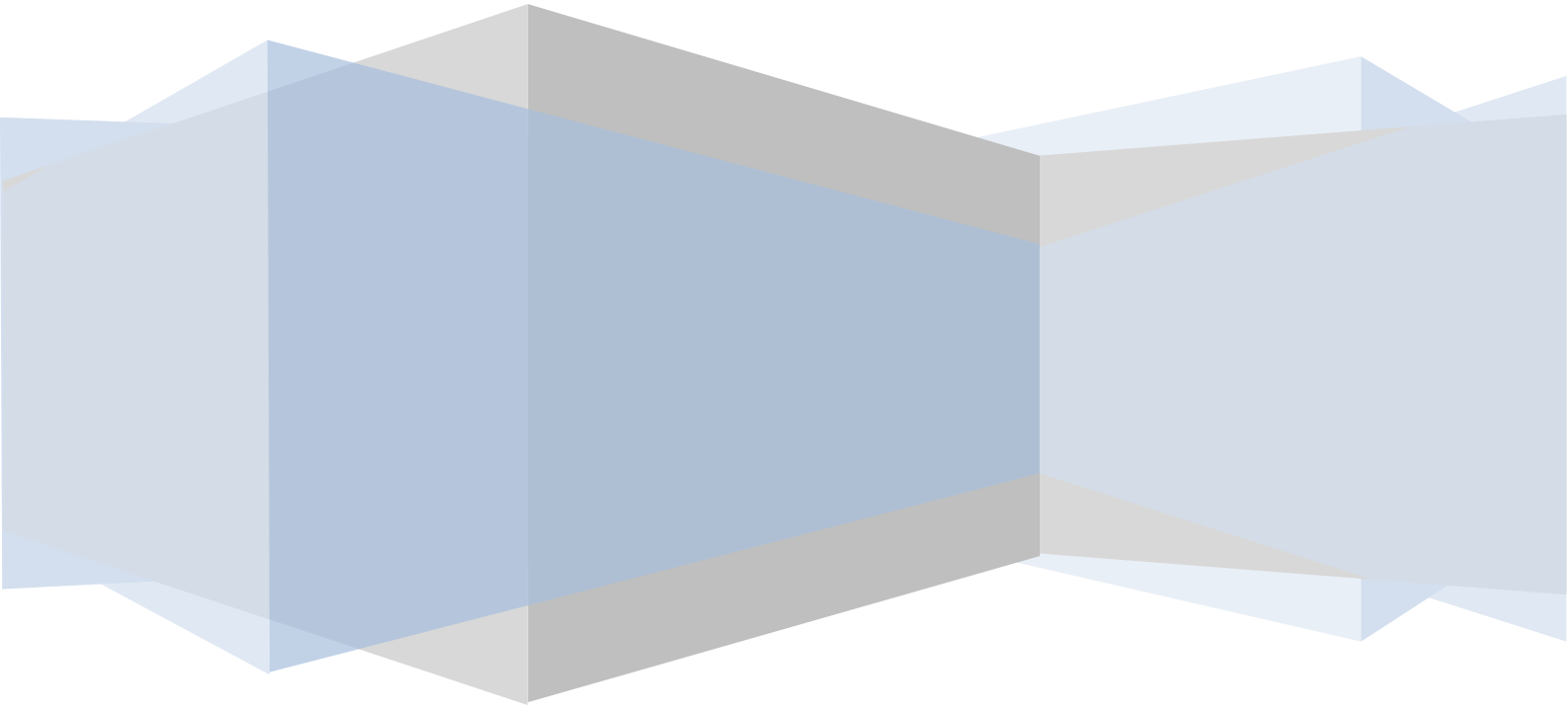

1. ROLE OF PTP1B IN APAP-INDUCED ACUTE LIVER FAILURE:-

1.1 Induction of cell death paralleled PTP1B expression during APAP-induced liver injury in human liver and APAP-treated human hepatocytes.

First, we investigated if PTP1B protein levels were modulated during APAP-induced human liver injury. For this goal, we analyzed PTP1B expression by immunohistochemistry in liver sections of individuals intoxicated with APAP. These samples were obtained from Dr Kenneth J. Simpson in the division of Clinical and Surgical Sciences, University of Edinburgh, Edinburgh EH164TJ, United Kingdom.

Characteristics of five patients transplanted following APAP overdose are shown in Table 1. Figure 6A shows elevated PTP1B expression in surviving hepatocytes, mainly in the areas surrounding the central veins (middle panel), during APAP intoxication as compared to a normal liver (left panel). In a more severe intoxication (right panel), where is difficult to detect surviving hepatocytes, strong staining was observed in precipitated proteins released from dead cells and not yet cleared (Characteristics of five patients transplanted following APAP overdose are shown in table 6).

In agreement with this, PTP1B protein content was up-regulated in human primary hepatocytes and in the human liver cell line CHL treated with APAP in a dose and time-dependent manner (Figures 6B, 6C, Figure 7). Elevated PTP1B expression was detected at 8 h after APAP addition whereas cells with death morphology were visualized at 16 h.

Patient Number	Age (years)	Sex	Acetamino phen dose	Staggered overdose	Admission Alanine aminotran sferase (IU/L)	Admission Creatinine (umol/L)	Prothromb in time (seconds)	Overdose to Transplant (hours)
1	42	Female	32g	No	12755	218	77	212
2	43	Female	NA*	NA	7106	192	182	NA
3	48	Male	16g	Yes	20800	124	96	NA
4	45	Female	10g	No	1097	142	69	176
5	36	Male	50g	No	9847	152	87	70

Table 6. Demographic and biochemical characteristics of patients with APAP hepatotoxicity. A= not available; Normal range alanine aminotransferase 10-50IU/L, creatinine 60 120 umol/L, prothrombin time 10.2-12.7 secons.

Moreover, in APAP-treated human hepatocytes in a dose-dependent manner for 24h, activation of c-Jun N-terminal kinases 1/2 (JNK) and p38 mitogen-activated protein kinase (p38 MAPK) and inhibition of Akt phosphorylation correlated with decreased levels of the anti-apoptotic Bcl2 family members BclxL

and Mcl1 (myeloid cell leukemia sequence 1) and with detection of the active caspase-3 fragment (Figure 6D).

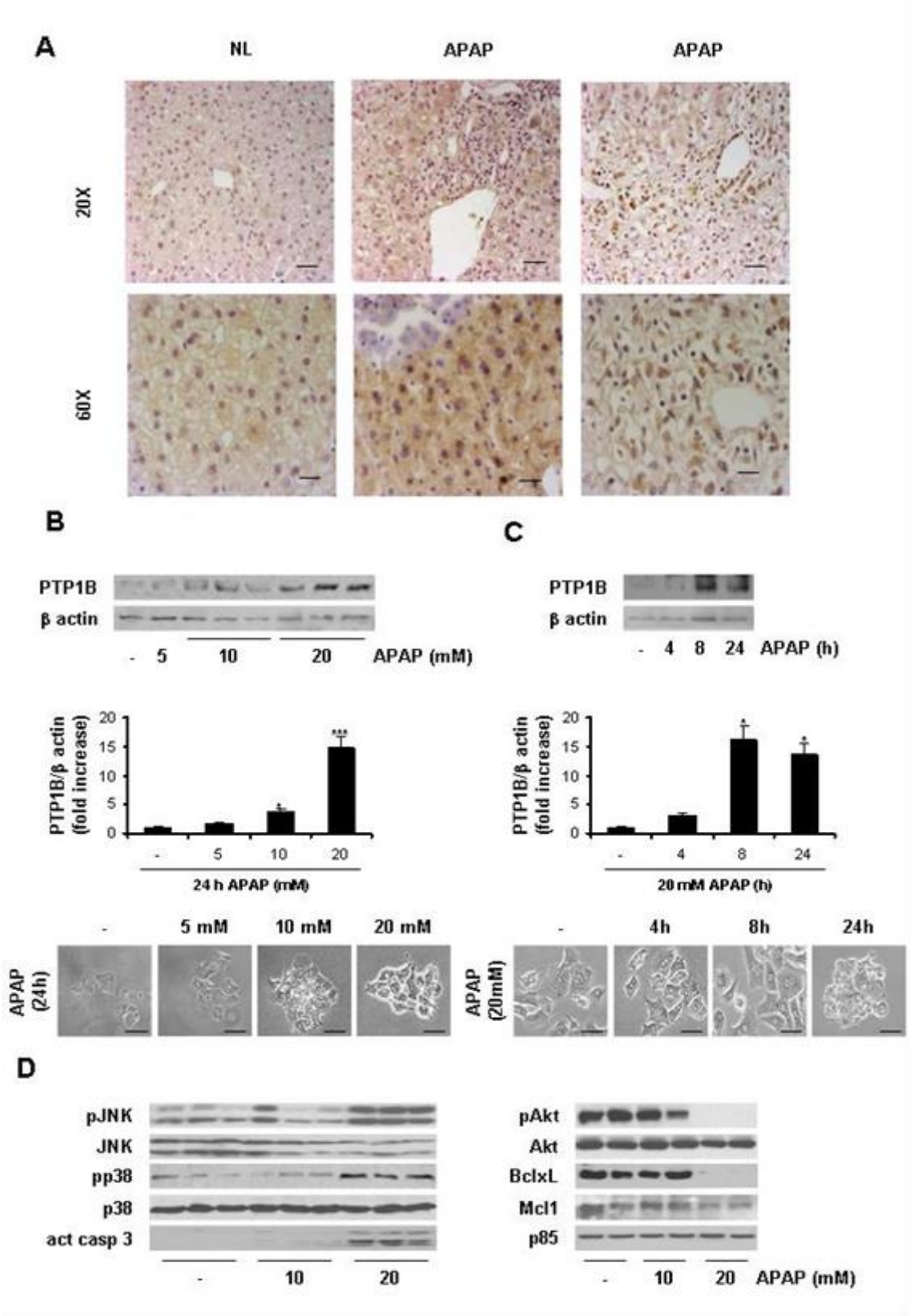

Figure 6. PTP1B expression is increased during APAP-induced liver injury and in human primary hepatocytes treated with APAP. A. Representative anti-PTP1B immunostaining of liver biopsy sections from patients with histologically normal liver

(NL) or with an APAP overdose (APAP) (n=7). Bar scale 50 µm. **B.** Human primary hepatocytes were treated with various doses of APAP (5-20 mM) for 24 h. Total cell lysates were analyzed by Western blot with the corresponding antibodies against PTP1B and b actin as a loading control. Autoradiograms corresponding were quantitated by scanning densitometry. Results are means ± SEM. *P<0.05 and ***P<0.001 APAP-treated versus non-treated cells. Representative phase-contrast microscopy images after APAP treatment. Bar scale 100 µm. **C.** Human primary hepatocytes were treated with 20 mM APAP for various time-periods (4, 8 and 24 h). Total cell lysates were analyzed by Western blot with the corresponding antibodies against PTP1B and b actin as a loading control. Autoradiograms corresponding were quantitated by scanning densitometry. Results are means ± SEM. *P<0.05 APAP-treated versus non-treated cells. Representative phase-contrast microscopy images after APAP treatment. Bar scale 100 µm. **D**. Human primary hepatocytes were treated with various doses of APAP for 24 h and total cell lysates were analyzed by Western blot with the antibodies against phospho-JNK1/2, JNK1/2, phospho-p38, p38, active caspase-3, phospho-Akt, Akt, BclxL, Mcl1 and p85-PI3K as a loading control. *P<0.05 and ***P<0.001 APAP-treated versus non-treated cells (n=3 independent experiments).

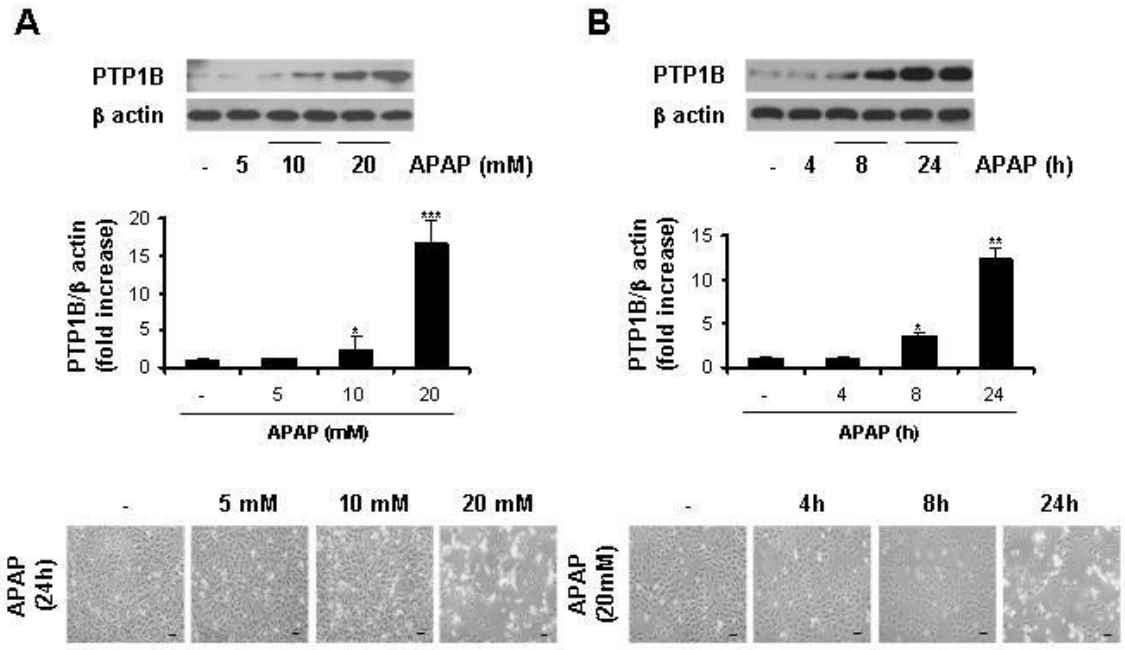

Figure7. PTP1B expression is increased in CHL liver cells treated with APAP. A. CHL human liver cells were treated with various doses of APAP for 24 h or with 20 mM APAP for various time-periods. B. (upper panels) Total cell lysates were analyzed by western blot with the corresponding antibodies against PTP1B and b actin as a loading control. (lower panels) Representative phase-contrast microscopy images after APAP treatment. Bar scale 100 µm.

1.2 PTP1B-deficient mouse hepatocytes are protected against APAP-induced cell death.

As occurred in human primary hepatocytes (Figure 6C), PTP1B was up-regulated in primary hepatocytes from wild-type ($PTP1B^{+/+}$) mice treated with APAP (10 mM) at 8 h whereas maximal cell death was observed at 16 h (Figure 8A).

Next, we explored the role of PTP1B in APAP-induced hepatotoxicity in mouse primary hepatocytes. Wild-type and $PTP1B^{-/-}$ primary hepatocytes were treated

with 5 and 10 mM APAP for 16 h and cell death was analyzed. Phase-contrast microscopy revealed many APAP-treated wild-type primary hepatocytes with death cell morphology.

By contrast, most of PTP1B$^{-/-}$ primary hepatocytes remained attached to the plate and only few cells displayed a death phenotype (Figure 8B).

Quantification analysis of crystal violet staining and released LDH activity showed that primary PTP1B$^{-/-}$ hepatocytes were more protected against APAP cytotoxicity. Analysis of nuclear morphology in cells treated with APAP for 16 h confirmed an increased incidence of condensed and/or fragmented nuclei in wild-type primary hepatocytes compared to PTP1B$^{-/-}$ cells (Figure 8C). Also, the percentage of hypodiploid (sub G0/G1) population increased in wild-type, but not in PTP1B$^{-/-}$ primary hepatocytes, as compared to their respective untreated cells.

Apoptosis in APAP-treated wild-type primary hepatocytes correlated with release of cytochrome C from mitochondria as revealed by the decrease in its content in the mitochondrial compartment and with the subsequent activation of caspase-3 (Figure 8D). These effects were significantly ameliorated in PTP1B$^{-/-}$ primary hepatocytes.

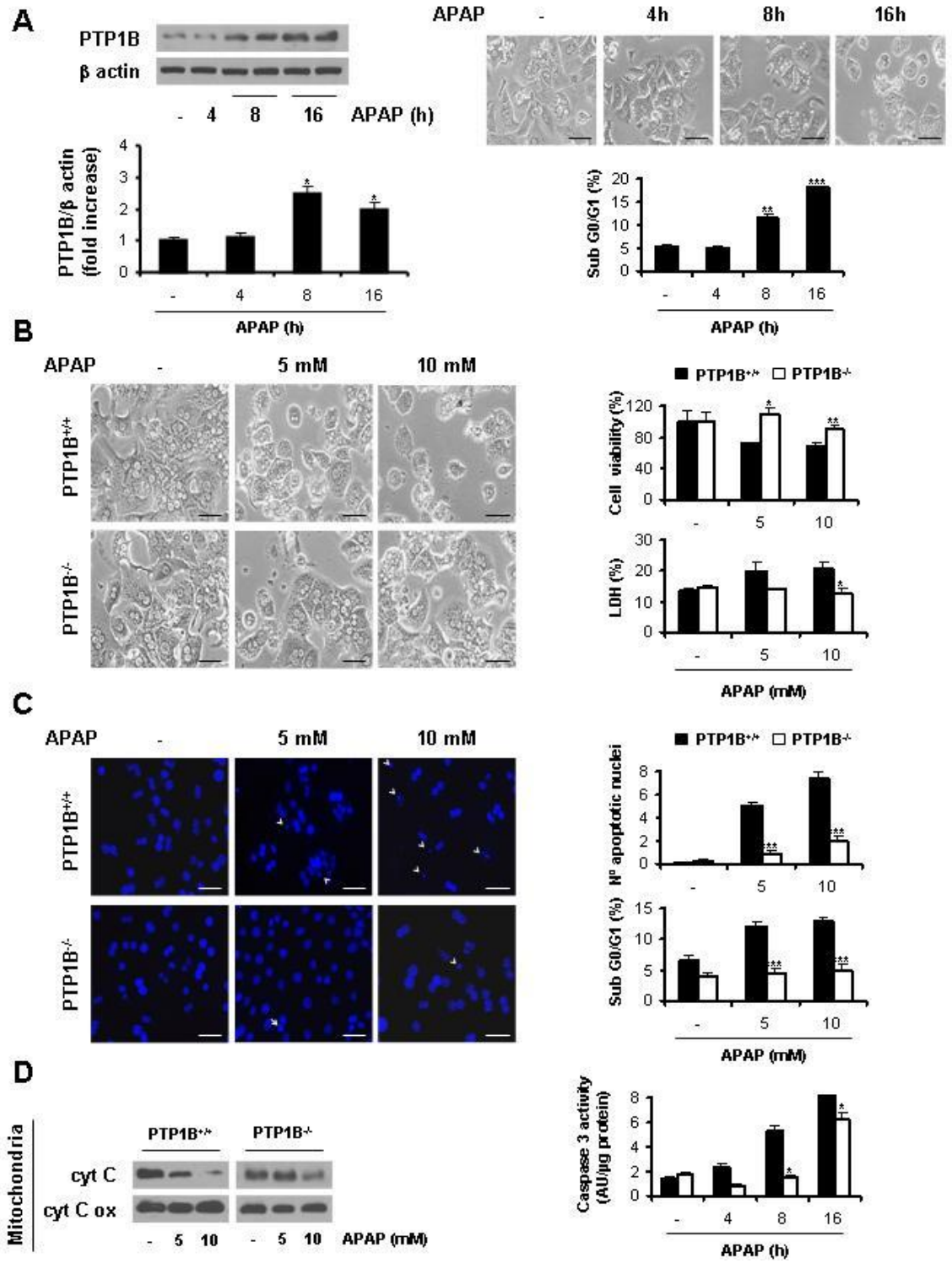

Figure 8 PTP1B-deficient hepatocytes are protected against APAP-induced cell death. A. (left panel) Wild-type ($PTP1B^{+/+}$) mouse primary hepatocytes were treated with 10 mM APAP for various time-periods. The expression of PTP1B was analyzed by Western blot. *P<0.05 APAP-treated versus non-treated cells (n=3 independent experiments). (right panel) Representative phase-contrast microscopy images and analysis of the percentage of sub G0/G1 cell population by flow cytometry. **B.** $PTP1B^{+/+}$ and $PTP1B^{-/-}$ primary hepatocytes were treated with APAP (5 and 10 mM) for 16 h. (left panel) Representative phase-contrast microscopy images. Bar scale 100 µm. (right panel) Cellular viability and released LDH activity. **C**. $PTP1B^{+/+}$ and $PTP1B^{-/-}$ primary hepatocytes were treated with APAP (5 and 10 mM) for 16 h. (left panel) Representative nuclear morphology images after DAPI staining and analysis by fluorescence microscopy. (right panel) Quantification of apoptotic nuclei. Percentage of

sub G0/G1 cell population analyzed by flow cytometry. **D**. (left panel) PTP1B$^{+/+}$ and PTP1B$^{-/-}$ primary hepatocytes were treated with APAP (5 and 10 mM) for 16 h. Western blot with anti-cytochrome C and anti-cytochrome C oxidase antibodies in mitochondrial extracts. (right panel) PTP1B$^{+/+}$ and PTP1B$^{-/-}$ primary hepatocytes were treated with APAP (10 mM) for various time-periods. Analysis of caspase-3 enzymatic activity. *P<0.05, **P<0.01 and ***P<0.001 PTP1B$^{-/-}$ versus PTP1B$^{+/+}$ (n=4 independent experiments.

1.3 PTP1B-deficient mouse immortalized hepatocytes are protected against APAP-induced cell death.

Immortalized PTP1B$^{+/+}$ hepatocytes were treated with APAP (1 mM) for different time periodes. PTP1B was up-regulated in PTP1B$^{+/+}$ immortalized hepatocytes treated with APAP (1 mM) at 8 h (maximal cell death was observed later at 16 h).

Phase-contrast microscopy revealed many APAP-treated wild-type hepatocytes with death cell morphology. But, most of PTP1B$^{-/-}$ immortalized hepatocytes remained attached to the plate and only few cells displayed a death phenotype (Figure 9A). Quantification analysis of crystal violet staining and released LDH activity showed that PTP1B-/- hepatocytes were more protected against APAP cytotoxicity. Analysis of nuclear morphology in cells treated with 1 mM APAP for 16 h confirmed an increased incidence of condensed and/or fragmented nuclei in wild-type hepatocytes compared to PTP1B-/- cells (Figure 4B). Also, the percentage of hypodiploid (sub G0/G1) population increased in wild-type, but not in PTP1B$^{-/-}$ hepatocytes, as compared to their respective untreated cells. In agreement with previous reports (Wiger et al., 1997), APAP arrested both kinds of hepatocytes in S phase, but this effect was significantly reduced in PTP1B-deficient cells (Figure 10). Apoptosis in APAP-treated wild-type hepatocytes correlated with release of cytochrome C from mitochondria (Figure 4C) and subsequent activation of caspase-3 at 8 (Figure 11) and 16 h (Figure 2C), this effect being ameliorated in PTP1B-/- hepatocytes. (Figure 9).

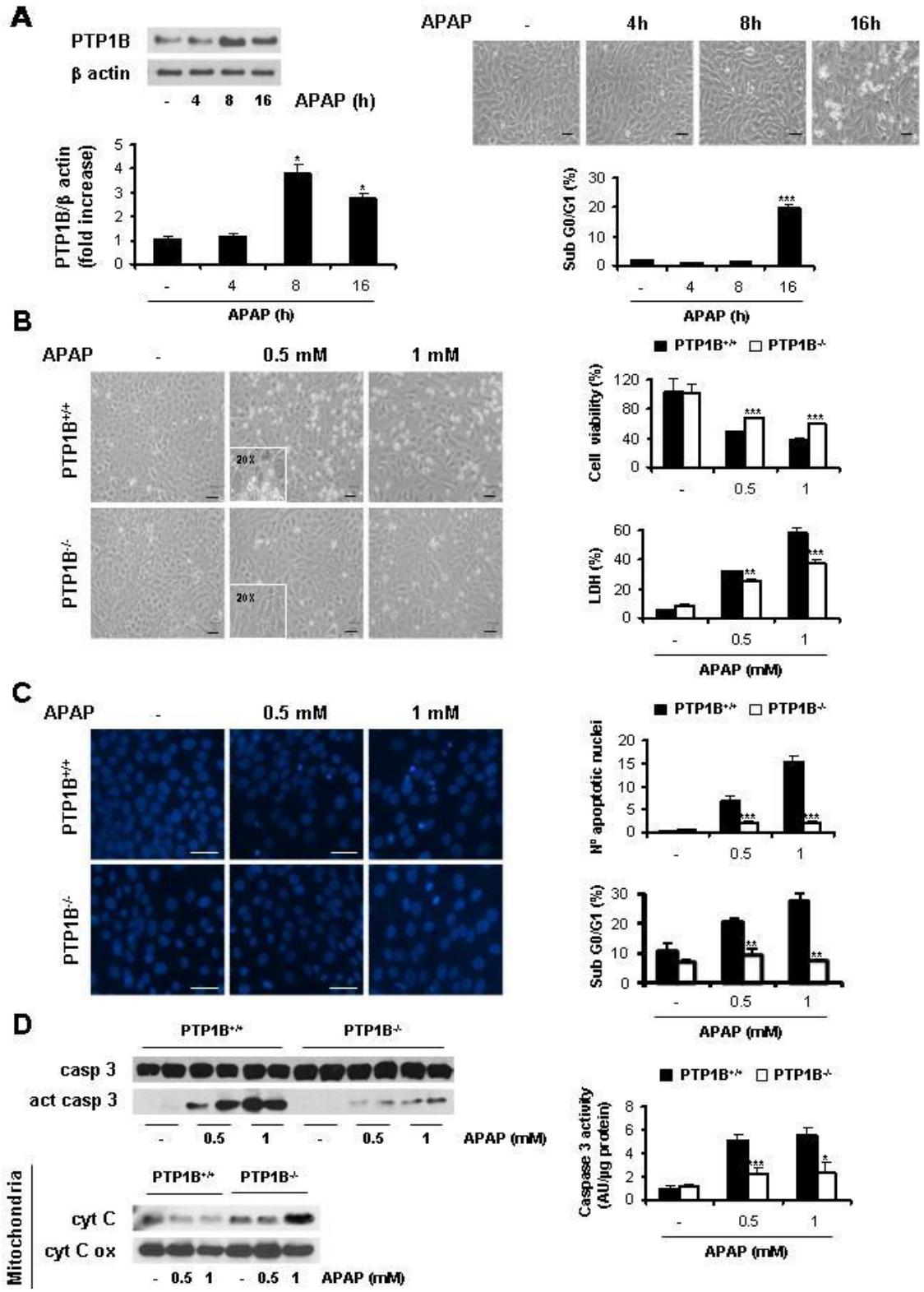

Figure 9. Immortalized PTP1B-deficient hepatocytes are protected against APAP-induced cell death. A. (left panel) Wild-type (PTP1B+/+) immortalized hepatocytes were treated with 1 mM APAP for various time-periods. The expression of PTP1B was analyzed by western blot. *P<0.05 APAP-treated vs. non-treated cells (n=3 independent experiments). (right panel) Representative phase-contrast microscopy images. Percentage of Sub G0/G1 cell population analyzed by flow cytometry. **B.** PTP1B+/+ and PTP1B-/- hepatocytes were treated with various doses of APAP for 16 h. (left panel) Representative phase-contrast microscopy images. (right panel) Cellular viability and released LDH activity. **C**. PTP1B+/+ and PTP1B-/- hepatocytes were treated with various doses of APAP for 16 h. (left panel) Representative nuclear morphology images after DAPI stainning and analysis by fluorescence microscopy. (right panel) Quantification of

fragmented nuclei and percentage of Sub G0/G1 cell population by flow cytometry. **D**. PTP1B+/+ and PTP1B-/- hepatocytes were treated with various doses of APAP for 16 h. (left panel) Western blot of cleavage caspase-3 in total lysates and cytochrome C in mitochondrial extracts. (right panel) Analysis of caspase-3 enzymatic activity. *P<0.05, **P<0.01 and ***P<0.005 PTP1B-/- vs. PTP1B+/+ (n=4 independent experiments). Bar scale 50 µm.

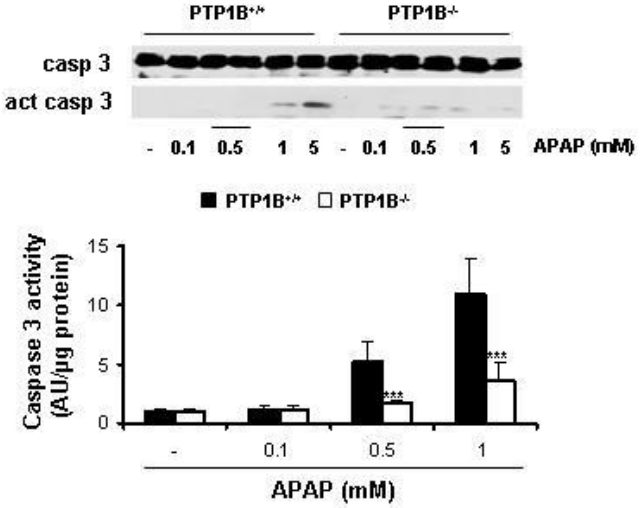

Figure 10. PTP1B-deficient hepatocytes are protected against APAP-induced S phase arrest. PTP1B+/+ and PTP1B-/- hepatocytes were treated with various doses of APAP for 16 h. A. S phase cell population percentage measured by flow cytometer. *P<0.05, **P<0.01 and ***P<0.005 PTP1B-/- vs. PTP1B+/+ (n=4 independent experiments).

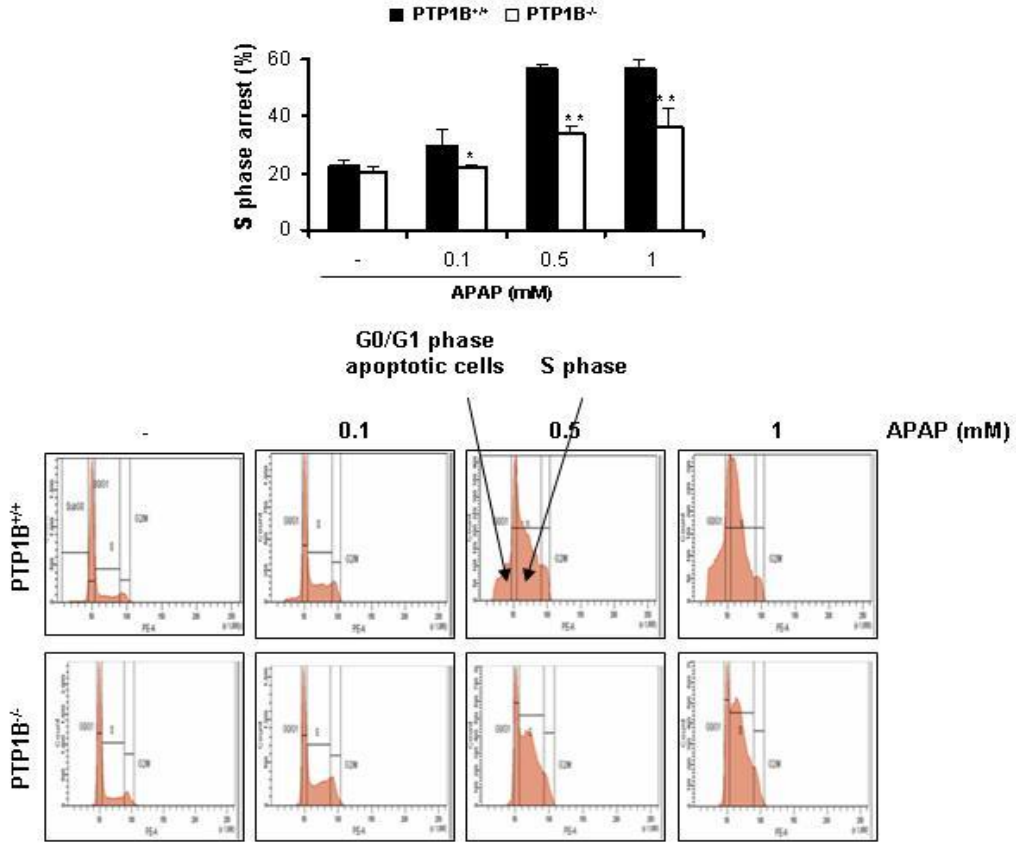

Figure 11. PTP1B-deficient hepatocytes are protected against APAP-induced caspase-3 activation. PTP1B+/+ and PTP1B-/- hepatocytes were treated with various doses of APAP for 8 h. A. (upper panel) Analysis of total cell lysates by western blot. (lower panel) Caspase-3 enzymatic activity. *P<0.05 and ***P<0.005 PTP1B-/- vs. PTP1B+/+ (n=4 independent experiments).

1.4 Effect of PTP1B deficiency on the activation of stress and survival-mediated signalling pathways in mouse primary and immortalized hepatocytes.

Next, we analyzed stress-mediated and survival signalling in primary hepatocytes from wild-type and PTP1B$^{-/-}$ mice. JNK and p38 MAPK phosphorylation was detected at 8 h in primary hepatocytes treated with 10 mM APAP, this response being ameliorated in PTP1B$^{-/-}$ cells (Figure 12A). Survival signalling monitored by IGFIR phosphorylation, levels of insulin receptor substrates 1 (IRS1) and 2 (IRS2) and Akt phosphorylation, was reduced in APAP-treated wild-type primary hepatocytes, but it was preserved in PTP1B$^{-/-}$ cells.

Consistently, anti-apoptotic markers BclxL and Mcl1 were decreased in wild-type primary hepatocytes treated with APAP, but again, this effect was reduced in PTP1B$^{-/-}$ hepatocytes.

As observed in human and primary hepatocytes, APAP increased PTP1B expression in immortalized mouse hepatocytes. With regard to stress-mediated signaling, both JNK and p38 MAPK phosphorylation increased in APAP-treated wild-type hepatocytes in a dose dependent-manner, these effects being ameliorated in PTP1B$^{-/-}$ cells. Survival signaling monitored by IGFIR phosphorylation, levels of insulin receptor substrates 1 (IRS1) and 2 (IRS2) and Akt phosphorylation, was significantly reduced in APAP-treated wild-type hepatocytes, but it was preserved in PTP1B$^{-/-}$ cells treated with APAP. Consistently, anti-apoptotic markers BclxL and Mcl1 were decreased in wild-type hepatocytes treated with APAP, but again, this effect was reduced in PTP1B$^{-/-}$ hepatocytes.

In order to exclude the possibility that the protection elicited by PTP1B deficiency against APAP-induced cell death could be secondary to compensatory adaptations in immortalized cell lines, we established siRNA assays. As similar responses have been found in APAP-treated wild-type and PTP1B$^{-/-}$ primary and immortalized hepatocytes (Figure 12A, 12B), we used immortalized cell lines to conduct siRNA assays. Reduction of PTP1B expression in wild-type immortalized hepatocytes decreased APAP-induced JNK phosphorylation and the levels of the active caspase-3 fragment (Figure 12C). Silencing of PTP1B also maintained IGFIR tyrosine phosphorylation, IRS1 and IRS2 expression, Akt phosphorylation and abolished down-regulation of BclxL upon APAP treatment.

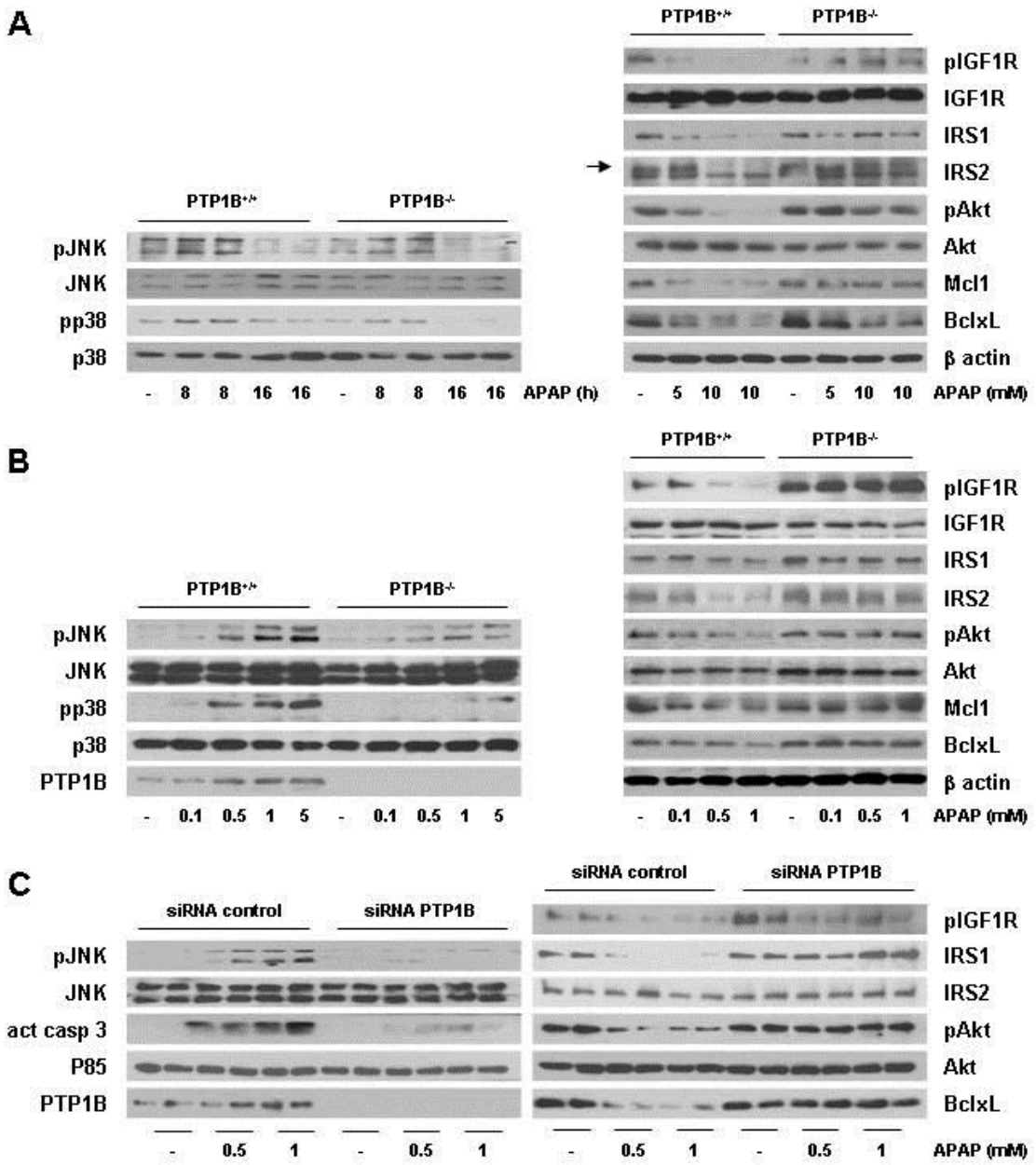

Figure 12. Effect of PTP1B deficiency in stress and survival signaling in hepatocytes. A. (left panel) PTP1B$^{+/+}$ and PTP1B$^{-/-}$ mouse primary hepatocytes were treated with APAP (10 mM) for various time periods. Total cell lysates were analyzed by Western blot with the antibodies against phospho-JNK1/2, JNK1/2, phospho-p38 MAPK and p38 MAPK. Representative autoradiograms corresponding to three independent experiments are shown. (right panel) PTP1B$^{+/+}$ and PTP1B$^{-/-}$ mouse primary hepatocytes were treated with APAP (5 and 10 mM) for 16 h. Total cell lysates were analyzed by Western blot with the antibodies against phospho-IGFIR, IGFIR, IRS1, IRS2, phospho-Akt, Akt, BclxL, Mcl1 and b actin as a loading control. Representative autoradiograms corresponding to three independent experiments are shown. **B.** PTP1B$^{+/+}$ and PTP1B$^{-/-}$ immortalized hepatocytes were treated with various doses of APAP for 16 h. Total cell lysates were analyzed by Western blot with the indicated antibodies. Representative autoradiograms corresponding to three independent experiments are shown. **C.** Immortalized PTP1B$^{+/+}$ hepatocytes transfected with 10 nM of control or PTP1B siRNA for 48 h were further treated with various doses of APAP for 16 h. Total cell lysates were analyzed by Western blot with the indicated antibodies. Representative autoradiograms corresponding to three independent experiments are shown.

1.5 PTP1B deficiency protects mouse hepatocytes against GSH depletion and elevation of ROS: prolonged Nrf2 nuclear accumulation

In the liver, Cyp2e1 converts APAP to NAPQI that rapidly depletes GSH, and therefore the degree of GSH consumption is a biomarker for APAP bioactivation (Kon et al., 2004). Since the expression of Cyp2e1 did not change in primary and immortalized hepatocytes from both genotypes of mice (Figure 13), we used immortalized cells for further experiments.

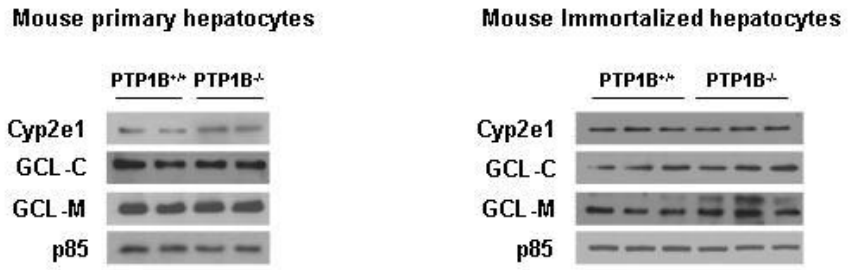

Figure 13. Basal expression of Cyp2e1, GCL-C and GCL-M in mouse primary and immortalized hepatocytes. Whole cell lysates from PTP1B$^{+/+}$ and PTP1B$^{-/-}$ mouse primary (left panel) and immortalized (right panel) hepatocytes were analyzed by western blot with the indicated antibodies. Representative autoradiograms are shown.

APAP-induced depletion of GSH was observed in wild-type immortalized hepatocytes after 4h treatment albeit this effect was absent in PTP1B$^{-/-}$ cells (Figure 14A). Likewise, a significant elevation of ROS (DCFH) was detected in APAP-treated wild type hepatocytes for 6 h, but not in PTP1B$^{-/-}$ cells.

Next, we measured the enzymatic activity of detoxifying enzymes glutathione peroxidase (GPx) and glutathione reductase (GR). As depicted (in Figure 14A), GPx activity increased in APAP-treated wild-type hepatocytes as compared to untreated controls as expected for an anti-oxidant defense. Conversely, GR was not increased by APAP suggesting impairment in replenish of GSH stores.

However, PTP1B$^{-/-}$ hepatocytes did not activate the GPx/GR system in response to APAP probably due to an insufficient threshold to trigger activation of detoxifying enzymes under these experimental conditions.

To inspect at molecular level the reasons for protection of PTP1B deficiency against APAP-induced oxidative stress, we analyzed the dynamics of Nrf2 nuclear accumulation. Since we did not observe differences in Nrf2 serine phosphorylation that leads to the dissociation of Nrf2 from its inhibitor Keap1 at early time-periods upon APAP treatment (Figure 15A), we studied nuclear accumulation of Nrf2 at later time-periods.

Both western blot and immunofluorescence analysis revealed that Nrf2 was maximally accumulated in the nucleus at 8h after APAP treatment in both

kinds of immortalized hepatocytes, but it was retained for up to 16 h exclusively in PTP1B$^{-/-}$ cells (Figure 14B). Tyrosine phosphorylation of Nrf2 results in its nuclear export, ubiquitination and degradation in the cytosol (Niture et al., 2011). As depicted in Figure 14C, in wild-type hepatocytes maximal Nrf2 tyrosine phosphorylation was observed at 8 h after APAP stimulation and total Nrf2 protein content decreased at 16h. In PTP1B$^{-/-}$ cells, maximal Nrf2 tyrosine phosphorylation was observed at 16 h, time at which total Nrf2 levels were maintained as in non-treated cells. Nuclear Nrf2 accumulation was accompanied by decreases in cytosolic expression (Figure 15B). These data correlated with a higher increase in the expression of the Nrf2downstream target heme oxygenase-1 (HO-1) in hepatocytes lacking PTP1B. As occurred in immortalized hepatocytes, Nrf2 levels were maintained and the induction of HO-1 was higher in APAP-treated mouse primary PTP1B$^{-/-}$ hepatocytes for 16 h as compared to the wild-type cells.

Next, ubiquitination analysis of Nrf2 was performed in immortalized hepatocytes treated with APAP for 8-24 h either in absence or presence of proteasome inhibitor MG132 (Figure 14D).

In APAP-treated wild-type cells, ubiquitinated Nrf2 was detected at earlier time-period (8 h) compared with PTP1B-/- cells that displayed this response at 16 h, this effect being enhanced when APAP was added in the presence of MG132.

In related experiments, over-expression of PTP1B in HEK 293T cells inhibited antioxidant response element (ARE)-mediated luciferase expression after treatment with APAP for 16 h (Figure 14E), reinforcing the involvement of this phosphatase in Nrf2-mediated antioxidant response to APAP.

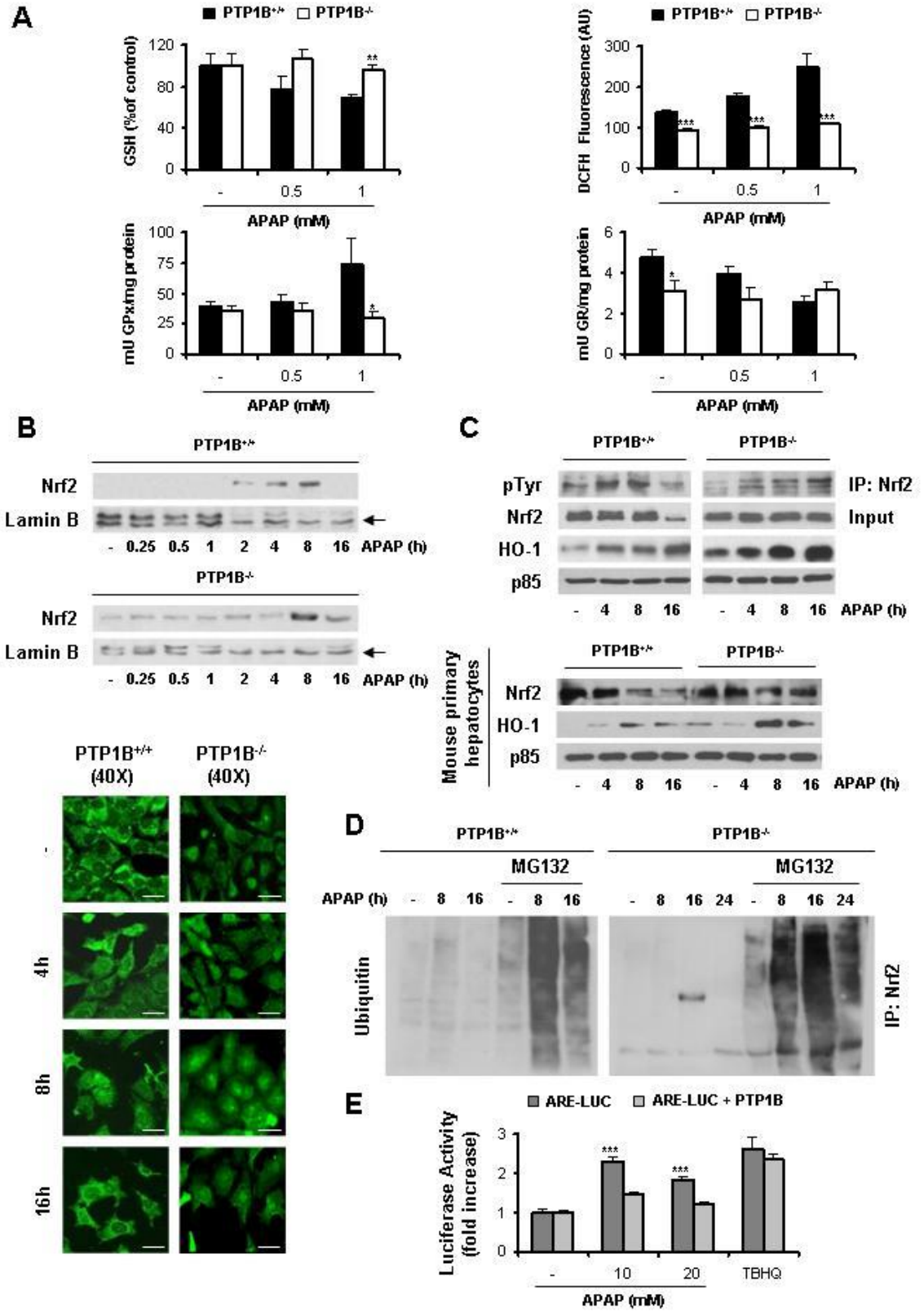

Figure 14. PTP1B deficiency protects hepatocytes against GSH depletion and elevation of ROS; effect on nuclear Nrf2 accumulation. PTP1B$^{+/+}$ and PTP1B$^{-/-}$ immortalized hepatocytes were treated with various doses of APAP for different time-periods. **A.** Analysis of GSH content (4 h), ROS levels (6 h) and GPx and GR activity (16 h) in three independent experiments. *P<0.05, **P<0.01 and ***P<0.005 PTP1B$^{-/-}$ versus PTP1B$^{+/+}$ **B**. (upper panel) Analysis of Nrf2 in nuclear cell lysates by Western blot in PTP1B$^{+/+}$ and PTP1B$^{-/-}$ immortalized hepatocytes treated with 1 mM APAP for several time-periods. Representative autoradiograms of 3-4 independent experiments are shown. (lower panel) Representative images

corresponding to the intracellular localization of Nrf2 by immunofluorescence microscopy in PTP1B$^{+/+}$ and PTP1B$^{-/-}$ immortalized hepatocytes treated with 1 mM APAP for several time-periods. Bar scale 50 μm. **C**. (upper panel) PTP1B$^{+/+}$ and PTP1B$^{-/-}$ immortalized hepatocytes were treated with 1 mM APAP for several time-periods. Nrf2 tyrosine phosphorylation was analyzed by inmunoprecipitation with the anti-Nrf2 antibody followed by Western blot with the anti-Tyr(P) antibody. Total Nrf2 and HO-1 was analyzed by Western blot. (lower panel) PTP1B$^{+/+}$ and PTP1B$^{-/-}$ mouse primary hepatocytes were treated with 10 mM APAP for various time-periods. Total Nrf2 and HO-1 was analyzed by Western blot. **D**. PTP1B$^{+/+}$ and PTP1B$^{-/-}$ immortalized hepatocytes were treated with MG132 (10 nM) for 30 min and then with 1 mM APAP for different time-periods. Whole cell lysates were analyzed by inmunoprecipitation with anti-Nrf2 antibody followed by Western blot with anti-ubiquitin antibody. **E**. Antioxidant response element (ARE)-mediated luciferase activity was measured in HEK 293T cells transfected with the expression vectors for pcDNA3.1mNrf2-V5/HisB and 3xARE-Luc combined with myc-PTP1B only in the indicated cases and treated with various doses of APAP for 16 h. tBHQ (15 mM) was used as a positive control (n=3 independent experiments performed in triplicate). ***P<0.005 PTP1B-transfected (Nrf2 ARE+PTP1B) versus empty vector-transfected (Nrf2 ARE) cells.

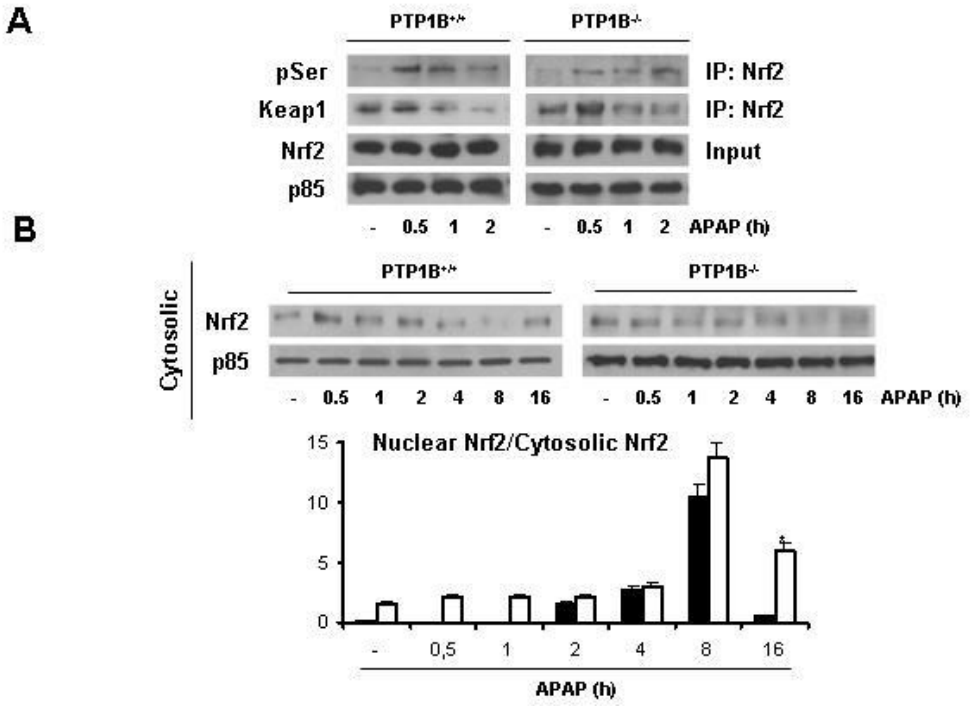

Figure 15. A. Serine phosphorilation of Nrf2 and dissociation with its inhibitor Keap1 at early time-periods upon APAP stimulation in wild-type and PTP1B-/- hepatocytes. PTP1B+/+ and PTP1B-/- hepatocytes were treated with 1 mM APAP for different time periods. Analysis of total cell lysates by inmunoprecipitation and western blot (n=3 independent experiments).

B. Nuclear/cytosolic ratio in wild-type and PTP1B$^{-/-}$ hepatocytes stimulated with APAP. Cells were stimulated with 1 mM APAP for various time-periods. Nrf2 was analyzed in cytosolic extracts by Western blot. The ratio between nuclear/cytosolic Nrf2 was calculated. *P<0.05 PTP1B$^{-/-}$ vs. PTP1B$^{+/+}$.

1.6 PTP1B modulates GSK3β/SKF-mediated Nrf2 nuclear accumulation in APAP-treated mouse hepatocytes.

In response to oxidative stress, GSK3β is activated by phosphorylation at Tyr 216 by an unknown tyrosine kinase. Then, activated GSK3β phosphorylates an activates Src kinase family (SKF) members in the cytosol allowing their nuclear

translocation and subsequent tyrosine phosphorylation of Nrf2 at Tyr 568, ultimately resulting in Nrf2 nuclear exclusion and degradation (Niture et al., 2011; Jain et al., 2007). Thus, we first examined if this molecular mechanism was triggered in APAP-treated hepatocytes. The efficacy of G3K3β siRNA in immortalized hepatocytes is shown in (Figure 16, 18).

Figure 16. Reduction of GSK3β expression by siRNA in PTP1B+/+ mouse hepatocytes. PTP1B$^{+/+}$ cells were transfected with various doses of GSK3β siRNA for 48 h following DharmaFECT General Transfection Protocol and total cell lysates were analyzed by western blot.

Silencing GSK3β in wild-type and PTP1B$^{-/-}$ cells hepatocytes prolonged Nrf2 nuclear accumulation up to 24 h upon APAP treatment similar to our observations in PTP1B$^{-/-}$ cells (Figures 14B, 17).

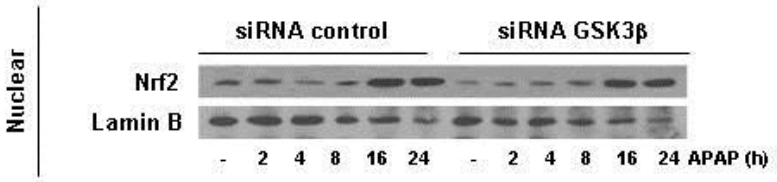

Figure 17. Reduction of GSK3β expression by siRNA in PTP1B$^{-/-}$ mouse hepatocytes. PTP1B$^{-/-}$ cells were transfected 25nm of GSK3β siRNA for 48 h following DharmaFECT General Transfection Protocol and total cell lysates were analyzed by western blot.

Moreover, nuclear translocation of Fyn and Src was also impaired in GSK3β silenced cells, although no effects of nuclear translocation of Yes were observed (results not shown). To obtain further support for the role of SKF in nuclear accumulation of Nrf2 in response to APAP, we treated wild-type hepatocytes with the SKF inhibitor PP2. As shown in Figure 18B, PP2 increased nuclear Nrf2 levels at 2-8 h after APAP treatment. In addition, mouse embryonic fibroblasts (MEFs) deficient in Src, Fyn and Yes (SYF$^{-/-}$) treated with 1 mM APAP showed nuclear Nrf2 accumulation up to 24 h. We next analyzed the effect of PTP1B deficiency on the GSK3β/SKF signaling pathway. In wild-type cells, APAP-induced GSK3β tyrosine phosphorylation was detected at 1 h and peaked at 4 h.

This response was parallel to the re-entry of Fyn and Src into the nucleus (Figure 18C). In PTP1B$^{-/-}$ hepatocytes, maximal GSK3β phosphorylation occurred at 8-16 h after APAP treatment and also paralleled with a latter re-entry of Src and Fyn into the nucleus as compared to wild-type.

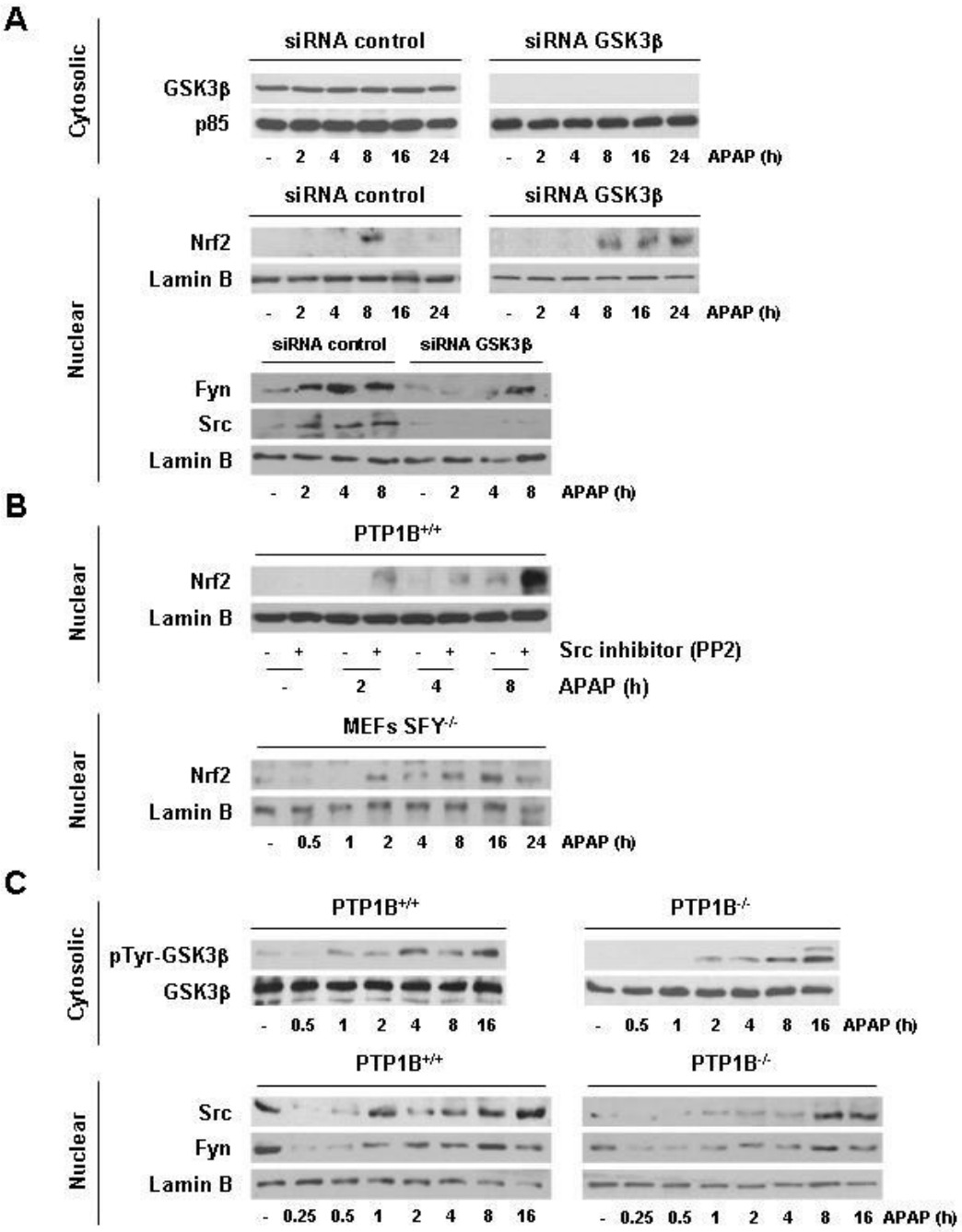

Figure 18. PTP1B modulates GSK3b/Src-Fyn-mediated Nrf2 nuclear accumulation in APAP-treated hepatocytes. A. PTP1B$^{+/+}$ immortalized hepatocytes were transfected with control or GSK3b siRNAs (25 nM) for 48 h followed by stimulation with 1 mM APAP. Nuclear and cytosolic extracts were analyzed by Western blot with antibodies against Nrf2, Fyn and Src. **B**. (upper panel) PTP1B$^{+/+}$ immortalized hepatocytes were treated with PP2 (5 mM) for 30 min following 1 mM APAP for different periods. Nrf2 in nuclear extracts was analyzed by Western blot. (lower panel) SYF$^{-/-}$ MEFs were treated with 1 mM APAP for different periods and Nrf2 was analyzed in nuclear extracts by Western blot. **C**. PTP1B$^{+/+}$ and PTP1B$^{-/-}$ immortalized hepatocytes were treated with 1 mM APAP for different periods. Phosphorylated GSK3β (Tyr 516) was analyzed

in cytosolic extracts by Western blot. Fyn and Src were analyzed in nuclear extracts. Similar results were obtained in 3 independent experiments.

1.7 PTP1B-deficient mice are protected against APAP-induced oxidative stress through the enhancement of Nrf2 nuclear accumulation and IGFIR-mediated survival signalling.

Next, we evaluated liver injury induced by APAP to wild-type and PTP1B$^{-/-}$ mice. Increased survival was observed in PTP1B$^{-/-}$ mice injected with an APAP overdose (300 mg/kg) (Figure 19A). Consistently, serum alanine transaminase (ALT) was seven-fold higher in wild-type mice than in PTP1B$^{-/-}$ mice at 6 h post-injection; these differences were maintained at 24 h (Figure 19B). At this time, necrotic lesions were observed exclusively in livers of wild-type mice (Figure 19C).

PTP1B deficiency also protected against a higher dose of APAP (500 mg/kg) (Figure 20). Next, we analyzed the expression of pro-inflammatory cytokines in livers of both genotypes of mice. At 6 h post APAP injection, elevated IL6 and IL1β mRNA levels were found in livers of wild-type mice, but not in PTP1B$^{-/-}$ animals (Figure 19D). Of note, APAP decreased TNFα mRNA levels in wild-type, but not in PTP1B-deficient mice.

Since hepatic PTP1B expression is modulated by inflammation (Zabolotny et al., 2008), we performed immunohistochemistry analysis of wild-type and PTP1B$^{-/-}$ livers. As shown in (Figure 19E), increased PTP1B staining was found in necrotic lesions of APAP-treated wild-type mice after 6h, particularly in areas surrounding the central veins.

By contrast, not histological signs of liver injury were observed in sections from PTP1B$^{-/-}$ mice. We next determined if reduced sensitivity of PTP1B$^{-/-}$ mice to APAP-induced liver injury was associated with alterations in GSH levels. In livers of both mouse strains, the basal expression of Cyp2e1, both the catalytic and the modifier subunits of γ-glutamyl cysteine ligase (GCL-C and GCL-M) and basal GSH level were comparable (Figure 21).

APAP administration depleted GSH at 3 and 6 h and increased APAP-protein aducts, but these effects being significantly ameliorated in the PTP1B$^{-/-}$ group (Figure 19F). Moreover, protein carbonyl levels, an indicator of tissue oxidative stress, were less elevated in APAP-injected PTP1B$^{-/-}$ mice than in wild-type controls and paralleled with reduced GSH depletion.

As intracellular redox state is chiefly regulated by Nrf2, we examined possible differences in nuclear levels of Nrf2. Nuclear Nrf2 was detected in wild-type mice at 3 and 6 h after APAP treatment (Figure 22A). In PTP1B$^{-/-}$ animals, basal nuclear Nrf2 was detected before APAP administration and increased at 3 and 6 h after injection, where the levels were higher than those of control mice. Similarly, HO-1 induction in response to APAP was higher in PTP1B-/- mice. Next, we analyzed Nrf2 target genes. As shown in Figure 22B, mRNA levels of GPx, HO-1 and GCL-M (γ-glutamyl cysteine ligase modulatory subtunit) significantly increased at 3 h post-APAP injection in livers of PTP1B$^{-/-}$ mice as compared to the wild-type controls and GPx, GCL-C (γ-glutamyl cysteine ligase catalytic subtunit), GCL-M and NQO1 (NAD(P)H quinone oxidoreductase) increased at 6 h.

1.8 Decreased activation of JNK and maintenance of IGFIR/Akt/BclxL survival signaling in APAP-treated PTP1B-deficient mice.

Activation of JNK was detected in APAP-treated wild-type mice at 3 and 6 h post-injection. As expected, this effect decreased in PTP1B$^{-/-}$ mice (Figure 22A). Regarding survival signaling, in wild-type mice phosphorylation of Insulin-like growth factor I receptor (IGFIR) was severely reduced at 6 h post-APAP injection and IRS1 protein levels were down-regulated in parallel with decreased Akt phosphorylation (Figure 22C). Consistently, anti-apoptotic BclxL protein was barely detected at 6 h post-APAP injection. Conversely, APAP-treated PTP1B$^{-/-}$ mice maintained IGFIR and Akt phosphorylation, as well as IRS1 and BclxL protein content to similar levels than those of mice injected with saline.

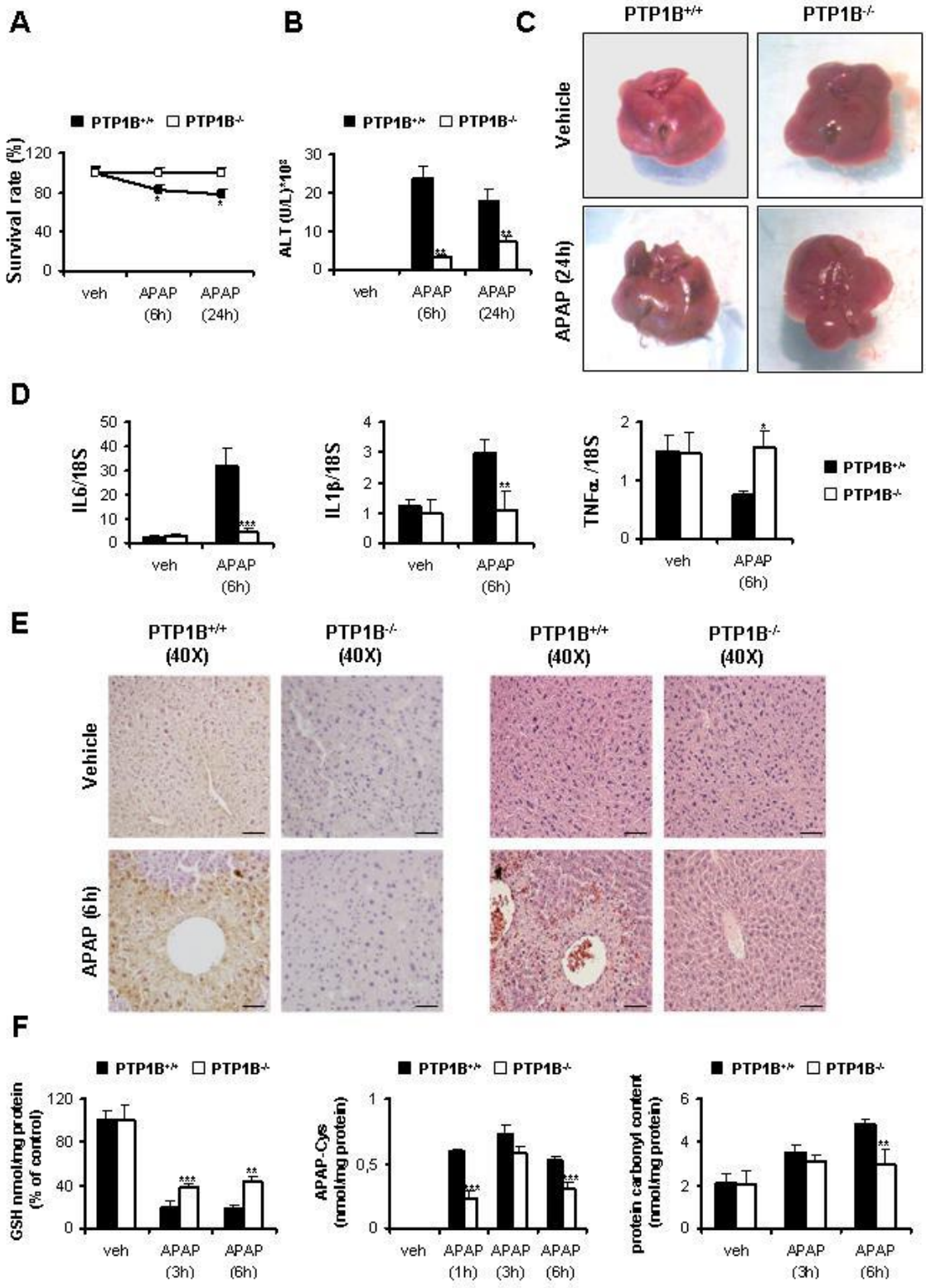

Figure 19. PTP1B-deficient mice are protected against APAP-induced, inflammation oxidative stress and liver damage. PTP1B$^{+/+}$ and PTP1B$^{-/-}$ mice were injected with 300 mg/kg APAP or saline for 6 or 24 h. **A**. Survival curves after 24 h of APAP injection. **B**. Serum transaminase (ALT) activity at 6 and 24 h. **C**. Representative images of whole livers from PTP1B$^{+/+}$ and PTP1B$^{-/-}$ mice 24 h after APAP injection. **D**. IL6, I1b and TNFa mRNA levels were determined by real-time PCR in livers from PTP1B$^{+/+}$ and PTP1B$^{-/-}$ mice at 6 h after APAP injection. **E**. Representative anti-PTP1B immunostaining (left panel) and Hematoxylin & Eosin staining (right panel) in livers from PTP1B$^{+/+}$ and PTP1B$^{-/-}$ mice 6 h after APAP injection. Bar scale 100 µm. **F**. GSH (left panel), APAP-protein aducts (middle panel) and carbonylated protein levels (right panel) were analyzed in livers from PTP1B$^{+/+}$ and PTP1B$^{-/-}$ mice at various time-periods after APAP injection. *P<0.05, **P<0.01 and ***P<0.005 PTP1B$^{-/-}$ versus PTP1B$^{+/+}$ (n= 6-8 mice of each condition).

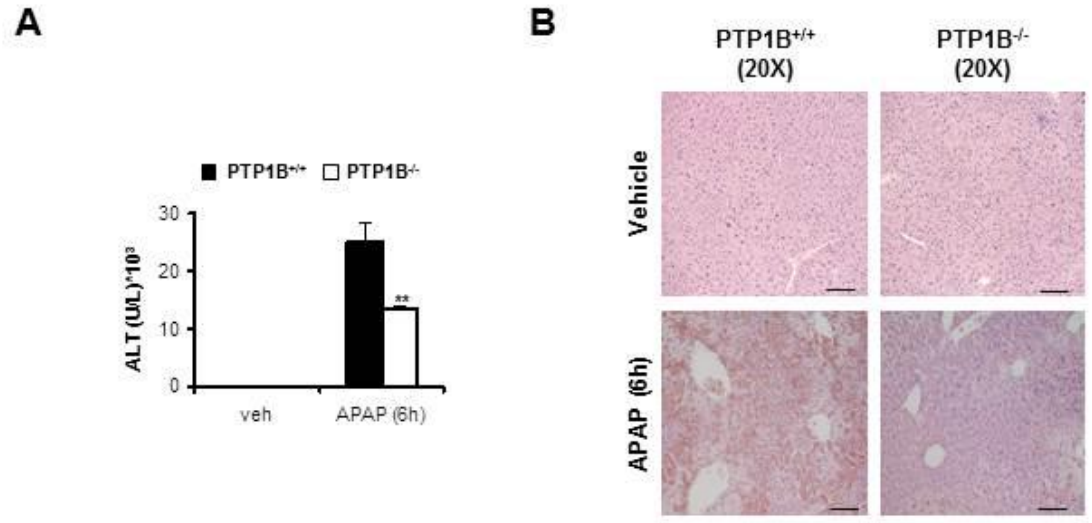

Figure20. PTP1B-deficient mice are protected against liver damage induced by a higher dose of APAP. $PTP1B^{+/+}$ and $PTP1B^{-/-}$ mice were injected with 500 mg/kg APAP or saline for 6 h. **A**. Serum transaminase (ALT) activity. **B**. Representative Hematoxylin & Eosin staining in livers from $PTP1B^{+/+}$ and $PTP1B^{-/-}$ mice 6 h after APAP injection. Bar scale 100 μm. $^{**}P<0.01$ $PTP1B^{-/-}$ vs. $PTP1B^{+/+}$ (n= 6-8 mice of each condition).

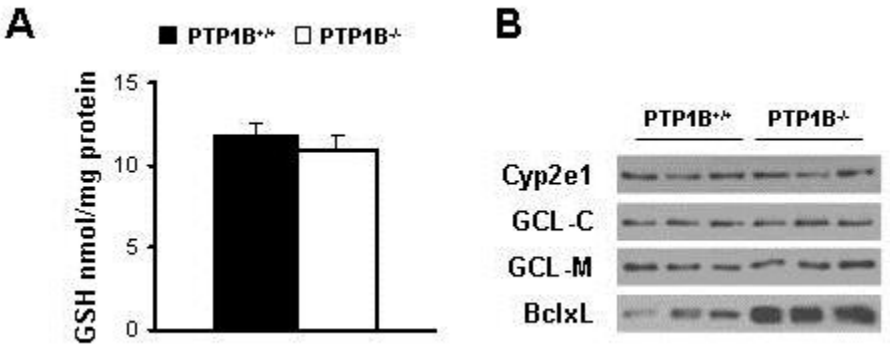

Figure 21. Basal GSH levels and expression of Cyp2e1, GCL-C, GCL-M and BclxL in livers from wild-type and $PTP1B^{-/-}$ mice. A. Basal GSH levels. **B.** Whole cell lysates from $PTP1B^{+/+}$ and $PTP1B^{-/-}$ mice were analyzed by Western blot with the indicated antibodies. Representative autoradiograms are shown.

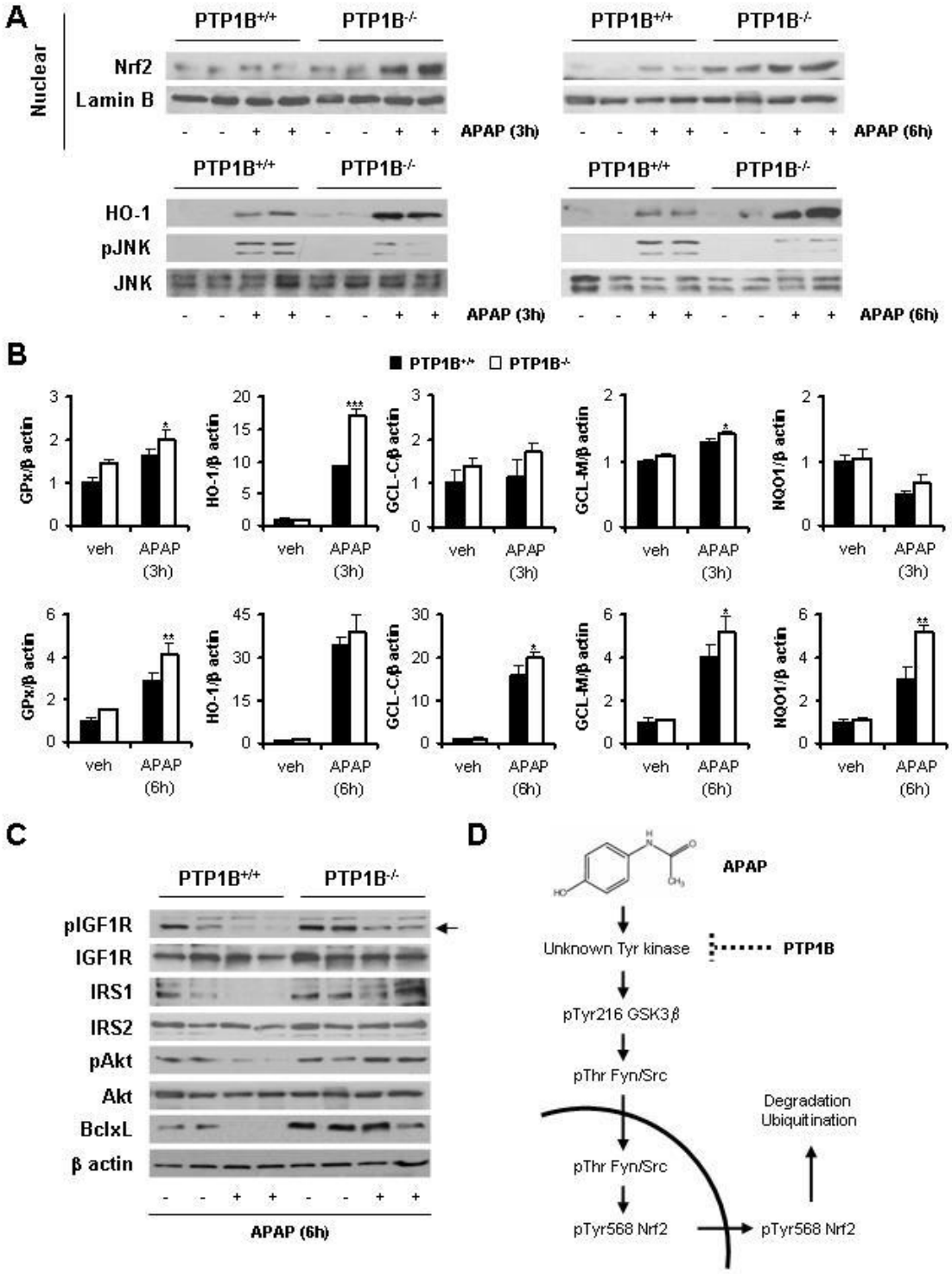

Figure 22. Beneficial effects of PTP1B deficiency on the induction of Nrf2-mediated anti-oxidant response and survival signaling in the liver. PTP1B$^{+/+}$ and PTP1B$^{-/-}$ mice were injected with 300 mg/kg APAP or saline for 3 or 6 h. **A**. Western blot analysis of Nrf2 in nuclear extracts and HO-1, phospho-JNK and JNK in total liver extracts. **B**. GPx, HO-1, GCL-M, GCL- C and NQO1 mRNA levels determined by qRT-PCR at 3 and 6 h post-APAP injection. *P<0.05, **P<0.01 and ***P<0.005 PTP1B$^{-/-}$ versus PTP1B$^{+/+}$ (n=6-8 mice of each condition). **C.** Western blot analysis of phospho-IGFIR, IGFIR, IRS1, IRS2, phospho-Akt, Akt and BclxL levels in total liver extracts from PTP1B$^{+/+}$ and PTP1B$^{-/-}$ mice 6 h after APAP injection. **D**. Schematic diagram illustrating the proposed mechanism by which PTP1B modulates Nrf2 nuclear accumulation. PTP1B might activate the unknown kinase upstream GSK3β by dephosphorylation, thereby, triggering activation of the GSK3 β /Src-Fyn axis in the nucleus that ultimately leads to Nrf2 tyrosine phosphorylation, ubiquitination and degradation.

2. EFFECT OF APAP TREATMENT IN HEPATIC INSULIN SIGNALING: ROLE OF PTP1B.

2.1 Effect of subtoxic and toxic doses of APAP in insulin-mediated signaling in human hepatocytes.

Since APAP activates stress-mediated signaling pathways that elicit a negative cross-talk with critical nodes of the insulin cascade (Aguirre et al., 2000), our first goal was to examine the effect of APAP treatment on insulin signaling in hepatocytes. Primary human hepatocytes were treated with subtoxic (10 mM) and toxic (20 mM) doses of APAP for 24 h. These doses were chosen on basis of experiments performed in Figure1. Then, hepatocytes were further stimulated with insulin (10 nM) for 10 minutes and insulin signaling cascade was analyzed. As shown in (Figure 23), insulin-induced IR tyrosine phosphorylation was significantly decreased in primary human hepatocytes treated with a subtoxic dose of APAP (10 mM) and was totally abolished at a toxic dose (20 mM).

Downstream from the IR, levels of IRS1 were also decreased in human hepatocytes treated with 10 or 20 mM APAP. By contrast, APAP treatment did not decrease IRS2 levels. In the light of these results, insulin-induced Akt phosphorylation at Ser 473 residue was impaired by APAP. As indicated in section 1.1, stress-mediated signaling monitored by phosphorylation of JNK and p38 MAPK was induced at both doses of APAP.

Due to the limitation in obtaining human primary hepatocytes for further experiments, we conducted similar assays in the hepatoma Huh7 human cell line. In these cells, APAP induced phosphorylation of JNK at 5 and 10 mM dose (Figure 24A). Cellular damage, monitored by microscopy analysis, crystal violet staining and released LDH activity, was elicited at 10 mM concentration whereas no toxicity was detected at 5 mM dose (Figure 24B, 24C). Thus, Huh7 hepatic cells were treated with 5 (subtoxic dose) and 10 (toxic dose) mM APAP for 24 h and then stimulated with 10 nM insulin for 10 minutes. As shown in Figure 24A, APAP attenuated insulin signaling as shown by reduced IR and IRS1 tyrosine phosphorylation as well as phosphorylation of Akt (Ser 473) at a subtoxic dose of APAP and almost suppressed all these effects at the toxic dose.

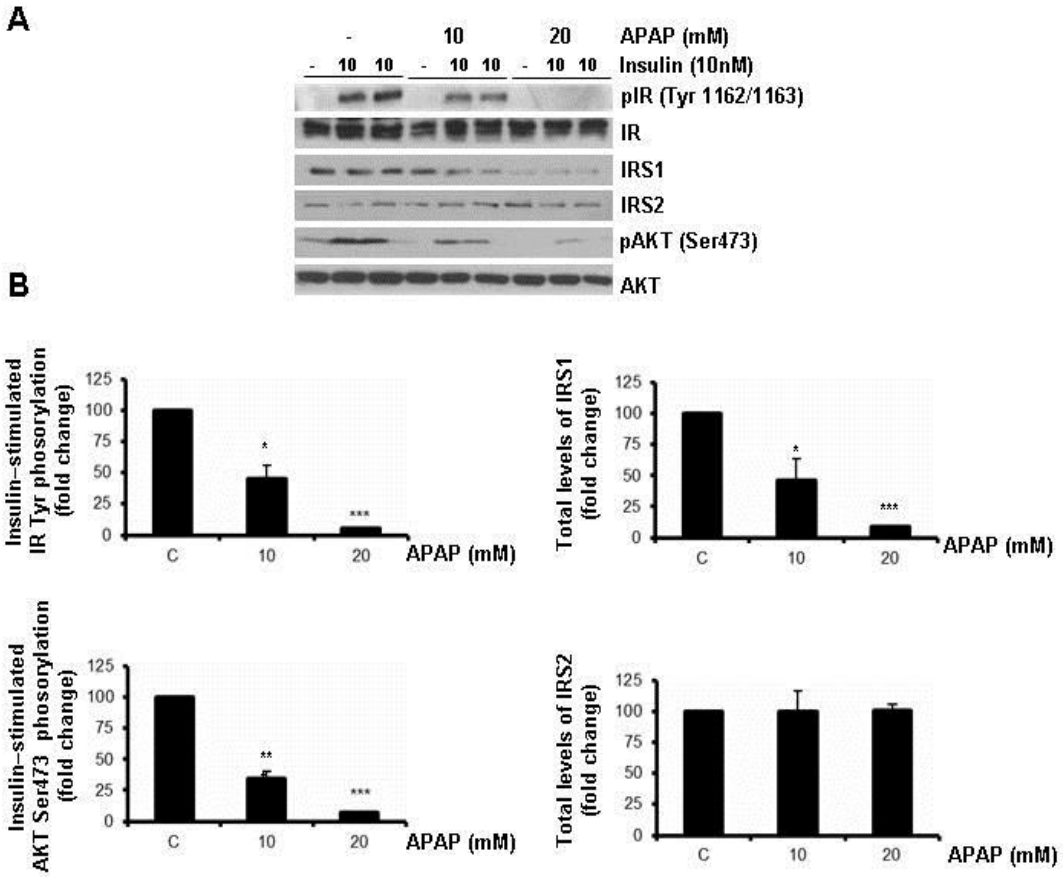

Figure 23. Effect of subtoxic and toxic doses of APAP in insulin-mediated signaling in human hepatocytes. A. Human primary hepatocytes were treated with two doses of APAP (10 and 20 mM) for 24 h. Then, hepatocytes were further stimulated with insulin (10 nM) for 10 min and insulin signaling cascade was analyzed by Western blot with the antibodies against phospho-IR, IR, IRS1, IRS2, phospho-Akt (Ser 473) and Akt. **B**. Autoradiograms were quantitated by scanning densitometry. Results are means ± SEM. *P<0.05, **P<0.01 and ***P<0.001 APAP-treated versus non-treated cells. (n=3 independent experiments).

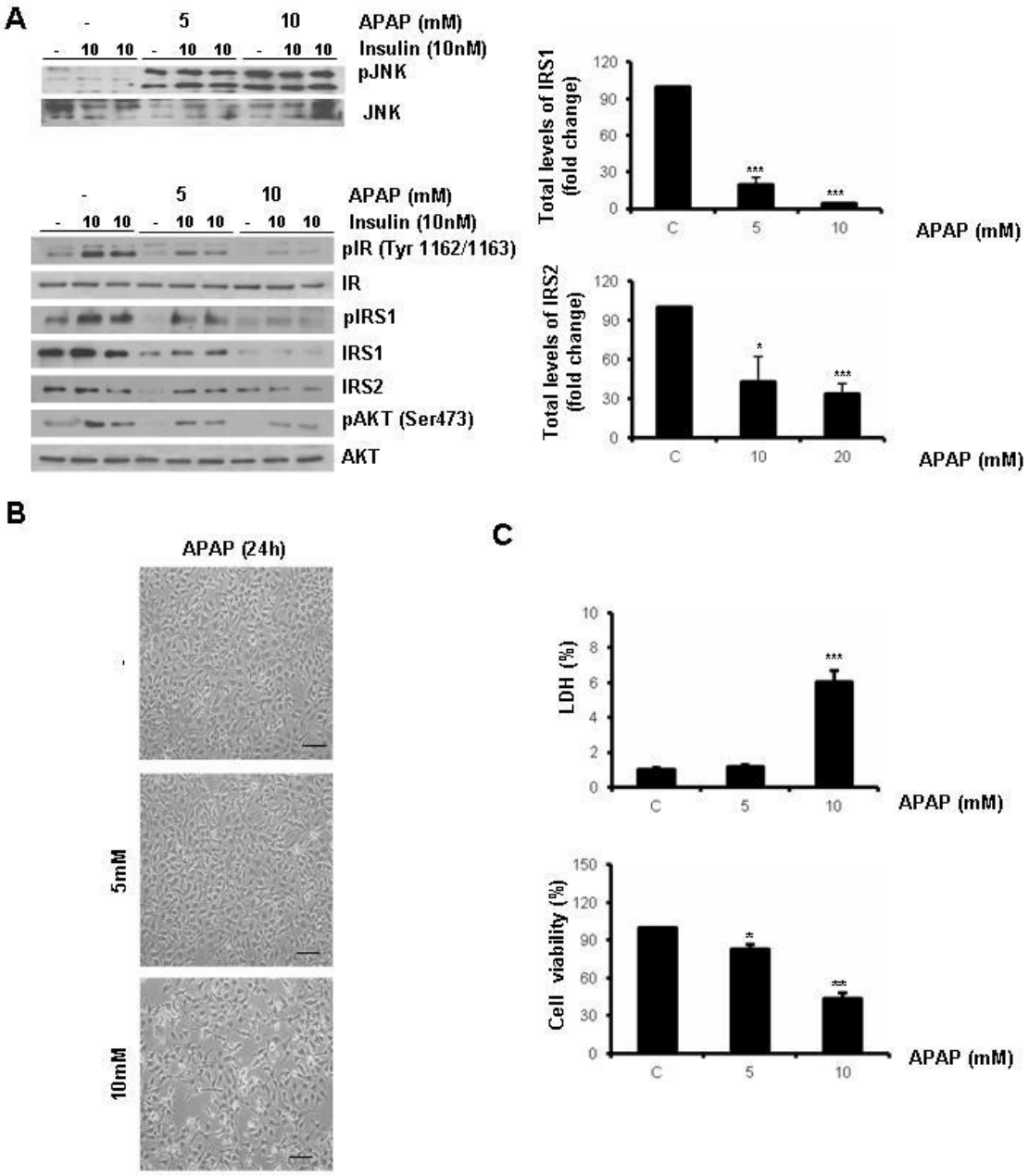

Figure 24.Effect of subtoxic and toxic doses of APAP in insulin-mediated signaling in hepatoma Huh7 human cell line. **A**. The hepatoma Huh7 human cell line was treated with two doses of APAP (5 and 10 mM) for 24 h. Then, cells were stimulated with insulin (10 nM) for 10 minutes and insulin signaling cascade was analyzed by Western blot with the antibodies against phospho-IR, IR, IRS1, IRS2, phospho-Akt (Ser 473), Akt, phospho-JNK1/2, and JNK1/2. n=3 independent experiments (left panel). Autoradiograms were quantitated by scanning densitometry. Results are means ± SEM. *P<0.05, **P<0.01 and ***P<0.001 APAP-treated versus non-treated cells. (n=3 independent experiments) (right panel). **B**. Huh7 cells were treated with two doses of APAP (5 and 10 mM) for 24 h. Representative phase-contrast microscopy images after APAP treatment. Bar scale 100 µm. **C**. Huh7 cells were treated with two doses of APAP (5 and 10 mM) for 24 h. Cellular viability and released LDH activity after APAP treatment. Results are means ± SEM. *P<0.05, **P<0.01 and ***P<0.001 APAP-treated versus non-treated cells (n=3 independent experiments).

2.2 Rosiglitazone decreased PTP1B and improved insulin signaling cascade in APAP-treated human primary hepatocytes.

Next, we investigated the effect of rosiglitazone, a well-known insulin sensitizer that binds to the peroxisome proliferator-activated (PPAR)-γ receptors, on APAP-mediated insulin resistance in hepatic cells. Human primary hepatocytes were treated with APAP (20 mM) without and with rosiglitazone (5 and 10 μM) for 24 h, after that the cells were stimulated with insulin (10 nM) for a further 10 min. As shown in (Figure 25), rosiglitazone decreased JNK and p38 MAPK phosphorylation triggered by APAP. Moreover, PTP1B levels were significantly decreased in human hepatocytes co-treated with APAP and 10 μM rosiglitazone. Interestingly, rosiglitazone increased Bcl-xL expression in APAP-treated hepatocytes. Regarding insulin signaling, rosiglitazone protected against APAP-mediated decreases in IR and IRS1 tyrosine phosphorylation, degradation of IRS1 and also maintained insulin-induced Akt Ser 473 phosphorylation.

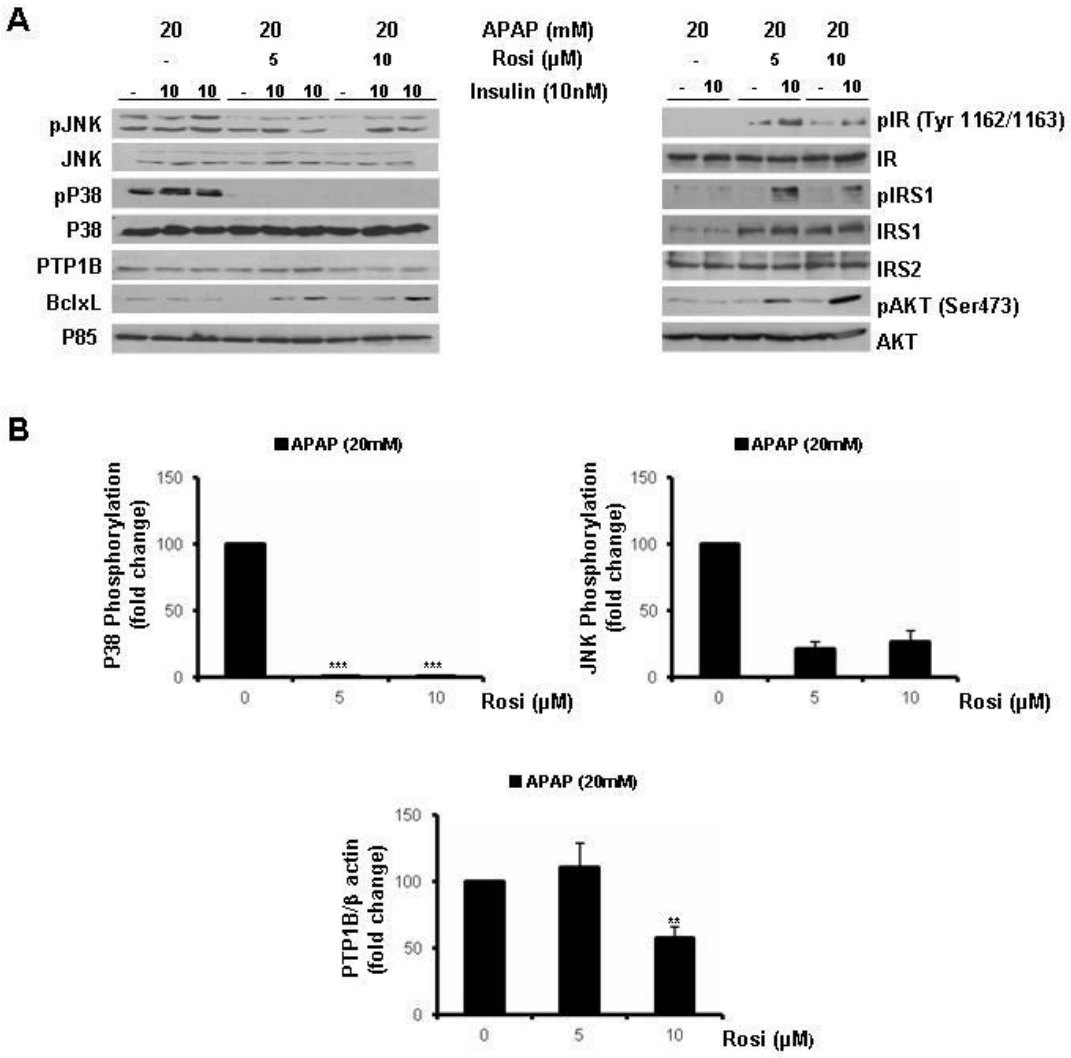

Figure 25.Rosiglitazone decreased PTP1B and improved insulin sensitivity in APAP-treated human primary hepatocytes. A.Human primary hepatocytes were treated with APAP (20 mM) without and with rosiglitazone (5 and 10 μM) for 24 h, after that the cells were stimulated with insulin (10 nM) for 10 minutes. Then, total cell lysates were analyzed by Western blot with the antibodies against phospho-JNK1/2, JNK1/2, phospho-p38 MAPF, p38 MAPK, PTP1B, BclxL, and p85-PI3K as a loading control. Also, insulin signaling cascade was analyzed by Western blot with the antibodies against phospho-IR, IR, IRS1, IRS2, phospho-Akt (Ser 473) and Akt. **B**. Autoradiograms were quantitated by scanning densitometry. Results are means ± SEM. *P<0.05 and ***P<0.001 APAP-treated versus non-treated cells (n=3 independent experiments).

2.3 Effect of reduction of PTP1B levels in insulin signaling in human hepatic cells.

PTP1B dephosphorylates tyrosine residues at the catalytic domain of the IR in the liver and skeletal muscle and, therefore, its deficiency increases insulin sensitivity (Elchebly et al., 1999; Klaman et al., 2000). In order to investigate if PTP1B levels modulate the sensitivity to insulin-mediated signaling cascade in human liver cells, we established siRNA assays (Figure 26A). Huh7 cells were transfected with human PTP1B siRNA and control (scrambled) oligos for 48 h and then stimulated with 1-10 nM insulin for a further10 min. As expected, IR tyrosine phosphorylation and Akt phosphorylation were increased in Huh7 cells with reduced PTP1B levels. To study the effect of PTP1B on the cross-talk between APAP and insulin signaling pathway, we generated stable Huh7 cell lines with reduced PTP1B levels by infection with lentivirus bearing PTP1B or scrambled short hairpin RNA (shRNA). As depicted in Figure 26B, PTP1B levels were reduced by 90% as compared with Huh7 cells infected with scrambled lentivirus. Next, cells were stimulated with insulin (1 and 10 nM) for 10 minutes and insulin signaling was analyzed. Tyrosine phosphorylation of IR as well as phosphorylation of Akt (Ser 473 and Thr 308) in response to insulin were enhanced in Huh7 hepatic cells transfected with siRNA PTP1B oligo, as well as in stable Huh7 cells with reduced PTP1B levels as compared to their corresponding controls expressing normal levels of PTP1B (Figure 26C and 26D).

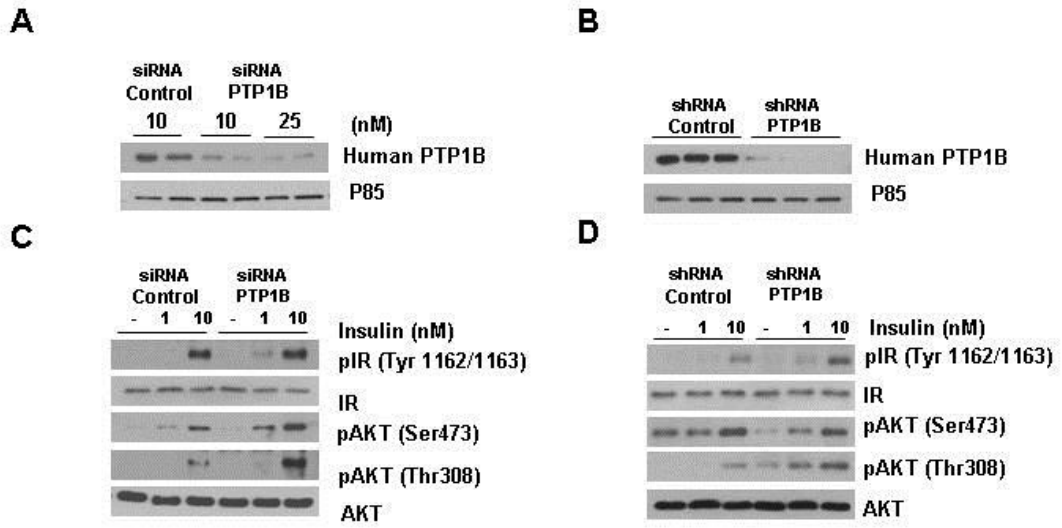

Figure 26. Effect of reduction of PTP1B levels in insulin signaling in hepatoma Huh7 human cell line. A. Hepatoma Huh7 human cell line was transfected with the human PTP1B siRNA(10 and 25 nM) or scrambled oligos (10nM) for 48 h or **B**. Hepatoma Huh7 human cell line was infected with lentivirus bearing scrambled or PTP1B short hairpin RNA (shRNA). Total cell lysates were analyzed by Western blot with the corresponding antibodies against

PTP1B and β actin as a loading control (n=3 independent experiments). **C.** Huh7 cells treated with siRNA oligos as described in A,then were stimulated with insulin (1 and 10 nM) for 10 minutes and insulin signaling cascade was analyzed by Western blot with the antibodies against phospho-IR, IR, phospho-Akt (Ser 473), phospho-Akt (Thr 308) and Akt. **D**. Huh7 cells infected with control and PTP1B shRNA lentiviral particles (B) were stimulated with insulin (1 and 10 nM) for 10 minutes and insulin signaling cascade was analysed as detailed in C. Representative autoradiograms are shown (n= 3 independent experiments).

2.4 PTP1B-deficient mouse hepatocytes are protected against APAP-mediated effects on insulin signaling.

To get further insights on the role of PTP1B in insulin signaling in APAP-treated hepatocytes, we used immortalized hepatocytes from wild-type ($PTP1B^{+/+}$) and PTP1B-deficient ($PTP1B^{-/-}$) mice. Cells from both genotypes were treated for 16 h with a low toxic APAP dose (0.5 mM) or a high toxic dose (1 mM) and then stimulated with 1-10 nM insulin for 10 minutes. As shown in (Figure 27), in wild-type immortalized hepatocytes stress-mediated signaling monitored by the phosphorylation of JNK and p38 MAPK and elevation of PTP1B levels, was observed at both APAP doses. In these cells insulin-mediated IR tyrosine phosphorylation was reduced at both APAP doses (Figure 27A). Likewise, IRS1 tyrosine phosphorylation was severely impaired in parallel with a marked reduction of total IRS1 levels. Regarding insulin-induced IRS2 tyrosine phosphorylation, it was partly (around 50%) or totally reduced when immortalized hepatocytes were pretreated with 0.5 and 1 mM APAP, respectively. Of note, total IRS2 levels were partly reduced at both APAP doses. Downstream IRS proteins, phosphorylation of Akt at both Ser 473 and Thr 308 in response to insulin were reduced with a more prominent effects in immortalized hepatocytes pretreated with 1 mM APAP. Next, we performed similar analysis in $PTP1B^{-/-}$ immortalized mouse hepatocytes (Figure 27B). As stated in section 1.4, these cells showed a lower response to APAP in the activation of stress kinases (JNK and p38 MAPK). In the light of these data, $PTP1B^{-/-}$ immortalized hepatocytes pretreated with 0.5 mM APAP were resistant to the decrease in IR tyrosine phosphorylation, IRS1 and IRS2 tyrosine phosphorylation and phosphorylation of Akt at both residues. When cells were pretreated with 1 mM APAP IRS2 tyrosine phosphorylation was further reduced. In addition, total levels of IRS1 and IRS2 were unaffected by APAP.

IRS1 phosphorylation at serine residues precedes its degradation via ubiquitination and proteosomal degradation (Terry et al., 2001). Among IRS1 serine kinases, JNK has been extensively study in insulin resistant states.

Therefore, we treated wild-type and PTP1B$^{-/-}$ immortalized hepatocytes with 1 mM APAP for short time-periods (1-4 hours) and phosphorylations of JNK, p38 MAPK and IRS1 at serine 307 were analyzed. As depicted in (Figure 28), both early JNK and p38 MAPK phosphorylation in response to APAP were delayed and reduced in PTP1B$^{-/-}$ immortalized hepatocytes as compared to the responses of the control cells. Similarly, phosphorylation of IRS1 at serine 307 was attenuated in PTP1B$^{-/-}$ cells.

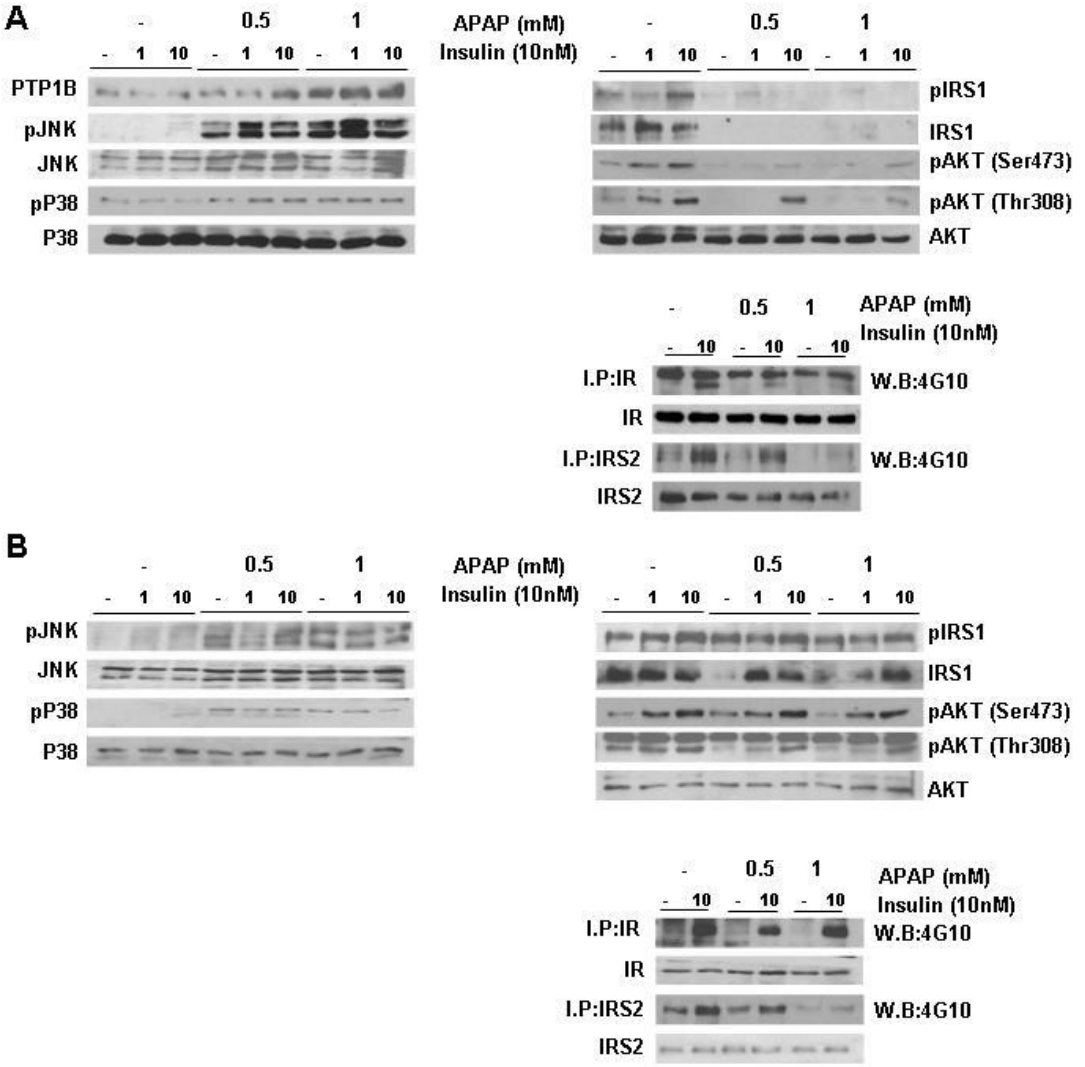

Figure 27. Effect of reduction of PTP1B levels in the effects of APAP on insulin signaling in mouse immortalized hepatocytes. Wild-type (PTP1B$^{+/+}$) immortalized mouse hepatocytes **(A)** or PTP1B$^{-/-}$ immortalized mouse hepatocytes **(B)** were treated with two doses of APAP (0,5 and 1 mM) for 16 h. Then, hepatocytes were stimulated with insulin (1 and 10 nM) for 10 minutes and insulin signaling cascade was analyzed by Western blot with the antibodies against phospho-IRS1, IRS1, phospho-Akt (Ser 473), phospho-Akt (Thr 308) and Akt. Also, total cell lysates were analyzed by Western blot with the antibodies against PTP1B, phospho-JNK1/2, JNK1/2, phospho-p38 and p38. In the lower panels IR and IRS2 tyrosine phosphorylation was analyzed by immunoprecipitation with the corresponding antibody followed by Western blot with the anti-Tyr(P) antibody (4G10). IR and IRS2 were analyzed in whole cell lysates. Representative autoradiograms are shown (n= 3 independent experiments).

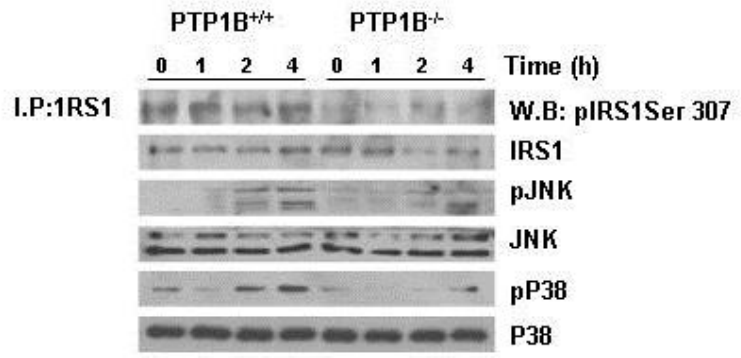

Figure 28. Effect of PTP1B deficiency in the early induction of the stress signaling by APAP in immortalized hepatocytes. Wild-type ($PTP1B^{+/+}$) and $PTP1B^{-/-}$ immortalized mouse hepatocytes were treated with APAP (1mM) for various time periods. IRS1 Ser 307 phosphorylation was analyzed by immunoprecipitation with the corresponding anti-IRS1 antibody followed by Western blot with the anti-phospho IRS1 (Ser 307) antibody. Total cell lysates were analyzed by Western blot with the antibodies against IRS1, phospho-JNK1/2, JNK1/2, phospho-p38 MAPK and p38 MAPK. Representative autoradiograms are shown (n= 3 independent experiments).

2.5 Effect of chronic APAP treatment on glucose homeostasis in wild-type and PTP1B-deficient mice.

As stated in the introduction, mice lacking the *ptpn1* gene exhibit increased insulin sensitivity owing to enhanced phosphorylation of IR in liver and skeletal muscle, resistance to weight gain on a high-fat diet, and an increased basal metabolic rate (Klaman et al., 2000; Elchebly et al., 1999). Accordingly, our next step was to study firstly if chronic APAP treatment at sub-toxic doses has an impact in whole body glucose homeostasis and insulin sensitivity and, secondly, the potential beneficial effects of the lack of PTP1B. Wild-type and $PTP1B^{-/-}$ mice were treated with APAP in the drinking water during 6 months accordingly with the protocol described in Materials and Methods (section 2.2.1.2). At this time-period there were no evidences of liver damage by APAP as reflected by normal serum ALT levels in all experimental groups and normal liver histology (Figure 29A and 29B).

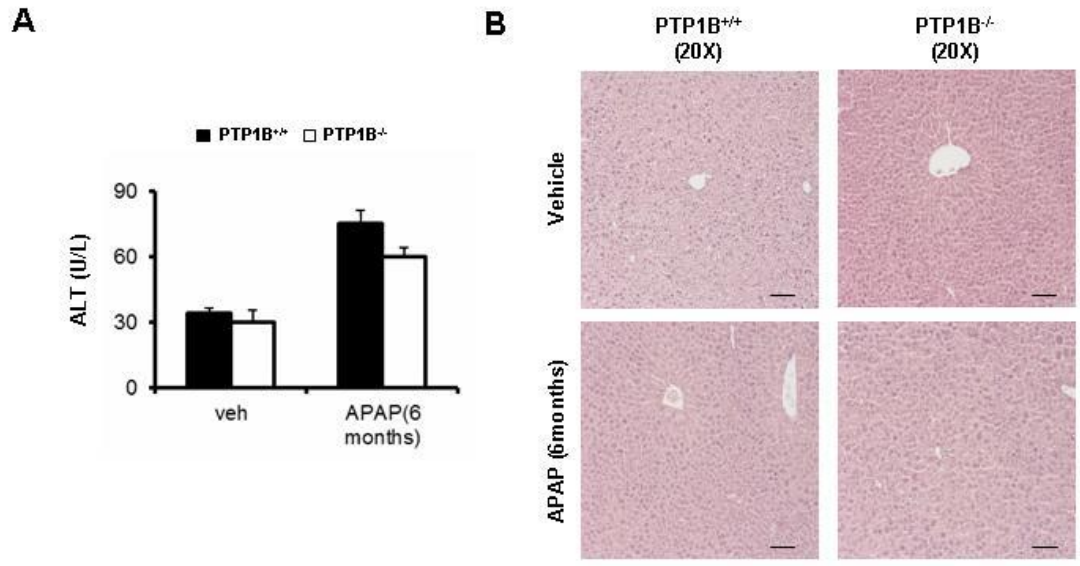

Figure 29. Chronic APAP treatment in mice did not induce liver liver damage. PTP1B$^{+/+}$ and PTP1B$^{-/-}$ mice were treated with APAP in the drinking water during 6 months (90-120 mg/kg/day). **A**. Serum transaminase (ALT) activity. **B**. Representative Hematoxylin & Eosin staining in livers from PTP1B$^{+/+}$ and PTP1B$^{-/-}$ mice after chronic APAP treatment. Bar scale 100 μm. **P<0.01 PTP1B$^{-/-}$ vs. PTP1B$^{+/+}$ (n= 6-8 mice of each condition).

Body weight was monitored through chronic APAP treatment. Wild-type mice increased body weight during the treatment, this effect was not observed in those mice receiving APAP (Figure 30A). However, body weight of PTP1B$^{-/-}$ mice was maintained during treatment, no differences being observed in mice receiving APAP.

We assessed whole-body glucose homeostasis at the end of the APAP treatment by performing the glucose tolerance test (GTT). (Figure 30B) shows that APAP slightly decreased glucose tolerance in wild-type, but not in PTP1B$^{-/-}$ mice. Of note, enhanced glucose tolerance was evident in PTP1B$^{-/-}$ as compared to the wild-type mice regardless of APAP treatment.

To further investigate the effects of chronic APAP treatment in insulin sensitivity, we performed insulin tolerance tests (ITT). As shown in (Figure 30C) PTP1B$^{-/-}$ mice displayed increased insulin sensitivity as compared to the wild-type control. However, chronic APAP treatment did not affect the ability of exogenously injected insulin to decrease glucose levels in both genotypes of mice.

In addition to the reduction in whole-body glucose disposal (mainly accounted by skeletal muscle-mediated glucose uptake), increased hepatic glucose production (HGP) has also been reported to contribute to glucose intolerance. To assess whether increased HGP was involved in glucose intolerance of the APAP-treated wild-type animals, we performed pyruvate tolerance tests (PTT).

The PTT measures the extension of the whole-body conversion of pyruvate into glucose and allows the assessment of the rate of gluconeogenesis, which is an important component of hepatic insulin action. In wild-type mice, we found increased glucose levels after pyruvate injection (Figure 30D). This effect was slightly enhanced in mice that had received the chronic APAP treatment. In PTP1B$^{-/-}$ mice blood glucose levels were less elevated after pyruvate injection in both vehicle and APAP-treated groups.

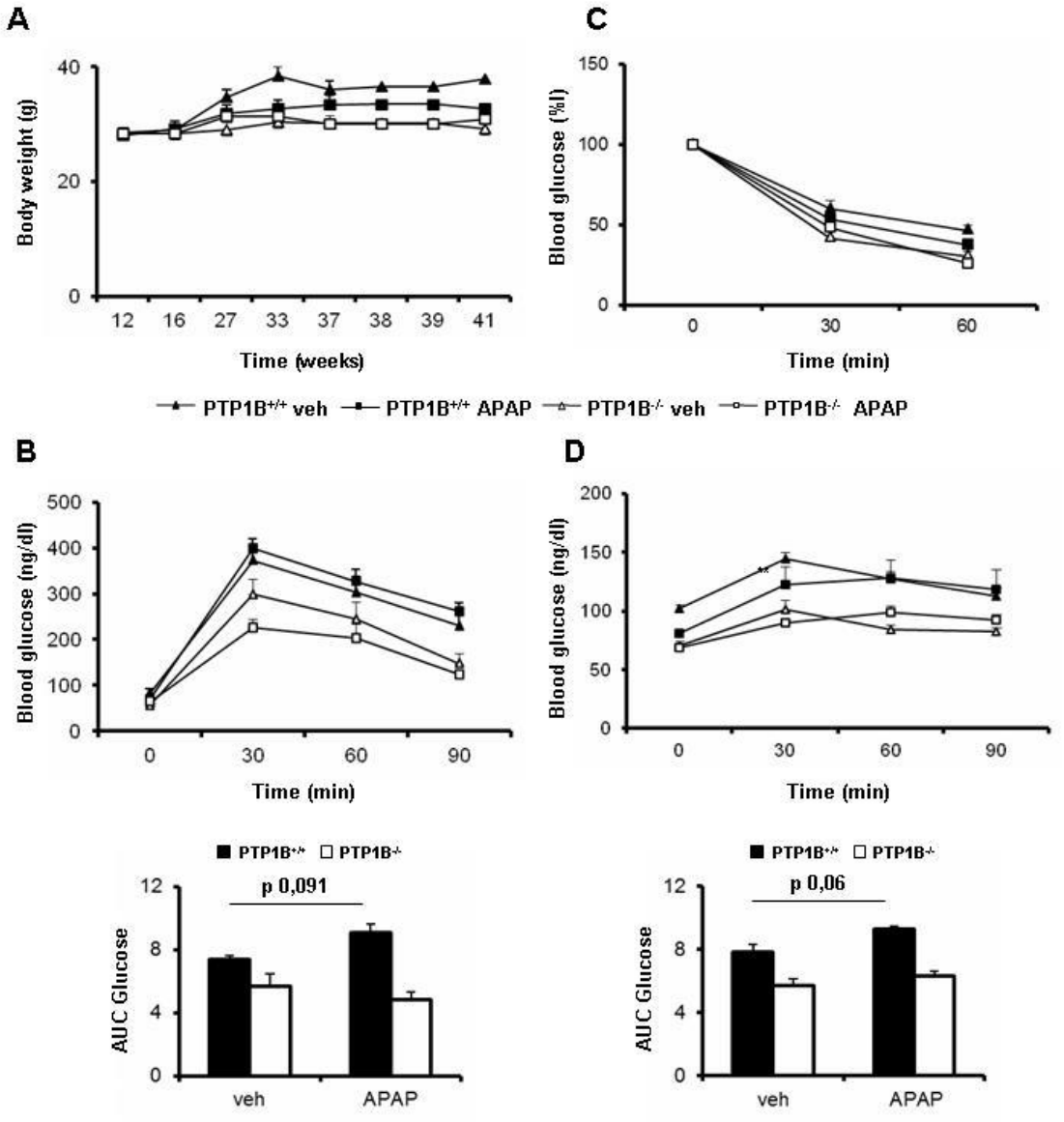

Figure 30. Effect of PTP1B deficiency in glucose homeostasis in mice treated chronically with APAP in the drinking water. PTP1B$^{+/+}$ and PTP1B$^{-/-}$ mice were treated with APAP in the drinking water during 6 months (90 mg/kg/day). **A**. Body weight of mice during the treatment. **B.** Glucose tolerance test (GTT) tolerance tests were performed in animals that had been fasted for 24 h and were given an intraperitoneal injection of glucose (2 g/kg). The area under the curve (AUC) was calculated as AUC_{Ground} (AUC $_G$mmol/L *min) and represented in graph (left panel). **C**. Insulin tolerance test (ITT) was performed in animals that had been fasted for 4 h and were given an intraperitoneal injection of (0.75 U/kg) of human regular insulin. **D**. Pyruvate tolerance test (PTT) tolerance test was performed on animals that had been fasted for 24 h and were given an intraperitoneal injection of pyruvate (2 g/kg). The area under the curve (AUC) was calculated as AUC_{Ground} (AUC $_G$mmol/L * min) (left panel). (n= 6-8 animals/group).

*p<0.05 and **p<0.01 PTP1B$^{+/+}$ APAP vs PTP1B$^{+/+}$ veh and PTP1B$^{-/-}$ APAP vs PTP1B^{--} veh.

Finally, we determined fasted insulin levels in serum in the four experimental groups. As depicted in Figure 31, insulin levels were significantly lower in PTP1B$^{-/-}$ mice as compared to the wild-type controls. This result is in agreement with the work of Bence and co-workers (Bence et al., 2000). Importantly, chronic APAP treatment decreased serum insulin in wild-type mice but not in mice lacking PTP1B.

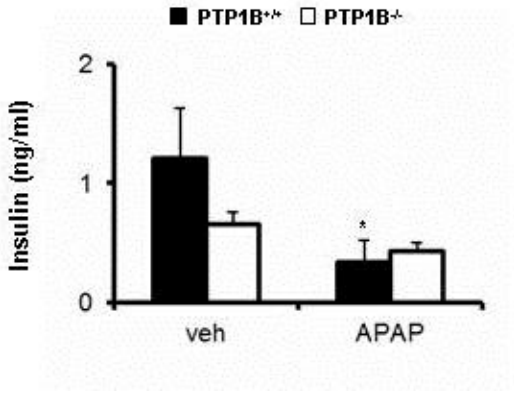

Figure 31. Effect of chronic APAP treatment on Insulin levels in PTP1B$^{+/+}$ and PTP1B$^{-/-}$ mice. PTP1B$^{+/+}$ and PTP1B$^{-/-}$ mice were treated with APAP in the drinking water during 6 months (90-120 mg/kg/day). Blood was collected from mice that had been fasted for 24 h and the serum insulin was determined by RIA. (n= 6-8 animals/group).

DISCUSSION

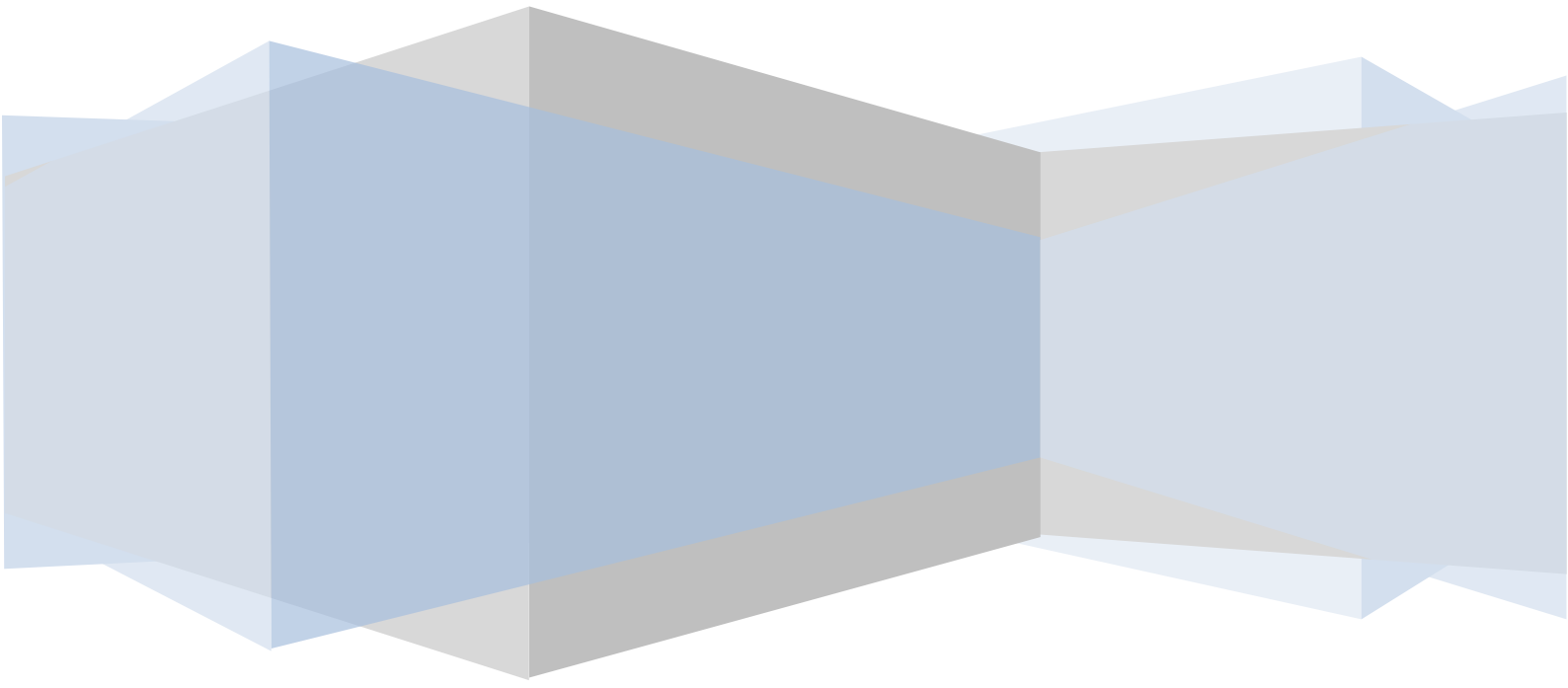

1. ROLE OF PTP1B IN APAP-INDUCED ACUTE LIVER FAILURE:-

There is evidence of increased PTP1B expression during the progression of non-alcoholic fatty liver disease that concurs with insulin resistance and liver damage (Sanderson et al., 2005; Garcia-Monzón et al., 2011). However, PTP1B functions in other *in vivo* physiological responses regulated by tyrosine kinase signaling, such as hepatic proliferation and, particularly, hepatocellular survival during drug injury are poorly understood. The current study has unraveled a central role of PTP1B in the molecular mechanism that mediates APAP-induced liver failure, thereby identifying PTP1B as a potential therapeutic target in the treatment of human APAP hepatotoxicity. In fact, this study emerged from the observation of elevated PTP1B expression in livers from individuals suffering of APAP intoxication. Moreover, in APAP-treated human and mouse hepatocytes up-regulation of PTP1B preceded cell death.

Our experiments in mouse hepatocytes demonstrated that PTP1B deficiency attenuates cellular damage in response to APAP treatment. The fact that released LDH activity was reduced in PTP1B$^{-/-}$ hepatocytes indicates that necrotic cell death was less severe than in wild-type controls. In wild-type hepatocytes APAP also increased percentage of sub G0/G1 cells, release of cytochrome C from mitochondria, activation of caspase-3 and decreased anti-apoptotic proteins BclxL and Mcl1. These results strongly suggest that APAP triggered apoptosis in hepatocytes and, again, these effects were ameliorated by PTP1B deficiency. In light of these data, we and others have shown that PTP1B inhibition protects hepatocytes against activation of mitochondrial (intrinsic) and death receptor (extrinsic)-mediated apoptotic pathways (Gonzalez-Rodriguez et al., 2007; Sangwan et al., 2006), reinforcing the role of this phosphatase in programmed cell death.

It is known that APAP-induced cell death in hepatocytes is, in part, the result of a series of events that increase cellular oxidative stress; mainly depletion of the GSH pool by conjugation with NAPQI and subsequent generation of ROS (Reid et al., 2005). Since these processes are significantly ameliorated in PTP1B$^{-/-}$ hepatocytes, we investigated the modulation of oxidative stress by PTP1B. In this regard, an unknown tyrosine kinase has been proposed to be the upstream activator of GSK3βby phosphorylation at tyrosine 216 (Niture et al., 2011; Jain et al., 2007). This phenomenon leads to

SKF-mediated tyrosine phosphorylation, nuclear export, ubiquitination, and degradation of Nrf2 in response to oxidative stress inducers. Our data demonstrated firstly that this signaling pathway is activated by APAP in hepatocytes and, secondly, as discussed below, that PTP1B deficiency mimicked the inhibition of GSK3β or SKF on the downstream mediators of this pathway. Therefore, silencing of GSK3 β delayed Src and Fyn nuclear translocation, which correlated with delayed Nrf2 nuclear exclusion in response to APAP. Likewise, chemical inhibition of SKF by PP2 in hepatocytes or, deletion of these kinases in MEFs ($SFY^{-/-}$), also augmented/prolonged Nrf2 nuclear accumulation in response to APAP. Importantly, the effect of PTP1B deficiency on this pathway was manifested by delayed Src-Fyn nuclear translocation, Nrf2 tyrosine phosphorylation and its subsequent ubiquitination and degradation, leading to enhanced HO-1 induction. These results suggest that PTP1B might activate this unknown kinase upstream from GSK3β probably by dephosphorylation, thereby, triggering activation of the GSK3β/Src-Fyn axis that, as stated above, ultimately leads to Nrf2 degradation. Consequently, as demonstrated in hepatocytes, PTP1B deficiency might delay and/or reduce activation of this complex axis resulting in prolonged nuclear accumulation of Nrf2 and enhanced anti-oxidant defense. Recent findings have reported a direct effect of GSK3β in APAP hepatotoxicity in mediating GCLC and Mcl1 protein degradation (Shinohara et al., 2010). Although our results point PTP1B as an upstream mediator of GSK3β activation (Figure 17D), additional direct effects of the PTP1B/GSK3β pathway independent of Nrf2-mediated transcription should not be excluded.

Besides the novel role of PTP1B in anti-oxidant defense reported in the present study, this phosphatase regulates duration and/or intensity of survival signals emerging from the tyrosine kinase receptor family (Zabolotny et al., 2002; Haj et al., 2003; Sangwan et al., 2006) . Since IGFIR triggers survival responses in hepatocytes (Tovar et al., 2010), the lack of PTP1B prevented the drop in the IGFIR/IRS1/2/Akt-mediated survival signaling in APAP-treated cells. In fact, this is the first report showing degradation of IRS proteins in hepatocytes by APAP, suggesting that high doses of this analgesic may also interfere with hepatic insulin signaling and increase the risk of metabolic diseases such as insulin resistance and type 2 diabetes mellitus. Thus, in wild-type hepatocytes, increased ROS-mediated JNK and p38 MAPK

phosphorylation by APAP are likely to be responsible for the feed-back mechanism on the IGFIR-mediated signaling leading to IRS1/2 serine phosphorylation that precedes degradation (Vinayagamoorthi et al., 2008) . Thus, in the absence of PTP1B the decrease in ROS-mediated activation of JNK and p38 MAPK and the increase in tyrosine phosphorylation of IGFIR might act in conjunction with the effects on the GSK3β/Src-Fyn axis thereby attenuating oxidative stress and increasing cell survival in response to APAP.

Several studies have shown the mechanistic importance of hepatic cytokine network in APAP-induced liver injury. In the liver, cytokines are mainly produced by non-parenchymal cells. Our *in vivo* data show significant lower expression levels of IL1β and IL6 mRNAs in livers of PTP1B$^{-/-}$ mice upon APAP injection as compared to the elevated levels of the wild-type controls, suggesting that PTP1B also modulate cytokine production by non-parenchymal cells in response to liver damage. Cytokines play an essential role as inducers of PTP1B in metabolic diseases. Activation of JNK together with elevated expression of PTP1B in response to IL6 has been reported in skeletal muscle of insulin resistant mice (Nieto-Vazquez et al., 2008). Likewise, IL4 induces PTP1B and enhances its protein stability to suppress IL4-induced STAT6 signaling in B cells (Lu et al., 2008). Since PTP1B is increased in the livers of APAP-injected wild-type mice, this effect is likely to be due to elevation of IL6 and IL1β .Therefore, cytokine-mediated increases in PTP1B expression might lead to enhancement of the GSK3β/Src-Fyn axis resulting in increased Nrf2 tyrosine phosphorylation and a rapid nuclear exclusion. Moreover, in the liver of APAP-injected wild-type mice, the negative cross-talk elicited by JNK on IRS proteins and also by PTP1B by direct dephosphorylation of the IGFIR might synergize with the enhancement of the GSK3β/Src-Fyn axis to reduce survival of hepatic cells. This mechanism is supported by lower activation of JNK, higher IGFIR tyrosine phosphorylation and nuclear Nrf2 accumulation in livers of APAP-injected PTP1B$^{-/-}$ mice as compared to wild-type controls. As a result, PTP1B-deficient livers are protected against APAP-induced oxidative stress and injury as manifested by decreased GSH depletion that might favour NAPQI detoxification lowering the formation of APAP-protein aducts. However, the effects of APAP *in vivo* are not exclusively mediated by elevation of PTP1B expression by pro-inflammatory cytokines secreted by non-parenchymal (i.e kuppfer) cells; our *in vitro* data have also demonstrated direct effects of APAP

in hepatocytes. Nevertheless, PTP1B deficiency protects against damage in hepatocytes in culture and in whole liver reinforcing the modulatory role of this phosphatase in multiple molecular mechanisms triggered in response to APAP in distinct liver cells.

In conclusion, we have demonstrated the unique role of PTP1B in the liver as a critical crossroad in the signaling pathways triggered in response to APAP by a dual modulation of Nrf2-mediated anti-oxidant response through the GSK3β/Src-Fyn kinases axis and survival signaling through its effects on the IGFIR/IRSs/Akt pathway. Our data suggest that inhibition of this phosphatase would be a suitable therapeutic approach against APAP-induced hepatotoxicity.

2. EFFECT OF APAP TREATMENT IN HEPATIC INSULIN SIGNALING: ROLE OF PTP1B.

Many drugs are associated with the development of glucose intolerance or with deterioration in glycaemic control in patients with pre-existing diabetes. Some of them show dose-dependent effects. For example, anti-inflammatory doses of corticosteroids may necessitate use of insulin in patients that are controlled with oral anti-diabetic agents. Such therapy not infrequently precipitates diabetes in middle-aged or elderly individuals with no history of glucose intolerance. Other notable examples include oral contraceptives, estrogen replacement therapy, cyclophilin immunosuppressants, protease inhibitors etc… (Reviewed in Insulin Resistance. A clinical Handbook. AJ Krentz Ed. 2002 Blackwell Science Ltd).

In the initial experiments of APAP-mediated toxicity in hepatocytes we found that APAP also increased PTP1B levels at subtoxic doses. Interestingly, PTP1B expression is elevated in hepatocytes treated with the proinflammatory cytokine TNFα that modulates insulin signaling in insulin-sensitive cellular models (Zabolotny et al. 2008; Nieto-Vazquez et al., 2007; Fernández-Veledo et al. 2006). In addition to the elevation of PTP1B, subtoxic doses of APAP also activated JNK. In this regard, it has been shown that JNK interferes with insulin signaling through the serine phosphorylation of IRS1 at serine 307 and subsequent degradation (Vincent et al., 2000). These data prompted us to evaluate a possible cross-talk between subtoxic doses of APAP and insulin signaling in hepatocytes.

Our results in three different hepatic cellular models (human primary hepatocytes, Huh7 human hepatic cell line and immortalized mouse hepatocytes) revealed a decreased response to insulin in IR tyrosine phosphorylation in cells pretreated with subtoxics doses of APAP. This effect is particularly relevant since indicated a negative cross-talk between APAP and insulin signaling at the level of IR that conforms together with IRS proteins the critical node 1 of insulin signaling (Taniguchi et al., 2006). As expected, downstream IR signaling was also attenuated in APAP treated hepatic cells reflected by decreased IRS1 and IRS2 tyrosine phosphorylation and Akt phosphorylation (Ser 473 and Thr 308).

IRS1 is particularly susceptible to proteasomal-mediated degradation by different triggers including oxidative stress. Acute oxidative stress leads to a short term activation of insulin signaling (Piwkowska et al., 2012), but if prolonged can have other effects including degradation of IRS1. In this regard, it has been shown that urea at concentrations that induce ROS production in cultured 3T3-L1 adipocytes increases modification of insulin signaling molecules by O-GlcNAc and reduces insulin-stimulated IRS1 and Akt phosphorylation and glucose transport (D'Apolito et al., 2010). Our data in the three hepatic cellular models clearly show that APAP triggers degradation of IRS1. In fact, we demonstrated in immortalized hepatocytes that APAP induces a rapid IRS1 serine phosphorylation at serine 307 in parallel to the phosphorylation of JNK. Therefore, in these cells the negative cross-talk elicited by JNK on IRS1 and by PTP1B on the IR might synergize to decrease Akt phosphorylation that is a critical node for insulin´s metabolic actions. Regarding IRS2, there are few data regarding the triggers and the molecular mechanisms responsible of its degradation (Copps and White 2012). However, it has been described decreased levels of IRS2 in response of oxidative stress induced by Bisphenol A in rat testis (D´Cruz et al., 2012). Another *in vitro* study demonstrated IRS2 degradation in muscle cells treated with H_2O_2 (Archuleta et al., 2009). Our results in hepatic human and mouse cell lines show IRS2 degradation upon subtoxic APAP doses. On the contrary, in primary human hepatocytes IRS2 levels were not affected by APAP indicating that IRS2 might be more resistant to degradation compared to IRS1 and also, the susceptibility to its degradation by oxidative stressors might vary among different cell systems. It has been well established that low chronic

inflammation in white adipose tissue induced in obesity leads to insulin resistance in the liver (Johnson and Olefsky 2013). In a similar manner, APAP at subtoxic doses might induce a low chronic oxidative stress that leads to the activation of some of the stress kinases such as JNK, also involved in the inflammatory negative cross-talk that ends up with the blockade of insulin signaling.

Although the past decade has proven that the ligands for PPARγ TZDs are effective insulin-sensitizing agents. Several studies have demonstrated compounds containing scaffolds similar to TZD exhibit inhibitory effects against PTP1B (Bhattarai et al., 2009). Similarly, Combs et al. reported isothiazolidinone-containing compounds as potent inhibitors of PTP1B (Combs et al., 2005). In an attempt to ameliorate the negative effects of APAP in insulin signaling, we treated human primary hepatic cells with the combination of APAP plus rosiglitazone. Under these experimental conditions the two APAP-mediated negative modulators of insulin signaling PTP1B and phospho-JNK were decreased, thereby recovering insulin sensitization. All together, these results in reinforce the importance of the modulation of PTP1B expression as a therapeutic strategy to ameliorate insulin resistance. Our previous work has evidence the beneficial effects of PTP1B inhibition to overcome hepatic insulin resistance due to IRS2 deficiency (González-Rodriguez et al., 2010) or aging (González-Rodriguez et al., 2012). In the light of these data, the results presented herein in immortalized hepatocytes lacking PTP1B showing a protection against APAP-mediated negative effects in insulin signaling, reinforce the benefits of inhibiting PTP1B in the liver to treat insulin resistance.

Finally, we have extended our investigations in an *in vivo* model of chronic APAP treatment in wild-type and PTP1B$^{-/-}$ mice (described in detail in Materials and Methods). This treatment did not produce changes in liver histology in both genotypes of mice, although ALT was increased by around twofold; this effect was less evident in PTP1B$^{-/-}$ mice. Even though, ALT values we maintained within normal range according to data provided from Laboratory Animal Resources at State University of Iowa (http://www.lar.iastate.edu/). Control wild-type mice (not receiving APAP) gained weight thorough the 6 months of the study, this effect being not observed in control PTP1B$^{-/-}$ mice. These data are in agreement with our recent

study regarding protection of PTP1B deficiency against age-mediated weight gain and adiposity (González-Rodriguez et al., 2012). If fact, the increase in body weight in wild-type mice correlated to increased adiposity (data not shown). Unexpectedly, weight loss was observed in wild-type mice that received a non-toxic dose of APAP for 6 months whereas weight loss was not observed in APAP-treated PTP1B$^{-/-}$ mice. One possible explanation for such an effect could be decreased food intake and/or increased energy expenditure. Daily food intake was similar among groups (results not shown). At present, we are performing indirect calorimetry to evaluate energy expenditure in light and dark cycles. Regarding whole body glucose homeostasis, the GTT tests revealed a trend towards an increased area under the curve (AUC) in wild-type mice that received APAP. Differences in glucose tolerance were not observed in both groups of APAP$^{-/-}$ mice. Importantly, PTP1B$^{-/-}$ mice displayed the phenotype of improved glucose tolerance initially reported by Elchebly et al., (1999) and Bence et al., (2000). However, data from the ITT tests indicated no differences in peripheral insulin sensitivity among groups. As skeletal muscle accounts for 85% of whole body glucose disposal (reviewed by Pillon et al., 2013), moderate alterations in hepatic insulin sensitivity are difficult to detect by the ITT. Therefore, we performed PTT and again, a trend towards an increase in the AUC was observed in wild-type mice treated with APAP, reflecting the possibility of decreased insulin suppression of hepatic glucose production (HGP). Again, the AUC was lower in PTP1B$^{-/-}$ mice due to the increased hepatic insulin sensitivity reported by several laboratories including ours, no tendency to increased AUC being observed in these mice by the chronic APAP treatment. At present, we are evaluating insulin signaling in both liver and skeletal muscle in the four experimental groups. Nevertheless, since APAP significantly decreased serum insulin in wild-type mice, it is possible that the chronic treatment induces alterations in beta cell mass and/or insulin secretion machinery. To unravel this critical issue, we are performing histological evaluation of beta cell mass, insulin and glucagon content, as well as markers of oxidative stress and apoptosis in pancreatic sections from the four experimental groups. Of note, the hypoinsulinemia characteristic of the insulin hypersensitivity phenotype of PTP1B$^{-/-}$ mice confirms again the maintenance of the phenotype of our colony.

CONCLUSIONS/ CONCLUSIONES

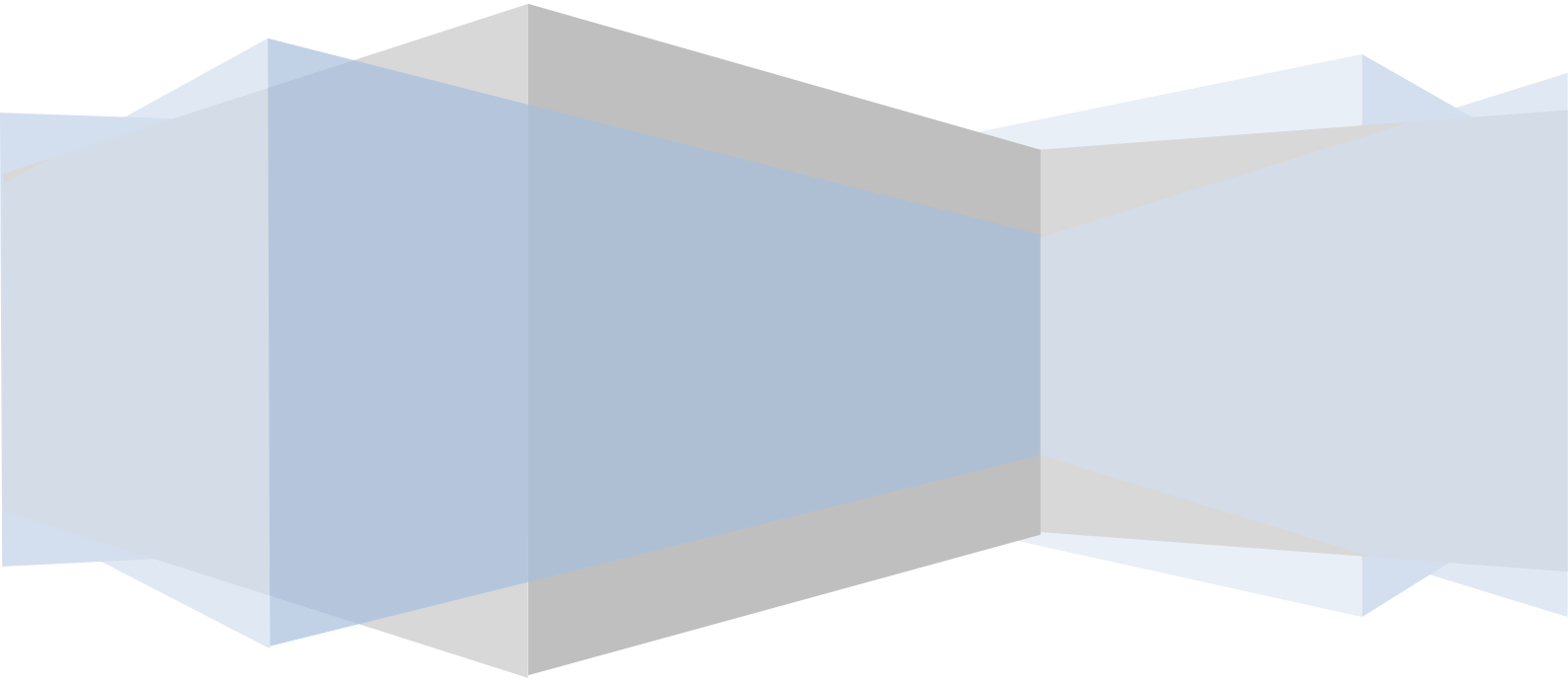

CONCLUSIONS

1-PTP1B expression was elevated during APAP-induced liver injury in humans. In APAP-treated human hepatocytes, elevation of PTP1B was detected before the induction of cell death.

2-PTP1B-deficiency protected against APAP-induced cell death in mouse hepatocytes.

3-PTP1B deficiency decreased the activation of stress-mediated signalling pathways and prolonged the survival-mediated signalling in hepatocytes.

4-PTP1B deficiency protected mouse hepatocytes against GSH depletion and elevation of ROS induced by the APAP treatment.

5-PTP1B deficiency modulated GSK3β/SKF-mediated Nrf2 nuclear accumulation in APAP-treated mouse hepatocytes, and delayed Nrf2 nuclear exclusion and degradation.

6-PTP1B-deficient mice were protected against APAP-induced oxidative stress through the decrease in the activation of JNK, enhancement of Nrf2 nuclear accumulation and maintenance of IGFIR/Akt/BclxL survival signalling.

7-Insulin signalling was decreased in hepatocytes pretreated with subtoxic and toxic doses of APAP.

8-Both rosiglitazone co-treatment and PTP1B inhibition protected against APAP-mediated effects on the insulin signalling cascade.

9-Chronic APAP treatment in wild-type mice showed a decrease in whole-body glucose homeostasis. This effect was not observed in PTP1B-deficient mice.

CONCLUSIONES

1- La expresión de PTP1B se encontraba aumentada en el hígado de individuos que habrían sufrido intoxicación por sobredosis de paracetamol. En hepatocitos tratados con dosis tóxicas de paracetamol, el aumento en la expresión de PTP1B era previo a la muerte celular.

2- La deficiencia en PTP1B confiere protección frente a la muerte celular inducida por paracetamol en hepatocitos de ratón.

3- La deficiencia en PTP1B disminuyó la activación de la señalización celular mediada por la activación de las quinasas de estrés a la vez que prolongaba la señalización de supervivencia celular en los hepatocitos.

4- La deficiencia en PTP1B protegía a los hepatocitos frente a la depleción de glutation reducido y la elevación de las especies reactivas de oxígeno tras el tratamiento con paracetamol.

5- La PTP1B modula la ruta GSK3β/SKF que conduce a la acumulación de Nrf2 en el núcleo. Los hepatocitos deficientes en PTP1B presentaron un retraso en la exclusión nuclear de Nrf2, así como en la posterior ubiquitinación y degradación del mismo.

6- En el hígado, los ratones deficientes en PTP1B presentaban protección frente al estrés oxidativo inducido por el paracetamol mediante la atenuación de la activación de JNK, el aumento en la acumulación de Nrf2 en el núcleo y el mantenimiento de la señalización de supervivencia IGFIR/Akt/BclxL.

7- La respuesta a la insulina en la activación de la cascada de señalización mediada por su receptor se encontraba disminuida cuando los hepatocitos habían sido pretratados con dosis subtóxicas y tóxicas de paracetamol.

8- El co-tratamiento con rosiglitazona ó la inhibición de PTP1B recuperaron la respuesta a la insulina en la activación de su ruta de señalización en hepatocitos tratados con paracetamol.

9-El tratamiento crónico con paracetamol en ratones de genotipo salvaje disminuyó la homeostasis glucídica. Dicho efecto no se observó en los ratones deficientes en PTP1B.

REFERENCE

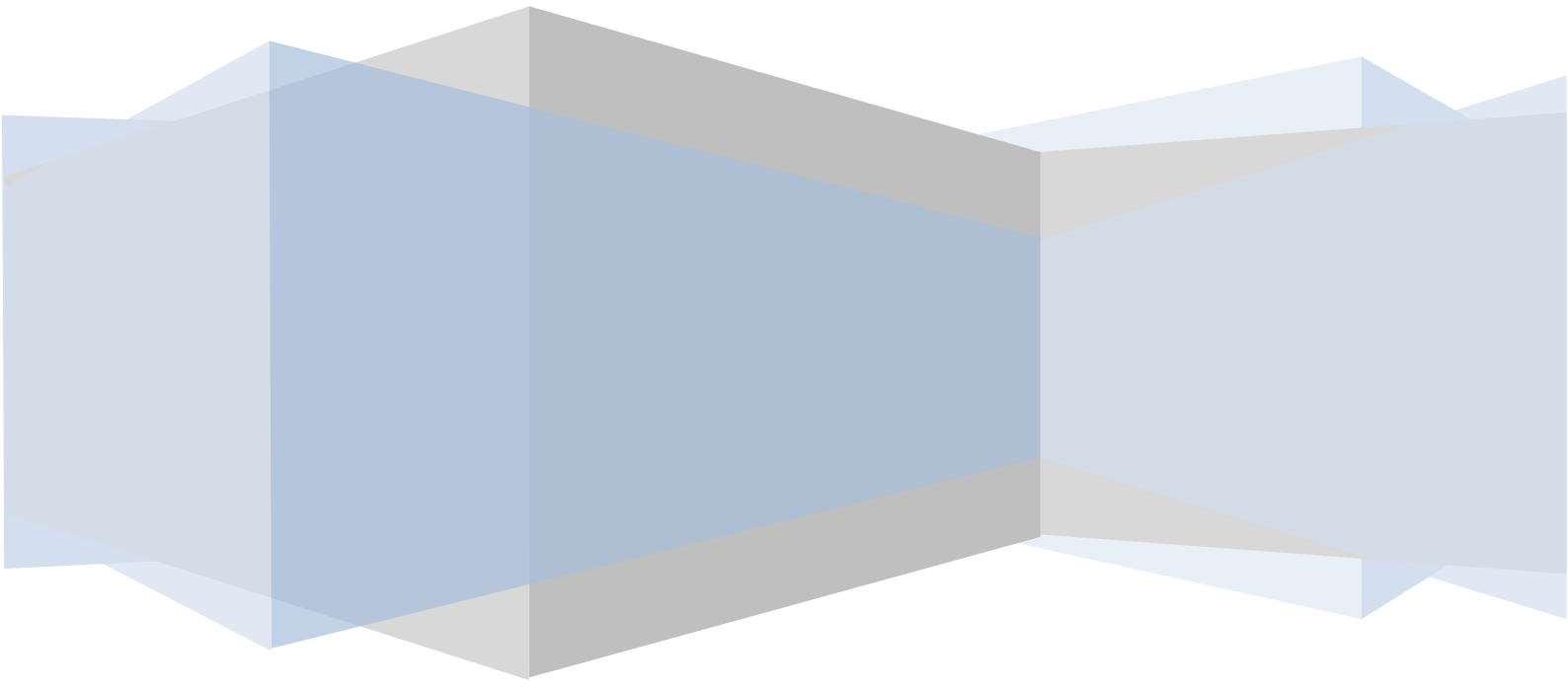

Aguirre V, Uchida T, Yenush L, Davis R, White MF (2000). The c-Jun NH(2)-terminal kinase promotes insulin resistance during association with insulin receptor substrate-1 and phosphorylation of Ser(307). J Biol Chem 275:9047-9054.

Alía M, Ramos S, Mateos R, Bravo L, Goya L (2005). Response of the antioxidant defense system to t-butyl hydroperoxide and hydrogen peroxide in a human hepatoma cell line (HepG2). J Biochem Mol Toxicol 19:119–128.

Ali AM, Ramos S, Mateos R, Bravo L, Goya L (2006). Quercetin protects human hepatoma cell line (HepG2) against oxidative stress induced by tert-butyl hydroperoxide. Toxicol. Appl. Pharmacol. 212:110–118.

Andrews NC, Faller DV (1991). A rapid micropreparation technique for extraction of DNA-binding proteins from limiting numbers of mammalian cells. Nucleic Acids Research 19: 2499.

Angulo P (2002). Nonalcoholic fatty liver disease. N Engl J Med 346:1221-1231.

Arias IM (1994). The Liver: Biology and Pathobiology. In: Lippincott-, Rabeen (eds), New York: 3th Edition.

Balsamo J, Leung T, Ernst H, ZainMKB, Hoffman S, Lilien J (1996). Regulated binding of PTP1B-like phosphatase to N-cadherin: control of cadherin-mediated adhesion by dephosphorylation of beta-catenin. J Cell Biol 134: 801-813.

Bandyopadhyay D, Kusari A, Kenner KA, Liu F, Chernoff J, Gustafson TA, Kusari J (1997). Protein-tyrosine phosphatase 1B complexes with the insulin receptor in vivo and is tyrosine-phosphorylated in the presence of insulin. J Biol Chem 272:1639–1645.

Bauer M, Schuppan D (2001). TGFbeta1 in liver fibrosis: time to change paradigms? FEBS Lett 502: 1-3.

Bessems JG, Vermeulen NP (2001). Paracetamol (acetaminophen)-induced toxicity: molecular and biochemical mechanisms, analogues and protective approaches. Crit Rev Toxicol 31: 55-138.

Bhattarai BR, Kafle B, Hwang JS, Khadka D, Lee SM, Kang JS, Ham SW, Han IO, Park H, Cho H (2009). Thiazolidinedione derivatives as PTP1B inhibitors with antihyperglycemic and antiobesity effects. Bioorg Med Chem Lett. 1:6161-6165.

Bloom DA, Jaiswal AK (2003). Phosphorylation of Nrf2 at Ser40 by protein kinase C in response to antioxidants leads to the release of Nrf2 from INrf2, but is not required for Nrf2 stabilization/accumulation in the nucleus and transcriptional activation of antioxidant response element-mediated NAD(P)H:quinone oxidoreductase-1 gene expression. J Biol Chem 278: 44675-44682.

Bouwens L, Baekeland M, De Zanger R, Wisse E (1986). Quantitation, tissue distribution and proliferation kinetics of Kupffer cells in normal rat liver. Hepatology 6: 718-722.

Brown-Shimer S, Johnson KA, Lawrence JB, Johnson, Walsh KA (1990). Molecular cloning and chromosome mapping of the human gene encoding protein phosphotyrosyl phosphatase 1B. Proc Natl Acad Sci U S A8713: 5148-5152.

Bugianesi E, Gastaldelli A, Vanni E, Gambino R, Cassader M, Baldi S, Ponti V, Pagano G, Ferrannini E, Rizzetto M (2005). Insulin resistance in non-diabetic patients with non-alcoholic fatty liver disease: sites and mechanisms. Diabetologia 48: 634-642.

Bursch W, Wastl U, Hufnagl K, Schulte-Hermann R (2005). No increase of apoptosis in regressing mouse liver after withdrawal of growth stimuli or food restriction. Toxicol Sci 85: 507-514.

Canbay A, Friedman S, Gores GJ (2004). Apoptosis: the nexus of liver injury and fibrosis. Hepatology 39: 273-278.

Chiarugi A, Meli E, Calvani M, Picca R, Baronti R, Camaioni E (2003). Novel isoquinolinone-derived inhibitors of poly(ADP-ribose) polymerase-1: pharmacological characterization and neuroprotective effects in an in vitro model of cerebral ischemia. J Pharmacol Exp Ther 305: 943-949.

Choi JH, Kim HS, Kim SH, Yang YR, Bae YS, Chang JS, Kwon HM, Ryu SH, Suh PG.(2006). Phospholipase C gamma1 negatively regulates growth hormone signalling by forming a ternary complex with Jak2 and protein tyrosine phosphatase-1B. Nat Cell Biol. 8:1389–1397.

Clampit JE, Meuth JL, Smith HT, Reilly RM, Jirousek MR, Trevillyan JM, Rondinone CM (2003). Reduction of protein-tyrosine phosphatase-1B increases insulin signaling in FAO hepatoma cells. Biochem Biophys Res Commun 300: 261-267.

Combs AP, Yue EW, Bower M, Ala PJ, Wayland B, Douty B, Takvorian A, Polam P, Wasserman Z, Zhu W, Crawley ML, Pruitt J, Sparks R, Glass B, Modi D,McLaughlin E, Bostrom L, Li M, Galya L, Blom K, Hillman M, Gonneville L, Reid BG, Wei M, Becker-Pasha M, Klabe R, Huber R, Li Y, Hollis G, Burn TC, Wynn R,Liu P, Metcalf B (2005.) Structure-based design and discovery of protein tyrosine phosphatase inhibitors incorporating novel isothiazolidinone heterocyclic phosphotyrosine mimetics. Journal of Medicinal Chemistry 48:6544–6548.

Copps KD, White MF (2012). Regulation of insulin sensitivity by serine/threonine phosphorylation of insulin receptor substrate proteins IRS1 and IRS2. Diabetologia 55:2565-2582.

Corcoran GB, Racz WJ, Smith CV, Mitchell JR (1985). Effects of N-acetylcysteine on acetaminophen covalent binding and hepatic necrosis in mice. J Pharmacol Exp Ther 232: 864-872.

Cullinan SB, Zhang D, Hannink M, Arvisais E, Kaufman RJ, Diehl JA (2003). Nrf2 is a direct PERK substrate and effector of PERK-dependent cell survival. Mol Cell Biol 23: 7198-7209.

Cullinan SB, Gordan JD, Jin J, Harper JW, Diehl JA (2004). The Keap1-BTB protein is an adaptor that bridges Nrf2 to a Cul3-based E3 ligase: oxidative stress sensing by a Cul3-Keap1 ligase. Mol Cell Biol 24: 8477-8486.

Czaja M J (2007). Liver Dis: Semin 27: 378–389.

Dadke S, Kusari A, Kusari J (2001). Phosphorylation and activation of protein tyrosine phosphatase (PTP) 1B by insulin receptor. Mol Cell Biochem 221: 147-154.

Dahlin DC, Miwa GT, Lu AY, Nelson SD (1984). N-acetyl-p-benzoquinone imine: a cytochrome P-450-mediated oxidation product of acetaminophen. Proc Natl Acad Sci U S A 81: 1327-1331

D'Apolito M, Du X, Zong H, Catucci A, Maiuri L, Trivisano T, Pettoello-Mantovani M, Campanozzi A, Raia V, Pessin JE, Brownlee M, Giardino I (2010). Urea-induced ROS generation causes insulin resistance in mice with chronic renal failure. J Clin Invest 120:203-213.

Darzynkiewicz Z, Bruno S, Del Bino G, Gorczyca W, Hotz MA, Lassota P, Traganos F (1992). Features of apoptotic cells measured by flow cytometry.Cytometry 13:795-808.

D'Cruz SC, Jubendradass R, Mathur PP (2012). Bisphenol A induces oxidative stress and decreases levels of insulin receptor substrate 2 and glucose transporter 8 in rat testis. Reprod Sci 19:163-172.

DeFronzo RA (2004). Pathogenesis of type 2 diabetes mellitus. Medical Clinics of North America 88:787–835.

Delibegovic M, Zimmer D, Kauffman C, Rak K, Hong EG, Cho YR, Kim JK, Kahn BB, Neel BG, Bence KK (2009). Liver-specific deletion of protein-tyrosine phosphatase 1B (PTP1B) improves metabolic syndrome and attenuates diet-induced endoplasmic reticulum stress. Diabetes 58: 590-599.

Dhakshinamoorthy S, Jaiswal AK (2001). Functional characterization and role of INrf2 in antioxidant response element-mediated expression and antioxidant induction of NAD(P)H:quinone oxidoreductase1 gene. Oncogene 20: 3906-3917.

Dixit R, Boelsterli UA (2007). Healthy animals and animal models of human disease(s) in safety assessment of human pharmaceuticals, including therapeutic antibodies. Drug Discov Today 12: 336-342.

Doherty DG, O'Farrelly C (2000). Innate and adaptive lymphoid cells in the human liver. Immunol Rev 174: 5-20.

Dong H, Haining RL, Thummel KE, Rettie AE, Nelson SD (2000). Involvement of human cytochrome P450 2D6 in the bioactivation of acetaminophen. Drug Metab Dispos 28: 1397-1400.

Egawa K, Maegawa H, Shimizu S, Morino K, Nishio Y, Bryer-Ash M, Cheung AT, Kolls JK, Kikkawa R, Kashiwagi A (2001). Protein-tyrosine phosphatase-1B negatively regulates insulin signaling in l6 myocytes and Fao hepatoma cells. J Biol Chem 276: 10207-10211.

Eichhorst ST, Krueger A, Muerkoster S, Fas SC, Golks A, Gruetzner U, Schubert L, Opelz C, Bilzer M, Gerbes AL, Krammer PH (2004). Suramin inhibits death receptor-induced apoptosis in vitro and fulminant apoptotic liver damage in mice. Nat Med 10: 602-609.

Elchebly M, Payette P, Michaliszyn E, Cromlish W, Collins S, Loy AL, Normandin D, Cheng A, Himms-Hagen J, Chan CC, Ramachandran C, Gresser MJ, Tremblay ML, Kennedy BP (1999). Increased insulin sensitivity and obesity resistance in mice lacking the protein tyrosine phosphatase-1B gene. Science 283: 1544-1548.

Enomoto A, Itoh K, Nagayoshi E, Haruta J, Kimura T, O'Conno T, Harada T, Yamamoto M (2001). High sensitivity of Nrf2 knockout mice to acetaminophen hepatotoxicity associated with decreased expression of ARE-regulated drug metabolizing enzymes and antioxidant genes. Toxicol Sci 59: 169-177.

Fabregat I, Roncero C, Fernandez M (2007). Survival and apoptosis: a dysregulated balance in liver cancer. Liver Int 27: 155-162.

Fernández-Millán E, de Toro-Martín J, Lizárraga-Mollinedo E, Escrivá F, Alvarez C (2013). Role of endogenous IL-6 in the neonatal expansion and functionality of Wistar rat pancreatic alpha cells. Diabetologia 56:1098-107.

Fernández-Veledo S, Nieto-Vazquez I, Rondinone CM, Lorenzo M (2006). Liver X receptor agonists ameliorate TNFalpha-induced insulin resistance in murine brown adipocytes by downregulating protein tyrosine phosphatase-1B gene expression.Diabetologia. 49:3038-3048.

Filippini M, Bazzani C, Zingarelli S, Ziglioli, T, Nuzzo M, Vianelli M, Biasini Rebaioli C, Cattaneo R, Gorla R (2008). Anti-TNFalpha agents in elderly patients with rheumatoid arthritis: a study of a group of 105 over sixty five years old patients. Reumatismo 60: 41-49.

Frangioni JV, Oda A, Smith M, Salzman EW, Neel BG (1993). Calpain-catalyzed cleavage and subcellular relocation of protein phosphotyrosine phosphatase1B (PTP1B) in human platelets. EMBO J.12: 4843-4856.

Friedman SL (2000). Molecular regulation of hepatic fibrosis, an integrated cellular response to tissue injury. J Biol Chem 275: 2247-2250.

Furukawa M, Xiong Y (2005). BTB protein Keap1 targets antioxidant transcription factor Nrf2 for ubiquitination by the Cullin 3-Roc1 ligase. Mol Cell Biol 25: 162-171.

Haj FG, Markova B, Klaman LD, Bohmer FD, Neel BG (2003) Regulation of receptor tyrosine kinase signaling by protein tyrosine phosphatase-1B. J Biol Chem 278: 739-744

-**Haj FG, Zabolotny JM, Kim YB, Kahn BB, Neel BG** (2005). Liver-specific protein-tyrosine phosphatase 1B (PTP1B) re-expression alters glucose homeostasis of PTP1B-/-mice. J Biol Chem 280:15038-15046.

Han D, Shinohara M, Ybanez MD, Saberi B, Kaplowitz N (2011). Signal transduction pathways involved in drug-induced liver injury. Handb Exp Pharmacol: 267-310.

Carmelo GM ,Oreste LL, Rafael M, Águeda GR, Maria MC, Tamara LR, Leonor GP, Javier VC, Marta C , Lisardo B, Ángela MV, Paloma MS (2011). Hepatic insulin resistance is associated with increased apoptosis and fibrogenesis in nonalcoholic steatohepatitis and chronic hepatitis C. J Hepatol 54: 142-152

Geyer R, Wee S, Anderson S, Yates J, Wolf DA (2003). BTB/POZ domain proteins are putative substrate adaptors for cullin 3 ubiquitin ligases. Mol Cell 12: 783-790.

Gillette JR, Nelson SD, Mulder GJ, Jollow DJ, Mitchell JR, Pohl LR, Hinson JA, Nelson SD, Mulder GJ (1981). Formation of chemically reactive metabolites of phenacetin and acetaminophen. Adv Exp Med Biol 136 Pt B: 931-950.

Ghosh A, Sil PC (2009). Protection of acetaminophen induced mitochondrial dysfunctions and hepatic necrosis via Akt-NF-kappaB pathway: role of a novel plant protein. Chem Biol Interact 177: 96-106.

Goldstein BJ (2001). Protein-tyrosine phosphatase 1B (PTP1B) a novel therapeutic target for type 2 diabetes mellitus, obesity and related states of insulin resistance. Curr Drug Targets Immune Endocr Metabol Disord 1: 265-275.

Gonzalez RA, Escribano O, Alba J, Rondinone CM, Benito M, Valverde AM (2007). Levels of protein tyrosine phosphatase 1B determine susceptibility to apoptosis in serum-deprived hepatocytes. J Cell Physiol 212: 76-88.

Gonzalez RA, Gutierrez JA, Sanz-Gonzalez S, Ros M, Burks DJ, Valverde AM (2010). Inhibition of PTP1B restores IRS1-mediated hepatic insulin signaling in IRS2-deficient mice. Diabetes 59:588-599.

González RA, Más-Gutierrez JA, Mirasierra M, Fernandez-Pérez A, Lee YJ, Ko HJ, Kim JK, Romanos E, Carrascosa JM, Ros M, Vallejo M, Rondinone CM, Valverde AM (2012). Essential role of protein tyrosine phosphatase 1B in obesity-induced inflammation and peripheral insulin resistance during aging. Aging Cell 11: 284-296.

Granado-Serrano AB, Martín MA, Izquierdo-Pulido M, Goya L, Bravo L, Ramos S (2007). Molecular mechanisms of (−)-epicatechin and chlorogenic

acid on the regulation of the apoptotic and survival/proliferation pathways in a human hepatoma cell line. J Agric Food Chem 55:2020–7.

Grisham MB (2004). Reactive oxygen species in immune responses. Free Radic Biol Med 36: 1479-1480.

Gum RJ, Gaede LL, Koterski SL, Heindel M, Clampit JE, Zinker BA, Trevillyan, JM, Ulrich RG, Jirousek MR, Rondinone CM (2003). Reduction of protein tyrosine phosphatase 1B increases insulin-dependent signaling in ob/ob mice. Diabetes 52: 21-28.

Gunawan BK, Liu ZX, Han D, Hanawa N, Gaarde WA, Kaplowitz N (2006). c-Jun N-terminal kinase plays a major role in murine acetaminophen hepatotoxicity. Gastroenterology 131: 165-178.

Gutterman DD, Miura H, Liu Y (2005). Redox modulation of vascular tone: focus of potassium channel mechanisms of dilation. Arterioscler Thromb Vasc Biol 25: 671-678.

Haj FG, Verveer PJ, Squire A, Neel BG, Bastiaens PI (2002). Imaging sites of receptor dephosphorylation by PTP1B on the surface of the endoplasmic reticulum. Science 295:1708-1711.

Haj FG, Markova B, Klaman LD, Bohmer FD, Neel BG (2003). Regulation of receptor tyrosine kinase signaling by protein tyrosine phosphatase-1B. J Biol Chem 278:739-744.

Haj FG, Zabolotny JM, Kim YB, Kahn BB, Neel BG (2005). Liver-specific protein-tyrosine phosphatase 1B (PTP1B) re-expression alters glucose homeostasis of PTP1B-/-mice. J Biol Chem 280:15038-15046.

Han D, Ybanez MD, Ahmadi S, Yeh K, Kaplowitz N (2009). Redox regulation of tumor necrosis factor signaling. Antioxid Redox Signal. 11: 2245–2263.

Hanawa N, Shinohara M, Saberi B, Gaarde WA, Han D, Kaplowitz N (2008). Role of JNK translocation to mitochondria leading to inhibition of mitochondria bioenergetics in acetaminophen-induced liver injury. J Biol Chem 283: 13565-13577.

Haque A, Andersen JN, Salmeen A,Barford D, Tonks I NK (2011). conformation-sensing antibodies stabilize the oxidized form of PTP1B and inhibit its phosphatase activity.Cell 147:185–198.

Henderson NC, Pollock KJ, Frew J, MackinnonAC, Flavell RA, Davis RJ, SethiT, Simpson KJ (2007). Critical role of c-jun (NH2) terminal kinase in paracetamol- induced acute liver failure. Gut 56: 982-990.

Hensley K, Robinson KA, Gabbita SP, Salsman S, Floyd RA (2000). Reactive oxygen species, cell signaling, and cell injury. Free Radic Biol Med 28: 1456-1462.

Hernandez MV, Sala MG, Balsamo J, Lilien J, Arregui CO (2006). ER-bound PTP1B is targeted to newly forming cell-matrix adhesions. J. Cell Sci.119: 1233–1243

Higuchi Y (2003). Chromosomal DNA fragmentation in apoptosis and necrosis induced by oxidative stress. Biochem Pharmacol 66: 1527-1535.

Hinson JA, Pohl LR, Monks TJ, Gillette JR, Guengerich FP (1980). 3-Hydroxyacetaminophen: a microsomal metabolite of acetaminophen. Evidence against an epoxide as the reactive metabolite of acetaminophen. Drug Metab Dispos 8: 289-294.

Huo Y, Qiu WY, Pan Q, Yao YF, Xing K, Lou MF (2009). Reactive oxygen species (ROS) are essential mediators in epidermal growth factor (EGF)-stimulated corneal epithelial cell proliferation, adhesion, migration, and wound healing. Exp Eye Res 89: 876-886.

Imai H, Nakagawa Y (2003). Biological significance of phospholipid hydroperoxide glutathione peroxidase (PHGPx, GPx4) in mammalian cells. Free Radic Biol Med 34: 145-169.

Ingley E (2008). Src family kinases: regulation of their activities, levels and identification of new pathways. Biochimica et Biophysica Acta 1784:56–65.

Itoh K, Wakabayashi N, Katoh Y, Ishii T, Igarashi K, Engel JD, Yamamoto M.
(1999). Keap1 represses nuclear activation of antioxidant responsive elements by Nrf2 through binding to the amino-terminal Neh2 domain. Genes Dev 13: 76-86.

Itoh K, Chiba T, Takahashi S, Ishii T, Igarashi K, Katoh Y, Oyake T, Hayashi N, Satoh K, Hatayama I, Yamamoto M, Nabeshima Y (1997). An Nrf2/small Maf heterodimer mediates the induction of phase II detoxifying enzyme genes through antioxidant response elements. Biochem Biophys Res Commun 236:313-22.

Jaeschke H, Bajt ML (2006). Intracellular signaling mechanisms of acetaminophen-induced liver cell death. Toxicol Sci 89: 31-41.

Jain AK, Bloom DA, Jaiswal AK (2005). Nuclear import and export signals in control of Nrf2. J Biol Chem 280: 29158-29168.

Jain AK, Jaiswal AK (2007). GSK-3beta acts upstream of Fyn kinase in regulation of nuclear export and degradation of NF-E2 related factor 2. J Biol Chem 282: 16502-16510.

James LP, Mayeux PR, Hinson JA (2003). Acetaminophen-induced hepatotoxicity. Drug Metab Dispos 31: 1499-1506.

Jollow DJ, Mitchell JR, Potter WZ, Davis DC, Gillette JR, Brodie BB (1973). Acetaminophen-induced hepatic necrosis. II. Role of covalent binding in vivo. J Pharmacol Exp Ther 187: 195-202.

Jollow DJ, Mitchell JR, Zampaglione N, Gillette JR (1974). Bromobenzene-induced liver necrosis. Protective role of glutathione and evidence for 3,4-bromobenzene oxide as the hepatotoxic metabolite. Pharmacology 11: 151-169.

Johnson GL, Nakamura K (2007). The c-jun kinase/stress-activated pathway: regulation, function and role in human disease. Biochim Biophys Acta 1773: 1341-1348.

Johnson AM, Olefsky JM (2013).The origins and drivers of insulin resistance. Cell 14:673-684.

Kang MI, Kobayashi A, Wakabayashi N, Kim SG, Yamamoto M (2004). Scaffolding of Keap1 to the actin cytoskeleton controls the function of Nrf2 as key regulator of cytoprotective phase 2 genes. Proc Natl Acad Sci U S A 101: 2046-2051

Kannoji A, Phukan S, Sudher Babu V, Balaji VN (2008). GSK3beta: a master switch and a promising target. Expert Opin Ther Targets 11:1443–1455.

Kaplowitz N (2004). Acetaminophen hepatoxicity: what do we know, what don't we know, and what do we do next? Hepatology 40: 23-26.

Kaplowitz N (2005). Idiosyncratic drug hepatotoxicity. Nat Rev Drug Discov 4: 489-499.

Kasibhatla B, Wos J, Peters KG (2007). Targeting protein tyrosine phosphatase to enhance insulin action for the potential treatment of diabetes. Curr Opin Investig Drugs 8:805–813.

Kaspar JW, Niture SK, Jaiswal AK (2009). Nrf2:INrf2 (Keap1) signaling in oxidative stress. Free Rad. Biol. Med. 47:1304-1309.

Klaman LD, Boss O, Peroni OD, Kim JK, Martino JL, Zabolotny JM, Moghal N, Lubkin M, Kim YB, Sharpe AH, Stricker-Krongrad A, Shulman GI, Neel BG, Kahn BB (2000). Increased energy expenditure, decreased adiposity, and tissue-specific insulin sensitivity in protein-tyrosine phosphatase 1B-deficient mice. Mol Cell Biol 20: 5479-5489.

Klover PJ, Mooney RA (2004). Hepatocytes: critical for glucose homeostasis. Int J Biochem Cell Biol 36: 753-758.

Kobayashi A, Kang MI, Okawa H, Ohtsuji M, Zenke Y, Chiba T, Igarashi K, Yamamoto M (2004). Oxidative stress sensor Keap1 functions as an adaptor for Cul3-based E3 ligase to regulate proteasomal degradation of Nrf2. Mol Cell Biol 24: 7130-7139.

Kobayashi A, Kang MI, Watai Y, Tong KI , Shibata T, Uchida K, Yamamoto M (2006). Oxidative and electrophilic stresses activate Nrf2 through inhibition of ubiquitination activity of Keap1. Mol Cell Biol 26: 221-229.

Kon K, Kim JS, Jaeschke H, Lemasters JJ (2004). Mitochondrial permeability transition in acetaminophen-induced necrosis and apoptosis of cultured mouse hepatocytes. Hepatology 40: 1170-1179

Kuchay SM, Kim N, Grunz EA, Fay WP. Chishti AH (2007). Double knockouts reveal that protein tyrosine phosphatase 1B is a physiological target of calpain-1 in platelets. Mol. Cell Biol. 27:6038-6052.

Kuntz ED (2008b). Morphology of the Liver in Hepatology. In: Heidelberg SB Textbook and Atlas, Berlin. (ed pp15-33).

Larson AM, Polson J, Fontana RJ, Davern TJ, Lalani E, Hynan LS, Reisch JS, Schiodt FV, Ostapowicz G, Shakil AO, Lee WM (2005). Acetaminophen-induced acute liver failure: results of a United States multicenter, prospective study. Hepatology 42: 1364-1372.

Larter CZ, Farrell GC (2006). Insulin resistance, adiponectin, cytokines in NASH: Which is the best target to treat?. J Hepatol 44: 253-261.

Latchoumycandane C, Goh CW, Ong MM, Boelsterli UA (2007). Mitochondrial protection by the JNK inhibitor leflunomide rescues mice from acetaminophen-induced liver injury. Hepatology 45: 412-421.

Lauer GM, Walker BD (2001). Hepatitis C virus infection. N Engl J Med 345: 41-52.

Lee WM (2004). Acetaminophen and the U.S. Acute Liver Failure Study Group: lowering the risks of hepatic failure. Hepatology 40: 6-9

Lee WM (2007). Acetaminophen toxicity: changing perceptions on a social/medical issue. Hepatology 46: 966-970.

Lembertas AV, Perusse L, Chagnon YC, Fisler JS, Warden CH, Purcell-Huynh DA, Dionne FT, Gagnon J, Nadeau A, Lusis AJ, Bouchard C (1997). Identification of an obesity quantitative trait locus on mouse chromosome 2 and evidence of linkage to body fat and insulin on the human homologous region 20q. J Clin Invest 100:1240–1247.

Liu H, Lo CR, Czaja MJ (2002). Hepatology 35: 772–778.

Lu X, Malumbres R, Shields B, Jiang X, Sarosiek KA, Natkunam PY, Tiganis T Lossos IS (2008). PTP1B is a negative regulator of interleukin 4-induced STAT6 signaling. Blood 112: 4098-4108.

Marieb EN (2001). Human Anatomy & Physiology. 5th Edition.

Meng TC, Tonks NK (2003). Analysis of the regulation of protein tyrosine phosphatases in vivo by reversible oxidation. Methods Enzymol. 366:304–318.

Mitchell JR, Jollow DJ, Gillette JR, Brodie BB (1973a) Drug metabolism as a cause of drug toxicity. Drug Metab Dispos 1: 418-423.

Mitchell JR, Jollow DJ, Potter WZ, Gillette JR, Brodie BB (1973b). Acetaminophen-induced hepatic necrosis. IV. Protective role of glutathione. J Pharmacol Exp Ther 187: 211-217.

Netter FH (2006) Atlas of human anatomy. In: Elsevier S (ed), Philadelphia.

Nguyen T, Sherratt PJ, Huang HC, Yang CS, Pickett CB (2003) Increased protein stability as a mechanism that enhances Nrf2-mediated transcriptional activation of the antioxidant response element. Degradation of Nrf2 by the 26 S proteasome. J Biol Chem 278: 4536-4541.

Nieto-Vazquez I, Fernández-Veledo S, de Alvaro C, Rondinone CM, Valverde AM, Lorenzo M (2007). Protein-tyrosine phosphatase 1B-deficient myocytes show increased insulin sensitivity and protection against tumor necrosis factor-alpha-induced insulin resistance. Diabetes 56:404-13.

Nieto-Vazquez I, Fernandez-Veledo S, de Alvaro C, Lorenzo M (2008). Dual role of interleukin-6 in regulating insulin sensitivity in murine skeletal muscle. Diabetes 57: 3211-3221.

Niture SK, Jaiswal AK (2009). Prothymosin-alpha mediates nuclear import of the INrf2/Cul3 Rbx1 complex to degrade nuclear Nrf2. J Biol Chem 284: 13856-13868.

Niture SK, Jain AK, Shelton PM, Jaiswal AK (2011). Src subfamily kinases regulate nuclear export and degradation of transcription factor Nrf2 to switch off Nrf2-mediated antioxidant activation of cytoprotective gene expression. J Biol Chem 286: 28821-28832.

Nordlie RC, Foster JD, Lange AJ (1999). Regulation of glucose production by the liver. Annu Rev Nutr 19: 379-406.

Ockner RK (2001). Apoptosis and liver diseases: recent concepts of mechanism and significance. J Gastroenterol Hepatol 16: 248-260.

Ortiz C, Caja L, Bertran E, Gonzalez-Rodriguez A., Valverde A.M., Fabregat I., Sancho P (2012) Protein-tyrosine Phosphatase 1B (PTP1B) Deficiency Confers Resistance to Transforming Growth Factor-beta (TGF-beta)-induced Suppressor Effects in Hepatocytes. J Biol Chem 287: 15263-15274.

Ostapowicz G, Fontana RJ, Schiodt FV, Larson A, Davern TJ, Han SH, McCashland TM, Obaid Shakil A, Hay JE, Hynan L, Crippin JS, Blei AT, Samuel G, Reisch J, Lee WM (2002). Results of a prospective study of acute liver failure at 17 tertiary care centers in the United States. Ann Intern Med 137: 947-954.

Perez M, Haschke B, Donato NJ (1999). Differential expression and translocation of protein tyrosine phosphatase 1B-related proteins in ME-180 tumor cells expressing apoptotic sensitivity and resistance to tumor necrosis factor: potential interaction with epidermal growth factor receptor. Oncogene 18: 967-978.

Peterson RG, Rumack BH (1977). Treating acute acetaminophen poisoning with acetylcysteine. JAMA 237: 2406-2407.

Pilkis SJ, Granner DK (1992). Molecular physiology of the regulation of hepatic gluconeogenesis and glycolysis. Annu Rev Physiol 54: 885-909.

Piperno E, Berssenbruegge DA (1976). Reversal of experimental paracetamol toxicosis with N-acetylcysteine. Lancet 2: 738-739.

Piwkowska A , Rogacka D, Angielski S, Jankowski M (2012). Hydrogen peroxide induces activation of insulin signaling pathway via AMP-dependent kinase in podocytes. Biochemical and biophysical research communications 428 :167-72.

Potter WZ, Davis DC, Mitchell JR, Jollow DJ, Gillette JR, Brodie BB (1973). Acetaminophen-induced hepatic necrosis. 3. Cytochrome P-450-mediated covalent binding in vitro. J Pharmacol Exp Ther 187: 203-210.

Potter DW, Hinson JA (1987). Mechanisms of acetaminophen oxidation to N-acetyl-P-benzoquinone imine by horseradish peroxidase and cytochrome P-450. J Biol Chem 262: 966-973.

Prescott LF (1977). Iatrogenic complications of drug overdosage and poisoning. Acta Pharmacol Toxicol (Copenh) 41 Suppl 2: 64.

Prescott LF (1980). Hepatotoxicity of mild analgesics. Br J Clin Pharmacol 10 Suppl 2: 373S-379S.

Prescott LF (1983). Paracetamol overdosage. Pharmacological considerations and clinical management. Drugs 25: 290-314.

Pruessner JC, Kirschbaum C, Meinlschmidt G, Hellhammer DH (2003). Two formulas for the computation of the area under the curve represent measures of total hormone concentration versus time-dependent change. Psychoneuroendocrinology 28: 916–931.

Rada P, Rojo AI, Chowdhry S, McMahon M, Hayes JD, Cuadrado A (2011). SCF/{beta}-TrCP promotes glycogen synthase kinase 3-dependent degradation of the Nrf2 transcription factor in a Keap1-independent manner. Mol Cell Biol. 31:1121–1133.

Radziuk J, Pye S (2001). Production and metabolic clearance of glucose under basal conditions in Type II (non-insulin-dependent) diabetes mellitus. Diabetologia *44*: 983-991.

Ramachandran R, Kakar S (2009). Histological patterns in drug-induced liver disease. J Clin Pathol 62: 481-492.

Raucy JL, Lasker JM, Lieber CS, Black M (1989). Acetaminophen activation by human liver cytochromes P450IIE1 and P450IA2. Arch Biochem Biophys 271: 270-283.

Ravichandran LV, Esposito DL, Chen J,Quan MJ (2001). Protein kinase C-zeta phosphorylates insulin receptor substrate-1 and impairs its ability to activate phosphatidylinositol 3-kinase in response to insulin. J. Biol. Chem. 276:3543-3549.

Reid AB, Kurten RC, McCullough SS, Brock RW, Hinson JA (2005). Mechanisms of acetaminophen-induced hepatotoxicity: role of oxidative stress and mitochondrial permeability transition in freshly isolated mouse hepatocytes. J Pharmacol Exp Ther 312: 509-516.

Richert S, Wehr NB, Stadtman ER, Levine RL (2002). Assessment of skin carbonyl content as a non-invasive measure of biological age. Arch Biochem Biophys 397:430–432.

Rockey DC (2001). Hepatic blood flow regulation by stellate cells in normal and injured liver. Semin Liver Dis 21: 337-349.

Rumack BH, Peterson RC, Koch GG, Amara IA (1981). Acetaminophen overdose. 662 cases with evaluation of oral acetylcysteine treatment. Arch Intern Med 141: 380-385.

Saberi B, Shinohara M, Ybanez MD, Hanawa N, Gaarde WA, Kaplowitz N, Han D (2008) Regulation of H(2)O(2)-induced necrosis by PKC and AMP-activated kinase signaling in primary cultured hepatocytes. Am J Physiol Cell Physiol 295: C50-63.

Salmeen A, Andersen JN, Myers MP, Tonks NK, Barford D (2000). Molecular basis for the dephosphorylation of the activation segment of the insulin receptor by protein tyrosine phosphatase 1B.Mol. Cell 6:1401–1412.

Saltiel AR, Kahn CR (2001). Insulin signalling and the regulation of glucose and lipid metabolism. Nature 414: 799-806.

Sanderson SO, Smyrk TC (2005). The use of protein tyrosine phosphatase 1B and insulin receptor immunostains to differentiate nonalcoholic from alcoholic steatohepatitis in liver biopsy specimens. Am J Clin Pathol 123: 503-509.

Sangwan V, Paliouras GN, Cheng A, Dube N, Tremblay ML, Park M (2006). Protein-tyrosine phosphatase 1B deficiency protects against Fas-induced hepatic failure. J Biol Chem 281: 221-228.

Schulte-Hermann R, Bursch W, Grasl-Kraupp B (1995). Active cell death (apoptosis) in liver biology and disease. Prog Liver Dis 13: 1-35.

Seely BL, Staubs PA, Reichart DR, Berhanu P, Milarski KL, Saltiel AR, Kusari J, Olefsky JM (1996). Protein tyrosine phosphatase 1B interacts with the activated insulin receptor. Diabetes. 45:1379–1385.

Seki S, Habu Y, , Kawamura T, Takeda K, Dobashi H, Ohkawa T, Hiraide H (2000). The liver as a crucial organ in the first line of host defense: the roles of Kupffer cells, natural killer (NK) cells and NK1.1 Ag+ T cells in T helper 1 immune responses. Immunol Rev 174: 35-46.

Shelton P, Jaiswal AK (2013). The transcription factor NF-E2-related factor 2 (Nrf2): a protooncogene. FASEB J. 27: 414-23.

Shinohara M, Ybanez MD, Win S, Than TA, Jain S, Gaarde WA, Han D, Kaplowitz N (2010). Silencing glycogen synthase kinase-3beta inhibits acetaminophen hepatotoxicity and attenuates JNK activation and loss of glutamate cysteine ligase and myeloid cell leukemia sequence 1. J Biol Chem 285: 8244-8255.

Schreiber E, Matthias P, Muller MM, Schaffner W (1989). Rapid detection of octamer binding proteins with "mini- extracts" prepared from a small number of cells. Nucleic Acids Res. 17: 6419.

Snawder JE, Roe AL, Benson RW, Roberts DW (1994). Loss of CYP2E1 and CYP1A2 activity as a function of acetaminophen dose: relation to toxicity. Biochem Biophys Res Commun 203: 532-539.

Stewart D, Killeen E, Naquin R, Alam S, Alam J (2003). Degradation of transcription factor Nrf2 via the ubiquitin-proteasome pathway and stabilization by cadmium. J Biol Chem 278: 2396-2402.

Taniguchi CM, Emanuelli B, Kahn CR (2006). Critical nodes in signalling pathways: insights into insulin action. Mol Cell Biol 7:85–96.

Thames G (2004). Drug-induced liver injury: what you need to know. Gastroenterol Nurs 27: 31-33.

Thummel KE, Lee CA, Kunze KL, Nelson SD, Slattery JT (1993). Oxidation of acetaminophen to N-acetyl-p-aminobenzoquinone imine by human CYP3A4. Biochem Pharmacol 45: 1563-1569.

Tong KI, Katoh Y, Kusunoki H, Itoh K, Tanaka T, Yamamoto M (2006). Keap1 recruits Neh2 through binding to ETGE and DLG motifs: characterization of the two-site molecular recognition model. Mol Cell Biol 26: 2887-2900.

Tong KI, Kobayashi A, Katsuoka F, Yamamoto M (2006b). Two-site substrate recognition model for the Keap1-Mrf2 system: a hinge and latch mechanism. Biol. Chem. 387:1311-1320.

Tonks NK, Diltz CD, Fischer EH (1988). Purification of protein-tyrosine phosphatases from human placenta. Journal of Biological Chemistry 263: 6722–6730.

Tovar V, Alsinet C, Villanueva A, Hoshida Y , Chiang DY, Sole M, Thung S, Moyano S, Toffanin S, Minguez B, Cabellos L, Peix J, Schwartz M, Mazzaferro V, Bruix J, Llovet JM (2010). IGF activation in a molecular subclass of hepatocellular carcinoma and pre-clinical efficacy of IGF-1R blockage. J Hepatol 52: 550-559.

Uetrecht J (2008). Idiosyncratic drug reactions: past, present, and future. Chem Res Toxicol 21: 84-92

Vinayagamoorthi R, Bobby Z, Sridhar MG (2008). Antioxidants preserve redox balance and inhibit c-Jun-N-terminal kinase pathway while improving insulin signaling in fat-fed rats: evidence for the role of oxidative stress on IRS-1 serine phosphorylation and insulin resistance. J Endocrinol 197: 287-296.

Wakabayashi N, Itoh K, Wakabayashi J, Motohashi H, Noda S, Takahashi S, Imakado S, Kotsuji T, Otsuka F, Roop DR, Harada T, Engel JD, Yamamoto M (2003). Keap1-null mutation leads to postnatal lethality due to constitutive Nrf2 activation. Nat. Genet. 35: 238–245.

Wang Y, Singh R, Lefkowitch JH, Rigoli RM, Czaja MJ (2006). Tumor necrosis factor-induced toxic liver injury results from JNK2-dependent activation of caspase-8 and the mitochondrial death pathway. J Biol Chem 281:15258–15267.

Welch KD, Wen B, Goodlett DR, Yi EC, Lee H, Reilly TP, Nelson SD, Pohl LR (2005). Proteomic identification of potential susceptibility factors in drug-induced liver disease. Chem Res Toxicol 18: 924-933.

Welch KD, Reilly TP, Bourdi M, Hays T, Pise-Masison , Radonovich MF, Brady JN, Dix dj, PohI LR (2006). Genomic identification of potential risk factors during acetaminophen-induced liver disease in susceptible and resistant strains of mice. Chem Res Toxicol 19: 223-233.

Welder AA, Acosta D (1994). Enzyme leakage as an indicator of cytotoxicity in culture cells. In: Tyson, C.A.; Franzier, J.M. In vitro toxicity indicators: methods in toxicology. New York: Academic press, pp 46-49.

Weston CR, Davis RJ (2002). The JNK signal transduction pathway. Current Opinion in Genetics and Development 12:14–21.

Wiger R, Finstad HS, Hongslo JK, Haug K, Holme JA (1997). Paracetamol inhibits cell cycling and induces apoptosis in HL-60 cells. Pharmacol Toxicol 81: 285-293.

Xiao L, Xie X, Zhai Y (2010). Functional crosstalk of CAR-LXR and ROR-LXR in drug metabolism and lipid metabolism. Adv Drug Deliv Rev 62: 1316-1321.

Zabolotny JM, Bence-Hanulec KK, Stricker-Krongrad A, Haj F, Wang Y, Minokoshi Y, Kim YB, Joel K (2002). PTP1B regulates leptin signal transduction in vivo. Dev Cell 2: 489-495.

Zabolotny JM, Kim YB, Welsh LA, Kershaw EE, Neel BG, Kahn BB (2008). Protein-tyrosine phosphatase 1B expression is induced by inflammation in vivo. J Biol Chem 283: 14230-14241.

ANNEX

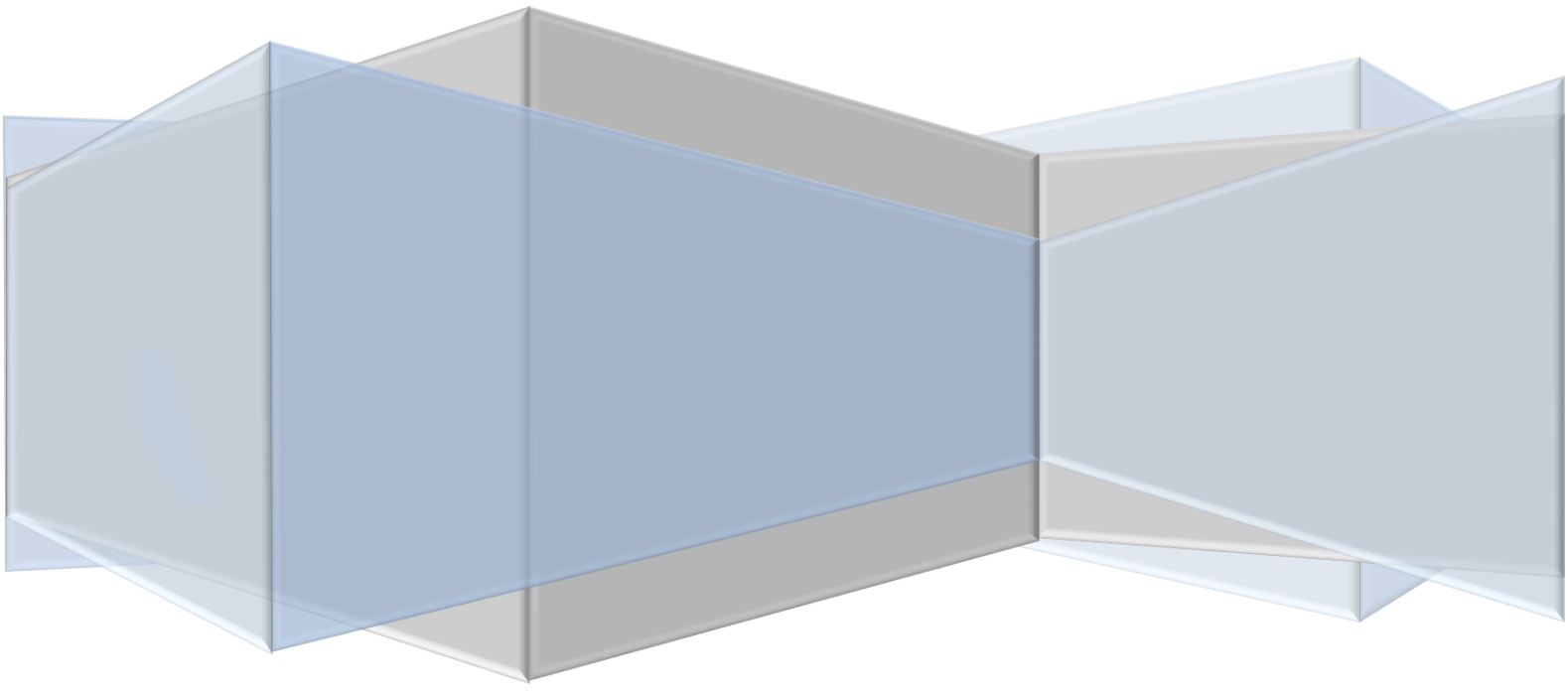

OPEN

Citation: Cell Death and Disease (2013) 4, e626; doi:10.1038/cddis.2013.150

www.nature.com/cddis

Protein tyrosine phosphatase 1B modulates GSK3β/Nrf2 and IGFIR signaling pathways in acetaminophen-induced hepatotoxicity

MA Mobasher[1,2], Á González-Rodriguez[1,2], B Santamaría[1,2], S Ramos[3], MÁ Martín[2,3], L Goya[3], P Rada[1,4], L Letzig[5], LP James[5], A Cuadrado[1,4], J Martín-Pérez[1], KJ Simpson[6], J Muntané[7,8] and AM Valverde*[,1,2]

Acute hepatic failure secondary to acetaminophen (APAP) poisoning is associated with high mortality. Protein tyrosine phosphatase 1B (PTP1B) is a negative regulator of tyrosine kinase growth factor signaling. In the liver, this pathway confers protection against injury. However, the involvement of PTP1B in the intracellular networks activated by APAP is unknown. We have assessed PTP1B expression in APAP-induced liver failure in humans and its role in the molecular mechanisms that regulate the balance between cell death and survival in human and mouse hepatocytes, as well as in a mouse model of APAP-induced hepatotoxicity. PTP1B expression was increased in human liver tissue removed during liver transplant from patients for APAP overdose. PTP1B was upregulated by APAP in primary human and mouse hepatocytes together with the activation of c-jun (NH2) terminal kinase (JNK) and p38 mitogen-activated protein kinase (p38 MAPK), resulting in cell death. Conversely, Akt phosphorylation and the antiapoptotic Bcl2 family members BclxL and Mcl1 were decreased. PTP1B deficiency in mouse protects hepatocytes against APAP-induced cell death, preventing glutathione depletion, reactive oxygen species (ROS) generation and activation of JNK and p38 MAPK. APAP-treated PTP1B$^{-/-}$ hepatocytes showed enhanced antioxidant defense through the glycogen synthase kinase 3 (GSK3)β/Src kinase family (SKF) axis, delaying tyrosine phosphorylation of the transcription factor nuclear factor-erythroid 2-related factor (Nrf2) and its nuclear exclusion, ubiquitination and degradation. Insulin-like growth factor-I receptor-mediated signaling decreased in APAP-treated wild-type hepatocytes, but was maintained in PTP1B$^{-/-}$ cells or in wild-type hepatocytes with reduced PTP1B levels by RNA interference. Likewise, both signaling cascades were modulated in mice, resulting in less severe APAP hepatotoxicity in PTP1B$^{-/-}$ mice. Our results demonstrated that PTP1B is a central player of the mechanisms triggered by APAP in hepatotoxicity, suggesting a novel therapeutic target against APAP-induced liver failure.

Cell Death and Disease (2013) **4,** e626; doi:10.1038/cddis.2013.150; published online 9 May 2013
Subject Category: Experimental Medicine

Acetaminophen (APAP) or paracetamol is a widely used analgesic and antipyretic, which is drug safe at therapeutic doses,[1] but accidental or intentional overdose induces severe hepatotoxicity in experimental animals and humans. APAP overdose is the most frequent cause of drug-induced liver failure in the United States[2,3] and most of Europe.[4,5] In these countries, APAP is a leading cause of urgent liver transplantation, which accounts for considerable levels of morbidity and mortality.[2] Therefore, APAP-induced acute toxicity has become an essential model for studying drug-induced liver and kidney failure. In the liver, APAP overdose produces centrilobular hepatic necrosis that can be fatal as it progresses to fulminant liver failure.[6] However, despite substantial progress in understanding APAP-induced hepatotoxicity,[7–9] additional injurious mechanisms responsible for the cellular damage induced by APAP remain unknown.

At normal dosage, the major elimination pathways of APAP involve glucuronide and sulfate conjugation. The initial step in toxicity is bioactivation of APAP by cytochrome *P*450 2e1 (Cyp2e1) to an electrophilic metabolite, *N*-acetyl-*p*-aminobenzoquinone imine (NAPQI).[10] At therapeutic doses, NAPQI is detoxified by glutathione (GSH) and eliminated in urine or bile as APAP-cysteine, APAP-*N*-acetylcysteine and APAP-APAP-GSH.[11] After an overdose, glucuronidation and sulfation routes become saturated and more extensive bioactivation of APAP occurs, leading to rapid depletion of

[1]Instituto de Investigaciones Biomédicas Alberto Sols (CSIC-UAM), Madrid 28029, Spain; [2]Centro de Investigación Biomédica en Red de Diabetes y Enfermedades Metabólicas Asociadas (CIBERDEM), ISCIII, Madrid, Spain; [3]Instituto de Ciencia y Tecnología de Alimentos y Nutrición (ICTAN-CSIC), Madrid 28040, Spain; [4]Centro de Investigación Biomédica en Red de Enfermedades Neurodegenerativas (CIBERNED), ISCIII, Madrid, Spain; [5]Section of Clinical Pharmacology and Toxicology, Arkansas Children's Hospital, Little Rock, AR 72207, USA; [6]Division of Clinical and Surgical Sciences, University of Edinburgh, Edinburgh EH164TJ, UK; [7]Oncology Surgery, Cell Therapy and Transplant Organs, Institute of Biomedicine of Seville (IBiS)/Virgen del Rocio Universitary Hospital/CSIC/University of Seville, Sevilla, Spain and [8]Centro de Investigación Biomédica en Red de Enfermedades Hepáticas y Digestivas (CIBERhed), Instituto de Salud Carlos III, Madrid, Spain
*Corresponding author: AM Valverde, Instituto de Investigaciones Biomédicas Alberto Sols (CSIC-UAM), Consejo Superior de Investigaciones Científicas c/Arturo Duperier 4, Madrid 28029, Spain. Tel: +34 915854497; Fax: +34 915854401; E-mail: avalverde@iib.uam.es
Keywords: liver injury; apoptosis; oxidative stress; survival signaling; tyrosine phosphorylation
Abbreviations: PTP1B, protein tyrosine phosphatase 1B; APAP, acetaminophen; JNK, c-jun (NH2) terminal kinase; Nrf2, nuclear factor-erythroid 2-related factor; IGFIR, insulin-like growth factor I receptor; ALT, alanine amino transaminase; GPx, glutathione peroxidase; GR, glutathione reductase; HO-1, heme oxigenase; GCL-C, γ-glutamyl cysteine ligase catalytic subunit; GCL-M, γ-glutamyl cysteine ligase modulatory subunit; SKF, Src kinase family
Received 05.1.13; revised 15.3.13; accepted 28.3.13; Edited by M Piacentini

the hepatic GSH pool. Subsequently, NAPQI binds to cysteine groups on cellular proteins forming APAP–protein adducts. NAPQI also binds to mitochondrial proteins, which, in turn, causes oxidative stress that may trigger signaling pathways through mitochondrial toxicity, leading to lethal cell injury. Moreover, generation of reactive oxygen (ROS) and nitrogen species, lipid peroxidation, mitochondrial dysfunction, disruption of calcium homeostasis and induction of apoptosis and necrosis are also involved in APAP-induced hepatotoxicity.[12–14] Therefore, tight control of ROS levels by antioxidant molecules and detoxifying enzymes is important to restore the balance between oxidants and antioxidants in cells challenged with oxidative insults. In this regard, nuclear factor erythroid-2-related factor 2 (Nrf2) activates detoxifying enzymes by binding to antioxidant response elements (AREs). Nrf2-deficient mice are highly susceptible to APAP-induced liver injury.[15] Thus, Nrf2 may serve as an endogenous regulator by which cells combat oxidative stress.

Protein tyrosine phosphorylation is crucial in the mechanisms by which growth factors and hormones regulate cellular metabolism, differentiation, growth and survival. Given the importance in maintaining survival and death fates of cells, the balance between tyrosine kinases and phosphatases is carefully regulated. Protein tyrosine phosphatases (PTPs) catalyze dephosphorylation of tyrosine-phosphorylated proteins.[16] Among them, protein tyrosine phosphatase 1B (PTP1B) is a widely expressed non-receptor PTP, which is associated with the endoplasmic reticulum by interaction through the C-terminal domain.[17] PTP1B has been proposed as a therapeutic target against type 2 diabetes and obesity via its capacity to dephosphorylate insulin and leptin receptors.[18,19] PTP1B also dephosphorylates and inactivates receptors of the tyrosine kinase superfamily, such as EGF receptor, PDGF receptor,[20] hepatocyte growth factor receptor/met [21] and insulin-like growth factor-I receptor (IGFIR),[22] which are involved in hepatocyte survival.[23,24] On this basis, the aim of this study was to investigate the role of PTP1B in APAP-induced hepatotoxicity.

Results

PTP1B expression increased during APAP-induced liver injury in human liver and APAP-treated human hepatocytes. We investigated if PTP1B was modulated during APAP-induced human liver injury. Figure 1a shows elevated PTP1B in surviving hepatocytes, mainly in the areas surrounding the central veins (middle panel), during APAP intoxication as compared with a normal liver (left panel). In a more severe intoxication (right panel), where it is difficult to detect surviving hepatocytes, strong staining was observed in precipitated proteins released from dead cells and not yet cleared. PTP1B protein content was also upregulated in human primary hepatocytes and in the human Chang liver cell line (CHL) treated with APAP in a dose- and time-dependent manner (Figures 1b and c and Supplementary Figure 1). Elevation of PTP1B was detected at 8 h after APAP addition, whereas cells with death morphology were visualized at 16 h. Moreover, in APAP-treated human hepatocytes activation of c-jun (NH2) terminal kinase (JNK) and p38 mitogen-activated protein kinase (p38 MAPK) and inhibition of Akt phosphorylation correlated with decreased levels of the antiapoptotic Bcl2 family members BclxL and Mcl1 and with detection of the active caspase-3 fragment (Figure 1d).

PTP1B-deficient mouse hepatocytes are protected against APAP-induced necrotic and apoptotic cell death. As observed in human hepatocytes (Figure 1c), PTP1B was upregulated in primary hepatocytes from wild-type ($PTP1B^{+/+}$) mice treated with APAP (10 mM) at 8 h, whereas maximal cell death was observed at 16 h (Figure 2a). Next, we explored APAP-induced hepatotoxicity in mouse primary hepatocytes from wild-type and $PTP1B^{-/-}$ mice. Cells were treated with 5 and 10 mM APAP for 16 h and cell death was analyzed. Phase-contrast microscopy revealed many APAP-treated wild-type primary hepatocytes with cell death morphology. Conversely, most of $PTP1B^{-/-}$ primary hepatocytes remained attached to the plate and only few cells displayed a death phenotype (Figure 2b). Quantification analysis of crystal violet staining and released lactate dehydrogenase (LDH) activity showed that primary $PTP1B^{-/-}$ hepatocytes were more protected against APAP-induced necrotic cell death. Moreover, APAP treatment also increased the incidence of condensed and/or fragmented nuclei and the percentage of hypodiploid (sub-G_0/G_1) population in wild-type primary hepatocytes indicating apoptotic cell death (Figure 2c). These effects were reduced in $PTP1B^{-/-}$ cells. Apoptosis in APAP-treated wild-type primary hepatocytes correlated with the release of cytochrome *C* from the mitochondrial compartment and with the subsequent activation of caspase-3 (Figure 2d). These effects were significantly ameliorated in $PTP1B^{-/-}$ primary hepatocytes. Similar results were obtained using wild-type and $PTP1B^{-/-}$ immortalized hepatocytes that express comparable levels of pro- and antiapoptotic proteins than primary hepatocytes and are highly sensitive to APAP-induced cell death[25] (Supplementary Figure 2).

Effect of PTP1B deficiency on the activation of stress- and survival-mediated signaling pathways in mouse hepatocytes. Next, we analyzed stress- and survival-mediated signaling in primary hepatocytes from wild-type and $PTP1B^{-/-}$ mice in response to APAP. JNK and p38 MAPK phosphorylation was detected at 8 h in primary hepatocytes treated with 10 mM APAP, this effect being ameliorated in $PTP1B^{-/-}$ cells (Figure 3a). Survival signaling monitored by IGFIR phosphorylation, levels of insulin receptor substrates 1 (IRS1) and 2 (IRS2) and Akt phosphorylation, was reduced in APAP-treated wild-type primary hepatocytes, but preserved in $PTP1B^{-/-}$ cells. Consistently, the antiapoptotic markers BclxL and Mcl1 were decreased in wild-type primary hepatocytes treated with APAP but, again, this effect was reduced in $PTP1B^{-/-}$ hepatocytes. Similar responses were found in immortalized hepatocytes that activate stress kinases at lower APAP doses (Figure 3b).

To exclude the possibility that the protection elicited by PTP1B deficiency against APAP-induced cell death could be secondary to compensatory adaptations in $PTP1B^{-/-}$ hepatocytes, we established siRNA assays. Reduction of

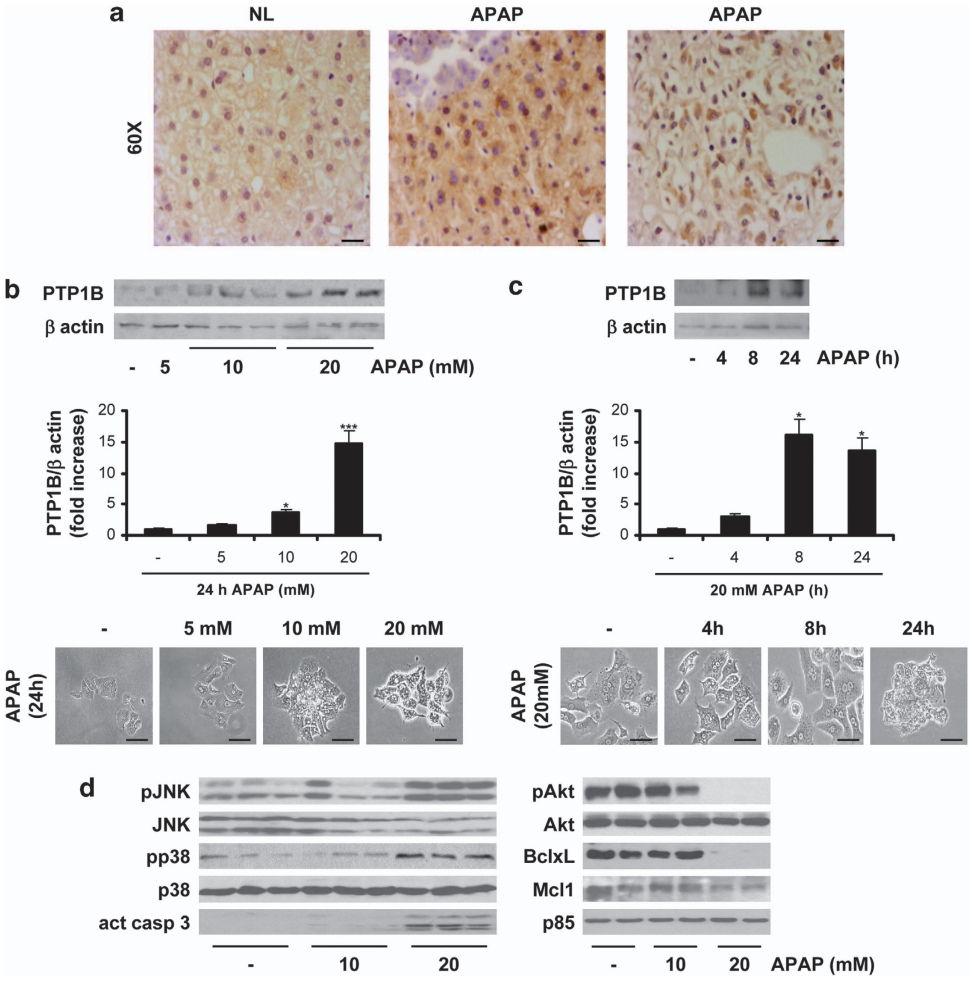

Figure 1 PTP1B expression is increased during APAP-induced liver injury and in human primary hepatocytes treated with APAP. (**a**) Representative anti-PTP1B immunostaining of liver biopsy sections from patients with histologically normal liver (NL) or with an APAP overdose (APAP) ($n=7$). Bar = 50 μm. (**b**) Human primary hepatocytes were treated with various doses of APAP (5–20 mM) for 24 h. Total cell lysates were analyzed by western blot with the antibodies against PTP1B and β-actin as a loading control. Autoradiograms corresponding were quantitated by scanning densitometry. Results are means ± S.E.M. *$P<0.05$ and ***$P<0.005$ APAP-treated *versus* non-treated cells. Representative phase-contrast microscopy images after APAP treatment. Bar = 100 μm. (**c**) Human primary hepatocytes were treated with 20 mM APAP for various time-periods (4, 8 and 24 h). Total cell lysates were analyzed by western blot with the antibodies against PTP1B and β-actin as a loading control. Autoradiograms corresponding were quantitated by scanning densitometry. Results are means ± S.E.M. *$P<0.05$ APAP-treated *versus* non-treated cells. Representative phase-contrast microscopy images after APAP treatment. Bar = 100 μm. (**d**) Human primary hepatocytes were treated with various doses of APAP for 24 h and total cell lysates were analyzed by western blot with the antibodies against phospho (p)-JNK1/2, JNK1/2, phospho-p38, p38, active caspase-3, phospho-Akt, Akt, BclxL, Mcl1 and p85-PI3K as a loading control. *$P<0.05$ and ***$P<0.005$ APAP-treated *versus* non-treated cells ($n=3$ independent experiments)

PTP1B in wild-type immortalized hepatocytes decreased APAP-induced JNK phosphorylation and levels of the active caspase-3 fragment, and also maintained IGFIR tyrosine phosphorylation, IRS1 and IRS2 expression, Akt phosphorylation and abolished downregulation of BclxL upon APAP treatment (Figure 3c).

PTP1B deficiency protects mouse hepatocytes against GSH depletion and elevation of ROS by prolonging Nrf2 nuclear accumulation. In the liver, Cyp2e1 converts APAP to NAPQI that depletes GSH and, therefore, the degree of GSH consumption is a biomarker for APAP bioactivation.[26] As the expression of Cyp2e1 did not change in primary and immortalized hepatocytes from both genotypes of mice (Supplementary Figure 3), we used immortalized cells for further experiments. APAP induced depletion of GSH in wild-type immortalized hepatocytes after 4 h, and this effect was absent in PTP1B$^{-/-}$ cells (Figure 4a). Likewise, a significant elevation of ROS was detected in APAP-treated wild-type hepatocytes for 6 h, but not in PTP1B$^{-/-}$ cells. Next, we measured the enzymatic activity of the detoxifying enzymes glutathione peroxidase (GPx) and glutathione reductase (GR). GPx activity increased in APAP-treated wild-type hepatocytes compared with untreated controls, as expected for an antioxidant defense system. Conversely, GR was not increased by APAP, suggesting impairment in pathways replenishing GSH stores. PTP1B$^{-/-}$ hepatocytes did not activate the GPx/GR system in response to APAP, probably due to an insufficient threshold to trigger the activation of detoxifying enzymes under these experimental conditions.

To investigate at the molecular level the mechanisms for protection of PTP1B deficiency against APAP-induced

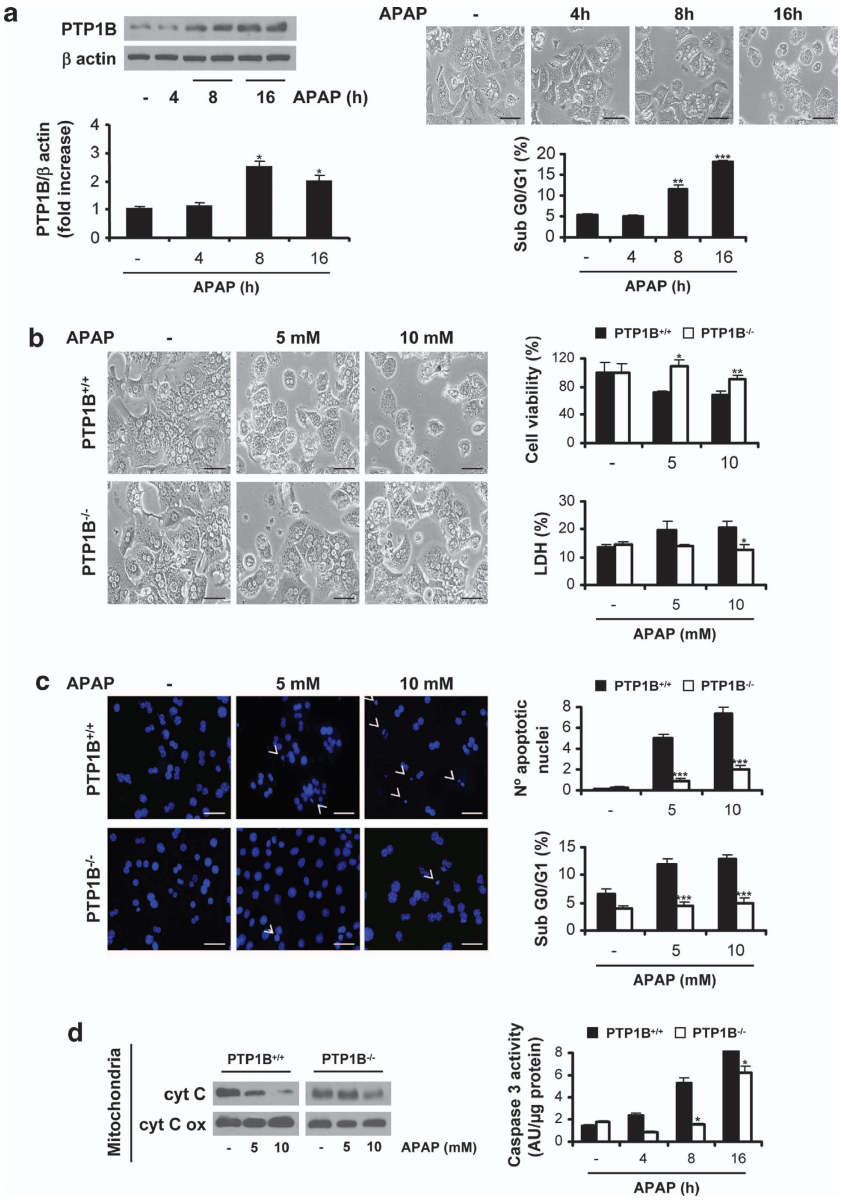

Figure 2 PTP1B-deficient primary hepatocytes are protected against APAP-induced cell death. (**a**, left panel) Wild-type ($PTP1B^{+/+}$) mouse primary hepatocytes were treated with 10 mM APAP for various time-periods. The expression of PTP1B was analyzed by western blot. $^{*}P<0.05$ APAP-treated *versus* non-treated cells ($n=3$ independent experiments). (Right panel) Representative phase-contrast microscopy images and analysis of the percentage of sub-G0/G1 cell population by flow cytometry. (**b**) $PTP1B^{+/+}$ and $PTP1B^{-/-}$ primary hepatocytes were treated with APAP (5 and 10 mM) for 16 h. (Left panel) Representative phase-contrast microscopy images. Bar = 100 μm. (Right panel) Cellular viability and released LDH activity. (**c**) $PTP1B^{+/+}$ and $PTP1B^{-/-}$ primary hepatocytes were treated with APAP (5 and 10 mM) for 16 h. (Left panel) Representative nuclear morphology images after DAPI staining and analysis by fluorescence microscopy. (Right panel) Quantification of apoptotic nuclei. Percentage of sub-G_0/G_1 cell population analyzed by flow cytometry. (**d**, left panel) $PTP1B^{+/+}$ and $PTP1B^{-/-}$ primary hepatocytes were treated with APAP (5 and 10 mM) for 16 h. Western blot with anticytochrome *C* and anti-cytochrome *C* oxidase antibodies in mitochondrial extracts. (Right panel) $PTP1B^{+/+}$ and $PTP1B^{-/-}$ primary hepatocytes were treated with APAP (10 mM) for various time-periods. Analysis of caspase-3 enzymatic activity. $^{*}P<0.05$, $^{**}P<0.01$ and $^{***}P<0.005$ $PTP1B^{-/-}$ *versus* $PTP1B^{+/+}$ ($n=4$ independent experiments)

oxidative stress, we analyzed the dynamics of Nrf2 nuclear accumulation. As no differences in Nrf2 serine phosphorylation that dissociates Nrf2 to its inhibitor Keap1 at early time-periods upon APAP treatment were found (Supplementary Figure 4A), we analyzed the nuclear accumulation of Nrf2 at later time-periods. Western blot and immunofluorescence revealed that Nrf2 was maximally accumulated in the nucleus at 8 h after APAP treatment in wild-type and $PTP1B^{-/-}$ hepatocytes, but was retained for up to 16 h exclusively in $PTP1B^{-/-}$ cells (Figure 4b). Nuclear Nrf2 accumulation was accompanied by decreases in cytosolic expression (Supplementary Figure 4B).

Tyrosine phosphorylation of Nrf2 results in its nuclear export, ubiquitination and degradation in the cytosol.[27] Figure 4c shows that in APAP-treated wild-type hepatocytes, maximal Nrf2 tyrosine phosphorylation was observed at 8 h and total Nrf2 protein content decreased at 16 h. In $PTP1B^{-/-}$ cells, maximal Nrf2 tyrosine phosphorylation

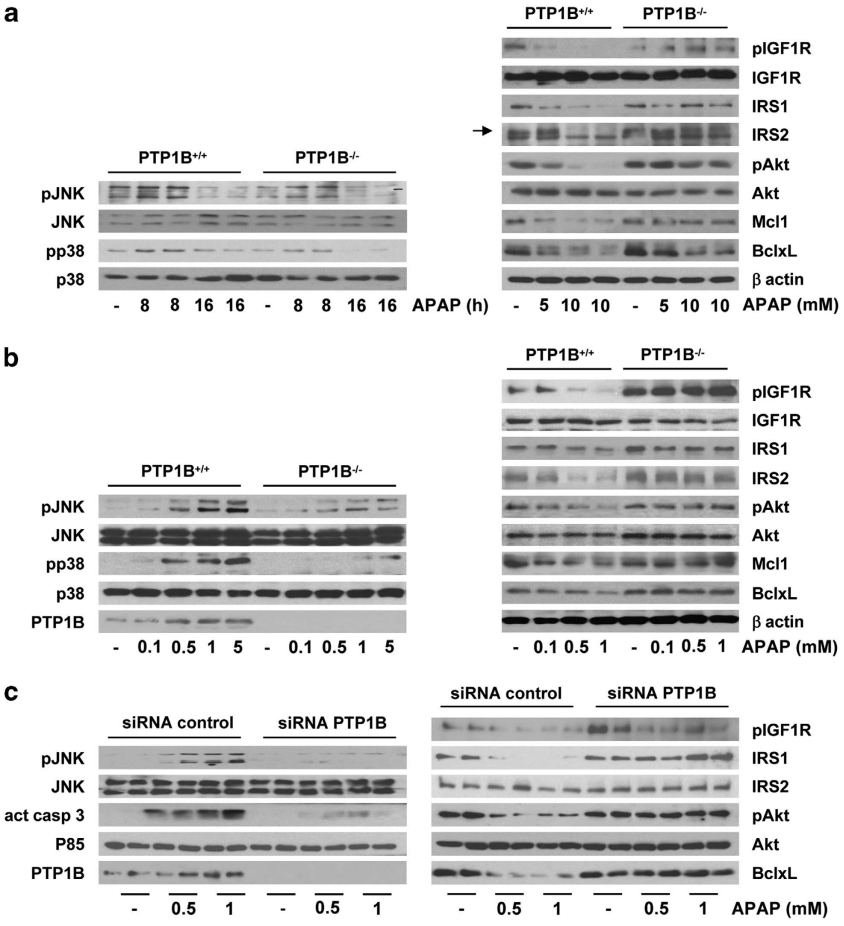

Figure 3 Effect of PTP1B deficiency in stress and survival signaling in hepatocytes. (**a**, left panel) PTP1B$^{+/+}$ and PTP1B$^{-/-}$ mouse primary hepatocytes were treated with APAP (10 mM) for various time periods. Total cell lysates were analyzed by western blot with the antibodies against phospho (p)-JNK1/2, JNK1/2, phospho-p38 MAPK and p38 MAPK. Representative autoradiograms corresponding to three independent experiments are shown. (Right panel) PTP1B$^{+/+}$ and PTP1B$^{-/-}$ mouse primary hepatocytes were treated with APAP (5 and 10 mM) for 16 h. Total cell lysates were analyzed by western blot with the antibodies against phospho (p)-IGFIR, IGFIR, IRS1, IRS2, phospho-Akt, Akt, BclxL, Mcl1 and β-actin as a loading control. Representative autoradiograms corresponding to three independent experiments are shown. (**b**) PTP1B$^{+/+}$ and PTP1B$^{-/-}$ immortalized hepatocytes were treated with various doses of APAP for 16 h. Total cell lysates were analyzed by western blot with the indicated antibodies. Representative autoradiograms corresponding to three independent experiments are shown. (**c**) Immortalized PTP1B$^{+/+}$ hepatocytes transfected with 10 nM of control or PTP1B small interfering RNA (siRNA) for 48 h were further treated with various doses of APAP for 16 h. Total cell lysates were analyzed by western blot with the indicated antibodies. Representative autoradiograms corresponding to three independent experiments are shown

occurred at 16 h, a time-point at which total Nrf2 levels were maintained as in non-treated cells. These data correlated with greater increase in the expression of the Nrf2 target heme oxygenase-1 (HO-1) in PTP1B$^{-/-}$ hepatocytes. As occurred in immortalized hepatocytes, Nrf2 levels were maintained and the induction of HO-1 was higher in APAP-treated mouse primary PTP1B$^{-/-}$ hepatocytes for 16 h as compared with the wild-type cells.

Next, ubiquitination analysis of Nrf2 was performed in immortalized hepatocytes treated with APAP for 8–24 h either in the absence or presence of the proteasome inhibitor MG132 (Figure 4d). In APAP-treated wild-type cells, ubiquitinated Nrf2 was detected at earlier time-points (8 h) compared with PTP1B$^{-/-}$ cells, which displayed this response at 16 h; this effect was enhanced when APAP was added with MG132. In related experiments, overexpression of PTP1B in HEK 293T cells inhibited ARE-mediated luciferase expression after treatment with APAP for 16 h (Figure 4e), reinforcing the involvement of PTP1B in Nrf2-mediated antioxidant response to APAP.

PTP1B modulates GSK3β/SKF-mediated Nrf2 nuclear accumulation in APAP-treated mouse hepatocytes. In response to oxidative stress, GSK3β is activated by phosphorylation at Tyr216 by an unknown tyrosine kinase. Activated GSK3β phosphorylates and activates Src kinase family (SKF) members in the cytosol, allowing their nuclear translocation and subsequent tyrosine phosphorylation of Nrf2 at Tyr568, ultimately resulting in Nrf2 nuclear exclusion and degradation.[27,28] We examined if this molecular mechanism was triggered in APAP-treated hepatocytes. Silencing GSK3β in immortalized wild-type hepatocytes (Supplementary Figure 5) prolonged Nrf2 nuclear accumulation up to 24 h upon APAP treatment as observed in PTP1B$^{-/-}$ cells (Figures 4b and 5a). Moreover, nuclear translocation of Fyn and Src was also impaired in GSK3β-silenced cells, although no effects of nuclear translocation of Yes were observed (results not shown). To reinforce the role of SKF in nuclear accumulation of Nrf2 in response to APAP, we treated wild-type hepatocytes with the

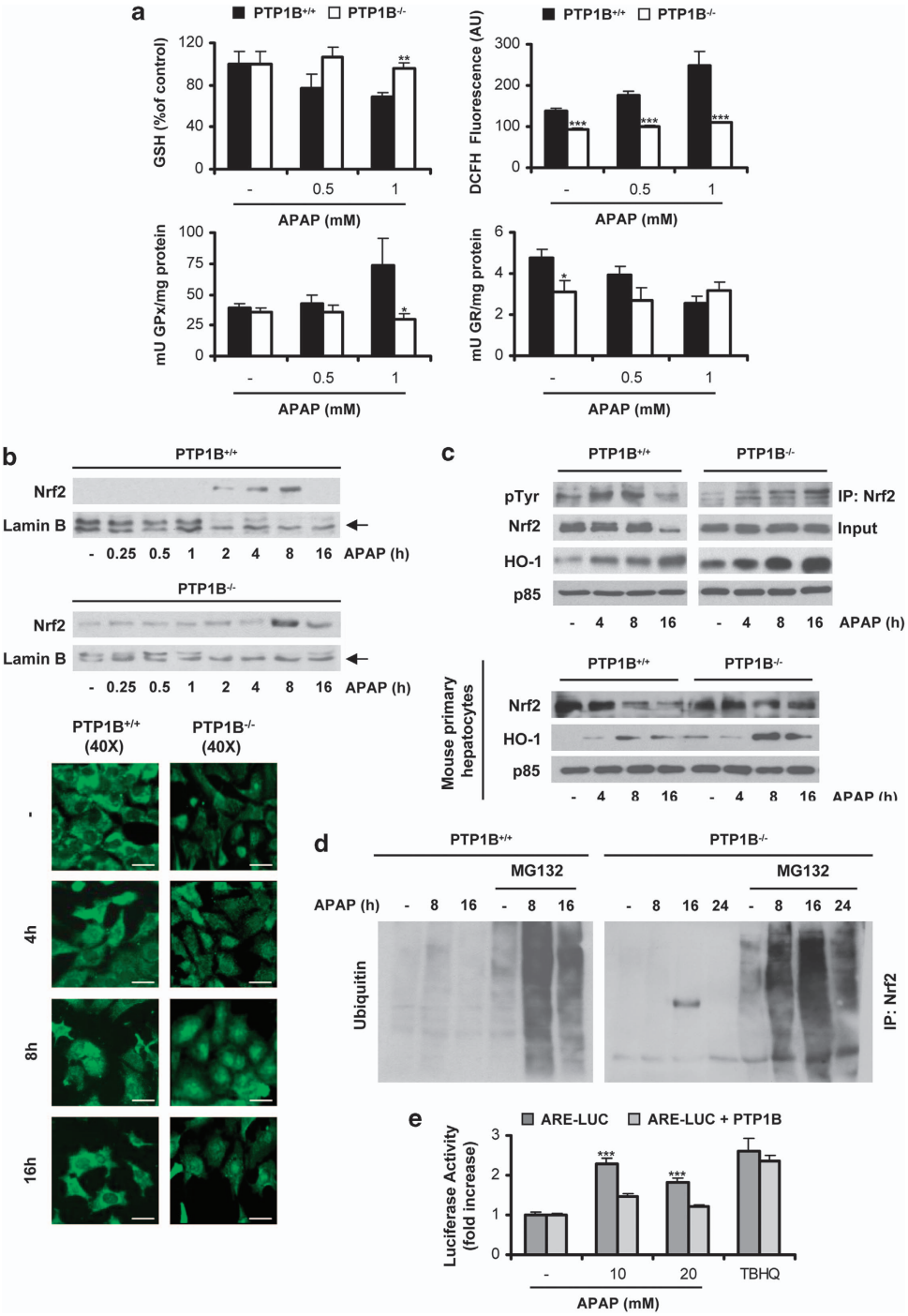

Figure 4 PTP1B deficiency protects hepatocytes against GSH depletion and elevation of ROS; effect on nuclear Nrf2 accumulation. PTP1B$^{+/+}$ and PTP1B$^{-/-}$ immortalized hepatocytes were treated with various doses of APAP for different time-periods. (**a**) Analysis of GSH content (4 h), ROS levels (6 h) and GPx and GR activity (16 h) in three independent experiments. *$P<0.05$, **$P<0.01$ and ***$P<0.005$ PTP1B$^{-/-}$ *versus* PTP1B$^{+/+}$ (**b**, upper panel) Analysis of Nrf2 in nuclear cell lysates by western blot in PTP1B$^{+/+}$ and PTP1B$^{-/-}$ immortalized hepatocytes treated with 1 mM APAP for several time-periods. Representative autoradiograms of three to four independent experiments are shown. (Lower panel) Representative images corresponding to the intracellular localization of Nrf2 by immunofluorescence microscopy in PTP1B$^{+/+}$ and PTP1B$^{-/-}$ immortalized hepatocytes treated with 1 mM APAP for several time-periods. Bar = 50 μm. (**c**) (Upper panel) PTP1B$^{+/+}$ and PTP1B$^{-/-}$ immortalized hepatocytes were treated with 1 mM APAP for several time-periods. Nrf2 tyrosine phosphorylation was analyzed by immunoprecipitation with the anti-Nrf2 antibody, followed by western blot with the anti-Tyr(P) antibody. Total Nrf2 and HO-1 was analyzed by western blot. (Lower panel) PTP1B$^{+/+}$ and PTP1B$^{-/-}$ mouse primary hepatocytes were treated with 10 mM APAP for various time-periods. Total Nrf2 and HO-1 was analyzed by western blot. (**d**) PTP1B$^{+/+}$ and PTP1B$^{-/-}$ immortalized hepatocytes were treated with MG132 (10 nM) for 30 min, and then with 1 mM APAP for different time-periods. Whole-cell lysates were analyzed by immunoprecipitation with anti-Nrf2 antibody, followed by western blot with anti-ubiquitin antibody. (**e**) Antioxidant response element (ARE)-mediated luciferase activity was measured in HEK 293T cells transfected with the expression vectors for pcDNA3.1mNrf2-V5/HisB and 3 × ARE-Luc combined with myc-PTP1B only in the indicated cases and treated with various doses of APAP for 16 h. tBHQ (15 μM) was used as a positive control ($n=3$ independent experiments performed in triplicate). ***$P<0.005$ PTP1B-transfected (Nrf2 ARE + PTP1B) *versus* empty vector-transfected (Nrf2 ARE) cells

SKF inhibitor PP2. As shown in Figure 5b, PP2 increased nuclear Nrf2 levels at 2–8 h after APAP treatment. In addition, in mouse embryonic fibroblasts (MEFs) deficient in SKF ($SYF^{-/-}$) treated with APAP Nrf2 was accumulated in the nucleus up to 24 h.

We next analyzed the effect of PTP1B deficiency on the GSK3β/SKF signaling pathway. In wild-type cells, APAP-induced GSK3β tyrosine phosphorylation was detected at 1 h and peaked at 4 h. This response paralleled the re-entry of Fyn and Src into the nucleus (Figure 5c). In $PTP1B^{-/-}$ hepatocytes, maximal GSK3β phosphorylation occurred later at 8–16 h after APAP treatment and also paralleled the re-entry of Src and Fyn into the nucleus as observed in wild-type cells.

PTP1B-deficient mice are protected against APAP-induced oxidative stress through the enhancement of Nrf2 nuclear accumulation. Increased survival was observed in $PTP1B^{-/-}$ mice injected with an APAP overdose (300 mg/kg) as compared with the wild-type control (Figure 6a). Consistently, serum alanine transaminase (ALT) was sevenfold higher in wild-type mice than in $PTP1B^{-/-}$ mice at 6 and 24 h after injection (Figure 6b). Of note, necrotic lesions were observed exclusively in livers of wild-type mice (Figure 6c). Next, we analyzed the hepatic expression of proinflammatory cytokines. At 6 h after APAP injection, elevated IL6 and IL1β mRNA levels were found in livers of wild-type mice, but not in $PTP1B^{-/-}$ animals (Figure 6d). APAP decreased TNFα mRNA levels in

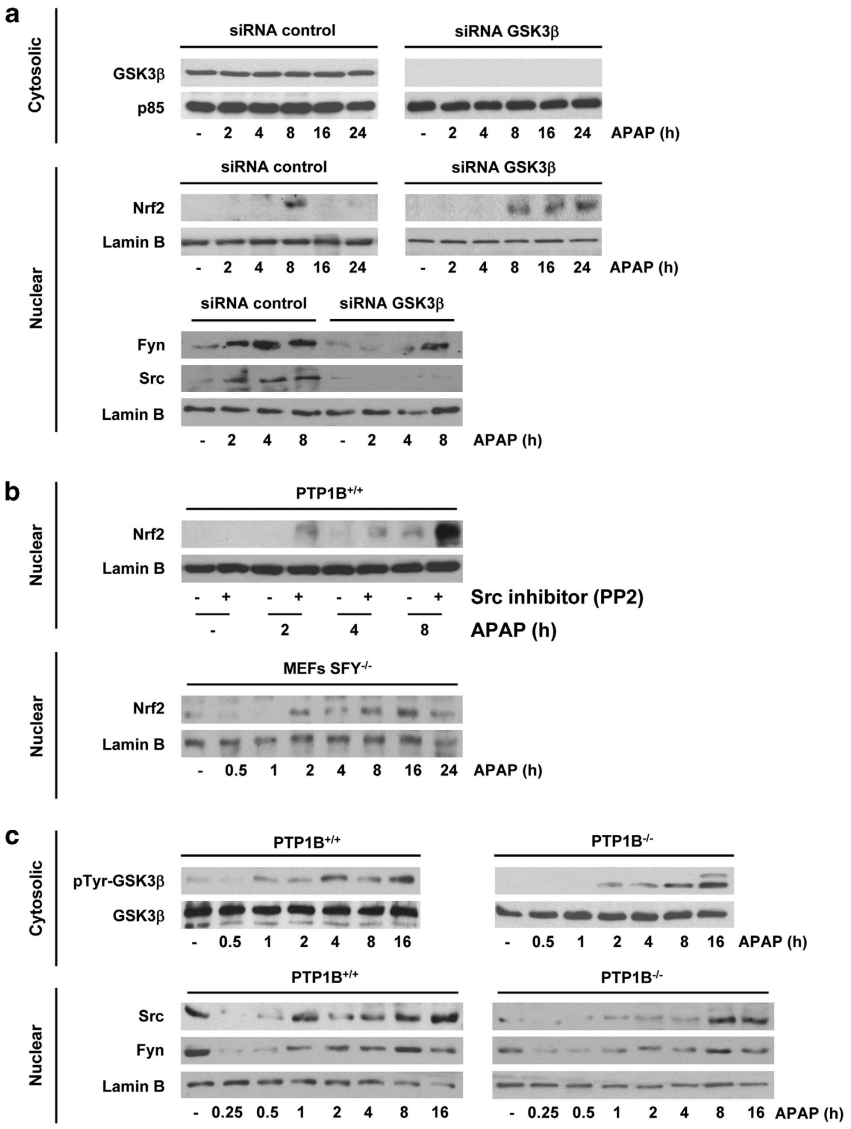

Figure 5 PTP1B modulates GSK3β/Src-Fyn-mediated Nrf2 nuclear accumulation in APAP-treated hepatocytes. (**a**) $PTP1B^{+/+}$ immortalized hepatocytes were transfected with control or GSK3β small interfering RNAs (siRNAs) (25 nM) for 48 h, followed by stimulation with 1 mM APAP. Nuclear and cytosolic extracts were analyzed by western blot with antibodies against Nrf2, Fyn and Src. (**b**, upper panel) $PTP1B^{+/+}$ immortalized hepatocytes were treated with PP2 (5 μM) for 30 min following 1 mM APAP for different periods. Nrf2 in nuclear extracts was analyzed by western blot. (Lower panel) $SYF^{-/-}$ MEFs were treated with 1 mM APAP for different periods and Nrf2 was analyzed in nuclear extracts by western blot. (**c**) $PTP1B^{+/+}$ and $PTP1B^{-/-}$ immortalized hepatocytes were treated with 1 mM APAP for different periods. Phosphorylated GSK3β (Tyr216) was analyzed in cytosolic extracts by western blot. Fyn and Src were analyzed in nuclear extracts. Similar results were obtained in three independent experiments

wild-type, but not in PTP1B-deficient mice. As hepatic PTP1B expression is modulated by inflammation,[29] we performed the immunohistochemistry analysis. Increased PTP1B staining was found in necrotic lesions of APAP-treated wild-type mice after 6 h, particularly in areas surrounding the central veins, but no signs of liver injury were observed in sections from PTP1B$^{-/-}$ mice (Figure 6e). We next determined if reduced sensitivity of PTP1B$^{-/-}$ mice to APAP-induced liver injury was associated with alterations in GSH levels. APAP administration depleted GSH at 3 and 6 h and increased APAP–protein adducts, these effects being significantly ameliorated in the PTP1B$^{-/-}$ group (Figure 6f). Protein carbonyl levels, an indicator of tissue oxidative stress, were less elevated in APAP-injected PTP1B$^{-/-}$ mice than in wild-type mice and paralleled the reduced GSH depletion.

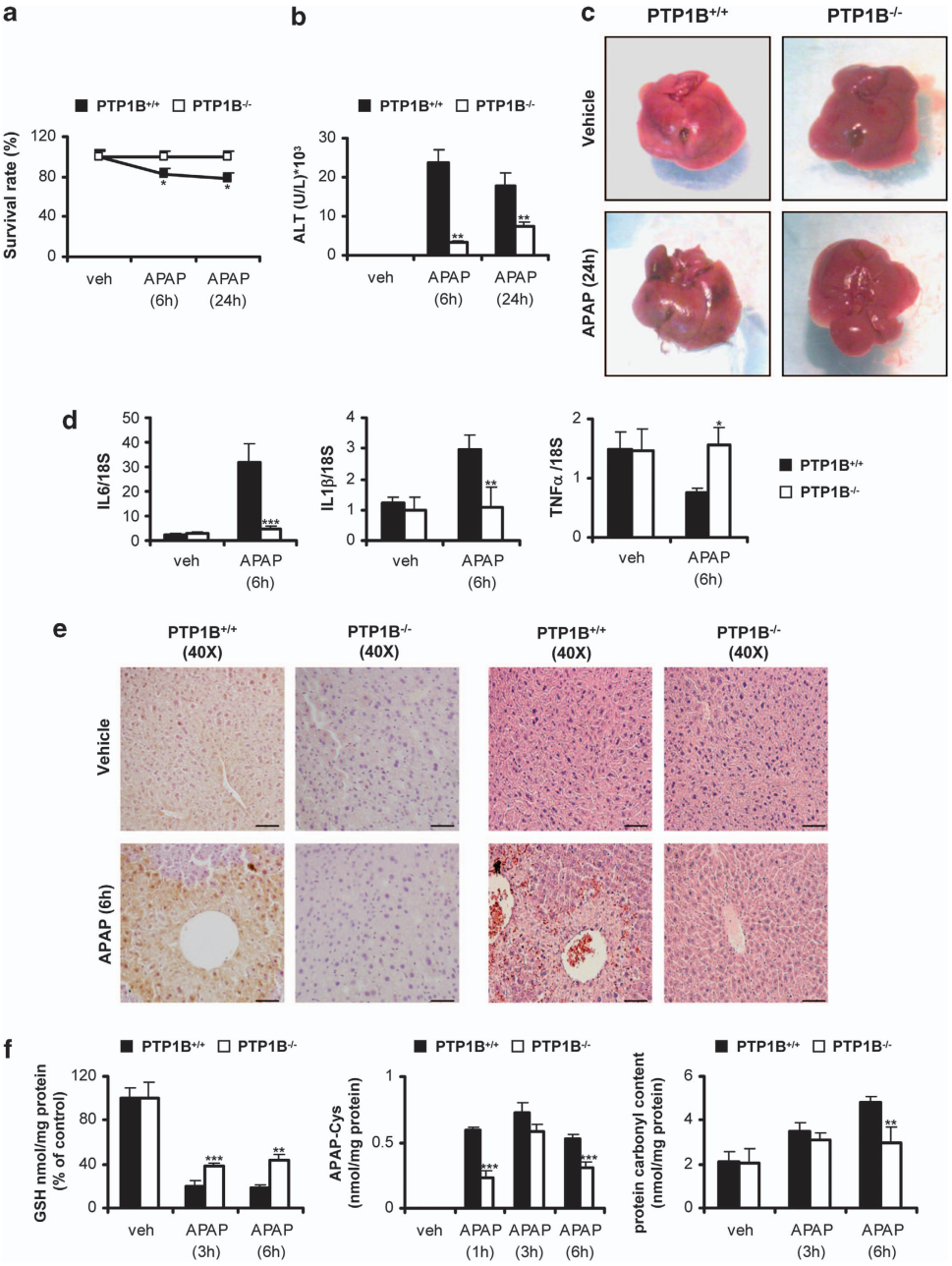

Figure 6 PTP1B-deficient mice are protected against APAP-induced, inflammation oxidative stress and liver damage. PTP1B$^{+/+}$ and PTP1B$^{-/-}$ mice were injected with 300 mg/kg APAP or saline for 6 or 24 h. (**a**) Survival curves after 24 h of APAP injection. (**b**) ALT activity at 6 and 24 h. (**c**) Representative images of whole livers from PTP1B$^{+/+}$ and PTP1B$^{-/-}$ mice 24 h after APAP injection. (**d**) IL6, IL1β and TNFα mRNA levels were determined by real-time polymerase chain reaction in livers from PTP1B$^{+/+}$ and PTP1B$^{-/-}$ mice at 6 h after APAP injection. (**e**) Representative anti-PTP1B immunostaining (left panel) and hematoxylin and eosin staining (right panel) in livers from PTP1B$^{+/+}$ and PTP1B$^{-/-}$ mice 6 h after APAP injection. Bar = 100 μm. (**f**) GSH (left panel), APAP–protein adducts (middle panel) and carbonylated protein levels (right panel) were analyzed in livers from PTP1B$^{+/+}$ and PTP1B$^{-/-}$ mice at various time-periods after APAP injection. *$P<0.05$, **$P<0.01$ and ***$P<0.005$ PTP1B$^{-/-}$ *versus* PTP1B$^{+/+}$ ($n=6$–8 mice of each condition). Cys, cysteine. Veh, vehicle

As intracellular redox state is chiefly regulated by Nrf2, we examined differences in nuclear levels of Nrf2 *in vivo.* Nuclear Nrf2 was detected in livers of wild-type mice at 3 and 6 h after APAP treatment (Figure 7a). In PTP1B$^{-/-}$ animals, basal nuclear Nrf2 was detected before APAP administration and increased at 3 and 6 h after injection, where the levels were higher than those of control mice. Similarly, APAP-induced HO-1 protein content was higher in PTP1B$^{-/-}$ mice. Then, we analyzed additional Nrf2 target genes. mRNA levels of GPx, HO-1 and γ-glutamyl cysteine ligase modulatory subunit (GCL-M) significantly increased at 3-h after APAP injection in livers of PTP1B$^{-/-}$ mice as compared with the wild-type and GPx, γ-glutamyl cysteine ligase catalytic subunit (GCL-C), GCL-M and NAD(P)H quinone oxidoreductase 1 (NQO1) mRNA increased at 6 h (Figure 7b).

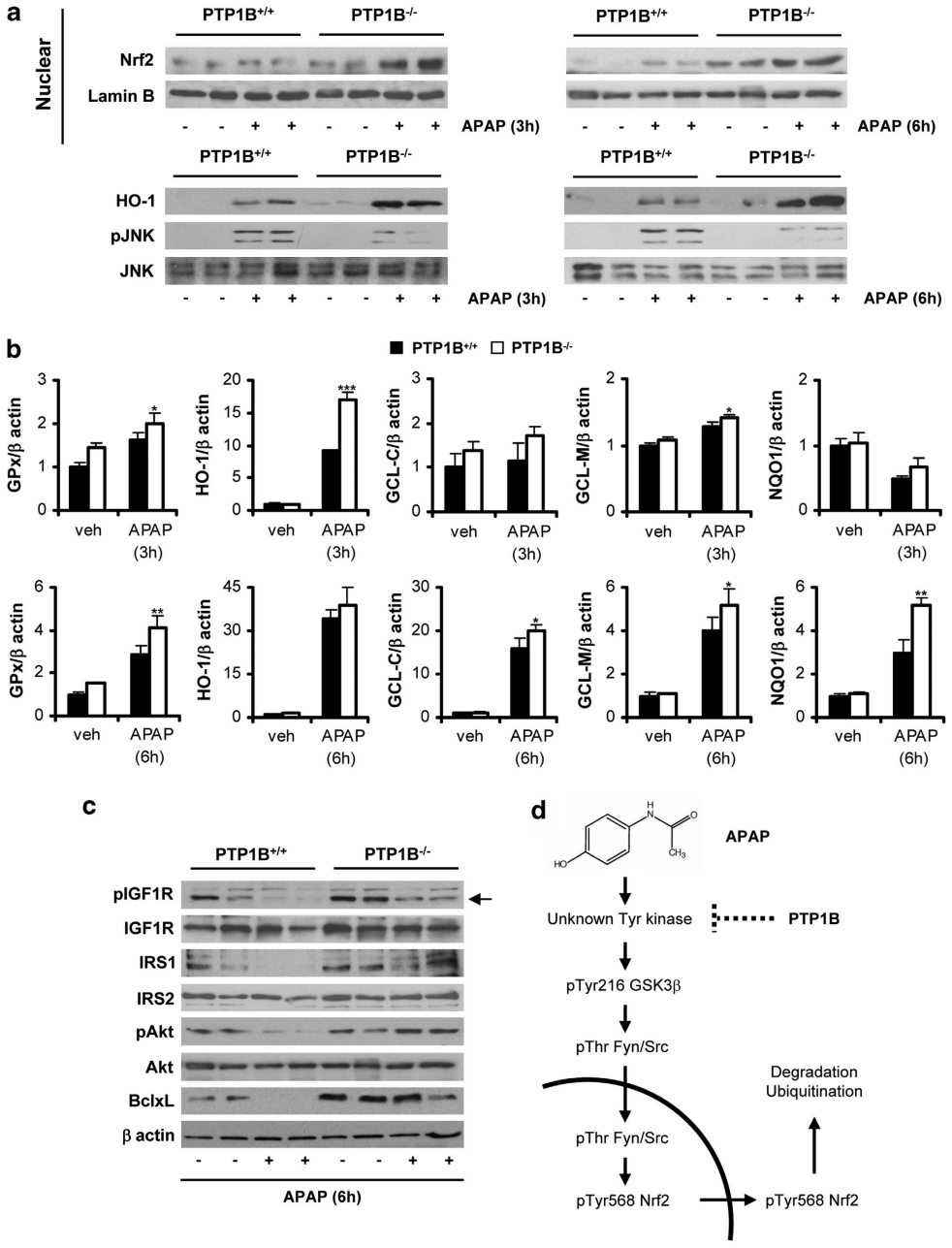

Figure 7 Beneficial effects of PTP1B deficiency on the induction of Nrf2-mediated antioxidant response and survival signaling in the liver. PTP1B$^{+/+}$ and PTP1B$^{-/-}$ mice were injected with 300 mg/kg APAP or saline for 3 or 6 h. (**a**) Western blot analysis of Nrf2 in nuclear extracts and HO-1, phospho (p)-JNK and JNK in total liver extracts. (**b**) GPx, HO-1, GCL-M, GCL-C and NQO1 mRNA levels determined by quantitative real-time polymerase chain reaction (qRT-PCR) at 3 and 6 h after APAP injection. *$P<0.05$, **$P<0.01$ and ***$P<0.005$ PTP1B$^{-/-}$ *versus* PTP1B$^{+/+}$ ($n=6$–8 mice of each condition). (**c**) Western blot analysis of phospho (p)-IGFIR, IGFIR, IRS1, IRS2, phospho-Akt, Akt and BclxL levels in total liver extracts from PTP1B$^{+/+}$ and PTP1B$^{-/-}$ mice 6 h after APAP injection. (**d**) Schematic diagram illustrating the proposed mechanism by which PTP1B modulates Nrf2 nuclear accumulation. PTP1B might activate the unknown kinase upstream GSK3β by dephosphorylation, thereby triggering activation of the GSK3β/Src-Fyn axis in the nucleus that ultimately leads to Nrf2 tyrosine phosphorylation, ubiquitination and degradation. Veh, vehicle

Decreased JNK activation and sustained IGFIR/Akt/BclxL survival signaling in APAP-treated PTP1B-deficient mice. Activation of JNK was detected in APAP-treated wild-type mice at 3 and 6 h after injection. As expected, this effect decreased in PTP1B$^{-/-}$ mice (Figure 7a). Regarding survival signaling, in wild-type mice IGFIR phosphorylation was severely reduced at 6 h after APAP injection and IRS1 protein levels were downregulated in parallel with decreased Akt phosphorylation (Figure 7c). Consistently, antiapoptotic BclxL protein was barely detected at 6 h after APAP injection. Conversely, APAP-treated PTP1B$^{-/-}$ mice maintained IGFIR and Akt phosphorylation, as well as IRS1 and BclxL protein content to similar levels than those of mice injected with saline.

Discussion

There is evidence of increased PTP1B expression during the progression of non-alcoholic fatty liver disease that concurs with insulin resistance and liver damage.[30,31] However, PTP1B functions in physiological responses regulated by tyrosine kinase signaling, such as hepatocellular survival during drug injury, are poorly understood. Our results have unraveled a central role of PTP1B in the molecular mechanism that mediates APAP-induced liver failure, identifying PTP1B as a potential therapeutic target in the treatment of human APAP hepatotoxicity. This study emerged from the observation of elevated PTP1B expression in livers from individuals suffering from APAP intoxication. Importantly, in APAP-treated human and mouse hepatocytes, upregulation of PTP1B preceded cell death.

Results in mouse hepatocytes demonstrated that PTP1B deficiency attenuates cellular damage in response to APAP. The fact that released LDH activity was reduced in PTP1B$^{-/-}$ hepatocytes indicates that necrotic cell death was less severe than in wild-type cells. In wild-type hepatocytes, APAP also increased the percentage of sub-G0/G1 cells and release of cytochrome *C* from the mitochondria. APAP also induced activation of caspase-3 and decreased expression of antiapoptotic proteins BclxL and Mcl1. These results strongly suggest that APAP also triggered apoptosis in hepatocytes and, again, these effects were ameliorated by PTP1B deficiency. The role of apoptosis in APAP-induced hepatocyte cell death is controversial. However, there are studies that clearly demonstrate both types of cell death following APAP overdose. Circulating apoptotic and necrotic cell death markers have been detected in patients with APAP-induced acute liver injury.[32–34] Cell death via necrosis and apoptosis has been reported in the livers removed during transplantation because of APAP intoxication.[35] These data have also been shown in mice during APAP poisoning.[36] In light of these results, we and others have shown that PTP1B inhibition protects hepatocytes against activation of mitochondrial (intrinsic) and death receptor (extrinsic)-mediated apoptotic pathways,[21,25] reinforcing the role of this phosphatase in programmed cell death.

As cellular oxidative stress processes (GSH depletion and ROS generation)[13] are ameliorated in PTP1B$^{-/-}$ hepatocytes, we investigated the modulation of oxidative stress by PTP1B. An unknown tyrosine kinase has been proposed to be the upstream activator of GSK3β by phosphorylation at Tyr216.[27,28] This phenomenon leads to SKF-mediated tyrosine phosphorylation, nuclear export, ubiquitination and degradation of Nrf2 in response to oxidative stress inducers. Our data demonstrated firstly that this signaling pathway is activated by APAP in hepatocytes and secondly that PTP1B deficiency mimics the inhibition of GSK3β or SKF on the downstream mediators of this pathway. Inhibition of GSK3β or SKF augmented and prolonged Nrf2 nuclear accumulation, delaying its nuclear exclusion in response to APAP. Importantly, the effect of PTP1B deficiency on this pathway was manifested by delayed Src-Fyn nuclear translocation, Nrf2 tyrosine phosphorylation and its subsequent ubiquitination and degradation, leading to enhanced HO-1 induction. These results suggest that PTP1B might activate this unknown kinase upstream from GSK3β, probably by dephosphorylation, and thereby triggering the activation of the GSK3β/Src-Fyn axis that ultimately leads to Nrf2 degradation. Consequently, as demonstrated in hepatocytes, PTP1B deficiency might delay and/or reduce activation of this complex axis, resulting in prolonged nuclear accumulation of Nrf2 and enhanced antioxidant defense.

Besides the novel role of PTP1B in antioxidant defense reported herein, this phosphatase regulates duration and/or intensity of survival signals emerging from the tyrosine kinase receptor family.[19–21] As IGFIR triggers survival responses in hepatocytes,[37] the lack of PTP1B prevented the reduction in IGFIR/IRS1/2/Akt-mediated survival signaling in APAP-treated cells. In fact, this is the first report showing degradation of IRS proteins in hepatocytes by APAP, suggesting that high doses of this analgesic may also interfere with hepatic insulin signaling and increase the risk of metabolic diseases such as type 2 diabetes mellitus. Thus, in wild-type hepatocytes, increased ROS-mediated JNK and p38 MAPK phosphorylation by APAP are likely to be responsible for the feedback mechanism on IGFIR-mediated signaling, leading to IRS1/2 serine phosphorylation that precedes degradation.[38] In the absence of PTP1B, the decrease in ROS-mediated activation of JNK and p38 MAPK and the increase in IGFIR tyrosine phosphorylation might act in conjunction with the effects on the GSK3β/Src-Fyn axis, resulting in attenuated oxidative stress and increased cell survival in response to APAP.

Several studies have shown the mechanistic importance of hepatic cytokines in APAP-induced liver injury. In the liver, cytokines are mainly produced by non-parenchymal cells. Our *in vivo* data show significant lower expression levels of IL1β and IL6 mRNAs in the livers of PTP1B$^{-/-}$ mice upon APAP injection as compared with the elevated levels of the wild-type controls, suggesting that PTP1B also modulates cytokine production by non-parenchymal (i.e. Kupffer) cells in response to liver damage. Cytokines have an essential role as inducers of PTP1B in metabolic diseases. Activation of JNK together with elevated expression of PTP1B in response to IL6 has been reported in skeletal muscle of insulin-resistant mice.[39] Likewise, IL4 induces PTP1B to suppress IL4-induced STAT6 signaling in B cells.[40] As PTP1B is increased in the livers of APAP-injected wild-type mice, this effect is likely to be due to elevation of IL6 and IL1β. Therefore, cytokine-mediated increases in PTP1B expression might enhance the GSK3β/Src-Fyn axis, resulting in increased Nrf2 tyrosine phosphorylation and a rapid nuclear exclusion. Moreover, in the liver of APAP-injected wild-type mice, the negative

cross-talk elicited by JNK on IRS proteins and also by PTP1B by direct dephosphorylation of the IGFIR might synergize with the enhancement of the GSK3β/Src-Fyn axis to reduce survival of hepatocytes *in vivo*. This mechanism is supported by lower activation of JNK, higher IGFIR tyrosine phosphorylation and nuclear Nrf2 accumulation in livers of APAP-injected PTP1B$^{-/-}$ mice as compared with the wild-type controls. As a result, PTP1B-deficient livers are protected against APAP-induced oxidative stress and injury as manifested by decreased GSH depletion favoring NAPQI detoxification and subsequently limiting the formation of APAP–protein adducts. However, the effects of APAP *in vivo* are not exclusively mediated by elevation of PTP1B expression induced by proinflammatory cytokines secreted by non-parenchymal cells; our *in vitro* data have also demonstrated direct effects of APAP in hepatocytes. Nevertheless, PTP1B deficiency protects against damage in hepatocytes in culture and in whole liver, reinforcing the regulatory role of this phosphatase in multiple molecular mechanisms triggered in response to APAP in distinct liver cells.

As summarized in Figure 7d, we have demonstrated the unique role of PTP1B in the liver as a critical crossroad in the signaling pathways triggered in response to APAP by dual modulation of the Nrf2-mediated antioxidant response through the GSK3β/Src-Fyn kinases axis and the survival signaling through its effects on the IGFIR/IRSs/Akt signaling pathway. Collectively, our data suggest that inhibition of PTP1B would be a suitable therapeutic approach against APAP-induced hepatotoxicity.

Materials and Methods

Reagents and antibodies. Fetal bovine serum and culture media were obtained from Invitrogen (Carlsbad, CA, USA). Protein A agarose was purchased from Roche Diagnostics. APAP and MG132 were from Sigma-Aldrich (St. Louis, MO, USA). PP2 was purchased from Tocris Bioscience (Ellsville, MO, USA). The antibodies used in this study were: anti-cleaved (Asp175) caspase-3 (no. 9661), anti-phospho-JNK (Thr183/Tyr185) (no. 4668), anti-phospho-p38 MAPK (Thr180/Tyr182) (no. 9211), anti-p38 MAPK (no. 9212), anti-Akt (no. 9272), and anti-ubiquitin (no. 3936) antibodies were from Cell Signaling Technology (Danvers, MA, USA). Anti-Bclx (no. 610211), anti-phospho-GSK3β (no. 612312), anti-GSK3β (no. 6102019) and anti-cytochrome *C* (no. 556433) antibodies were from BD Biosciences (San Diego, CA, USA). Anti-phospho-IGF-IR (Tyr1165/1166) (sc-101704), anti-JNK (sc-571), anti-phospho-Akt1/2/3 (Ser473) (sc-7985-R), anti-Nrf2 (C-20, sc-722), anti-Mcl1 (sc-819), anti-Fyn (sc-16), anti-Keap1 (sc-33569), anti-Lamin B (sc-20682 in Figure 4b) and anti-human PTP1B (sc-14021) were from Santa Cruz Biotechnology (Palo Alto, CA, USA). The anti-IRS1 (06-248), anti-IRS2 (06-506), anti-p85α (06-195), anti-mouse PTP1B (07-088), anti-HO1 (AB1284), anti-phospho-Ser (clone 4A4, 05-1000X) and anti-phospho-Tyr (clone 4G10, 05-321) antibodies were purchased from Merck Millipore (Merck KGaA, Darmstadt, Germany). Anti-IGF-IR antibody was a gift from S Pons (CSIC, Madrid, Spain). Anti-β-actin (A-5441) antibody was from Sigma Chemical Co. (St. Louis, MO, USA). Anti-Lamin B (aB16048) and anti-Cyp2e1 antibody (aB19140) were from Abcam (Cambridge, UK). Mouse monoclonal antibody (mAb) 327 against c-Src was from Calbiochem (Merck KGaA, Darmstadt, Germany). Anti-cytochrome *C* oxidase subunit I antibody (A-6403) was from Molecular Probes (Eugene, OR, USA).

Human liver biopsies. Human liver samples were obtained from the Department of Pathology, University of Edinburgh (Edinburgh, UK). Written informed consent was obtained from each patient. Characteristics of five patients transplanted following APAP overdose are shown in Table 1.

Animal models. Three-month-old male PTP1B$^{+/+}$ (wild-type) and PTP1B$^{-/-}$ mice on the C57Bl/6J $\times$ 129Sv/J genetic background and maintained as described previously[41] were used throughout this study. Animal experimentation was approved by the ethic committee at CSIC and was conducted according to the accepted guidelines for animal care of the Comunidad de Madrid (Spain). Overnight fasted mice were intraperitoneally (i.p.) injected with 300 mg/kg APAP dissolved in physiological saline. Mice were killed at 1, 3, 6 and 24 h and livers and blood were collected.

Cell culture. Human hepatocytes were prepared from liver biopsies obtained from 12 patients (eight male, four female aged 58 $\pm$ 4.0 years) submitted to a surgical resection for liver tumors after obtaining patients' written consent. Hepatocytes' isolation was based on the two-step collagenase procedure.[42] Mouse hepatocytes were isolated from male mice (8–12 weeks old) by perfusion with collagenase and cultured as described.[41] CHLs, purchased from the ATCC, (Manassas, VA, USA) were a gift from P Martin-Sanz (CSIC). The generation and characterization of immortalized hepatocyte cell lines from wild-type and PTP1B$^{-/-}$ mice has been described previously.[43] Cells were grown in DMEM plus 10% heat-inactivated fetal calf serum and stimulated with various doses of APAP.

Liver histology. Histological grading of hepatic necrosis was performed by two blinded observers using hematoxylin and eosin (H&E)-stained sections as follows: 30% of the total area necrotic (one point); 30–60% of the total area necrotic (two points); and 60% of the total area necrotic (three points). PTP1B immunohistochemistry was performed as described previously.[44]

Analysis of ALT activity. Blood was collected in tubes containing heparin and diluted 1/30 with saline (0.9% NaCl). ALT activity was determined by direct measurement with the Reflotron test (Ref. 10745120; Roche Diagnostics, Indianapolis, IN, USA).

Transient transfection with siRNA. siRNA oligonucleotides were synthesized by Dharmacon RNAi Technologies (Fisher Scientific-USA, Pittsburgh, PA, USA) for gene silencing of mouse PTP1B and GSK3β. Wild-type immortalized hepatocytes were seeded in 6-cm dishes and incubated overnight at 37 °C with 5% CO_2. When 40–50% confluence was reached, cells were transfected with 10 nM of PTP1B or 25 nM GSK3β siRNAs or with a scrambled control siRNA following DharmaFECT General Transfection Protocol. After 48 h, cells were used for experiments.

Immunofluorescence. Cells were grown in glass coverslips until 80% confluence was reached. Then, cells were washed two times with PBS, fixed in methanol (-20 °C) for 2 min and processed to immunofluorescence. Primary anti-Nrf2 antibody was applied for 1 h at 37 °C in PBS–1% bovine serum albumin (BSA), followed by 4 $\times$ 5 min washes in PBS, a 45-min incubation with fluorescence-conjugated secondary antibody (Alexa 488 goat anti-rabbit) and

Table 1 Demographic and biochemical characteristics of patients with APAP hepatotoxicity

Patient number	Age (years)	Sex	Acetaminophen dose	Staggered overdose	Admission alanine aminotransferase (IU/l)	Admission creatinine (μmol/l)	Prothrombin time (s)	Overdose to transplant (h)
1	42	Female	32 g	No	12755	218	77	212
2	43	Female	NA	NA	7106	192	182	NA
3	48	Male	16 g	Yes	20800	124	96	NA
4	45	Female	10 g	No	1097	142	69	176
5	36	Male	50 g	No	9847	152	87	70

NA, not available
Normal range alanine aminotransferase 10–50 IU/l, creatinine 60—120 μmol/l and prothrombin time 10.2–12.7 s

four final washes of 5 min each in PBS. Immunofluorescence was examined in a Nikon Eclipse 90i microscope (Nikon Instruments, Inc., Melville, NY, USA). Immunofluorescence mounting medium was from Vector Laboratories Inc. (Burlingame, CA, USA). For 4,6-diamidino-2-phenylindole (DAPI) staining, cells were washed with PBS, fixed in methanol (− 20 °C) for 2 min and stained with 1 μM DAPI for 5 min in the dark. After washing with PBS, nuclear morphology was analyzed by fluorescence microscopy.

Evaluation of cell viability by LDH leakage assay. Cellular damage was evaluated by LDH leakage assay as described.[45]

Analysis of cellular viability by crystal violet. After cell incubation with APAP, the medium was discarded, and the remaining viable adherent cells were stained with crystal violet (0.2% (w/v) in 2% ethanol) for 20 min. After this time, plates were rinsed with tap water and allowed to dry, and 1% SDS was added to solubilize them. The absorbance of each plate was read spectrophotometrically at 560 nm. Dishes without cells were processed in parallel to correct the nonspecific adhesion of crystal violet to the plastic. The remaining viable cells were calculated as the percentage of absorbance with respect to control cells (incubated in the absence of APAP).

Quantification of apoptotic cells by flow cytometry. After induction of apoptosis, adherent and non-adherent cells were collected by centrifugation, washed with PBS and fixed with cold ethanol. The cells were then washed, resuspended in PBS and incubated with RNAse A (25 μg/10^6 cells) for 30 min at 37 °C. After addition of 0.05% propidium iodide, cells were analyzed by flow cytometry.

Analysis of caspase-3 activity. Cells were scraped off, collected by centrifugation at 2500 × *g* for 5 min and lysed at 4 °C in 5 mM Tris/HCl (pH 8), 20 mM EDTA and 0.5% Triton X-100. Caspase-3 activity was determined as described previously.[25] Protein concentration of cell lysates was determined, and the results are presented as caspase-3 activity per micrograms of total protein.

Luciferase assays. HEK 293T cells were seeded on 24-well plates (100 000 cells per well), cultured for 16 h and transfected using calcium phosphate. Transient transfections of HEK 293T cells were performed with the expression vectors for pcDNA3.1mNrf2-V5/HisB (a gift from Dr. JD Hayes, Biomedical Research Institute, Ninewells Hospital and Medical School, University of Dundee, Dundee, UK), *Renilla* (Promega, Madison, WI, USA) and 3 × ARE-Luc (a gift from Dr. J Alam, Department of Molecular Genetics, Ochsner Clinic Foundation, Baton Rouge, LA, USA) combined with myc-PTP1B (a gift from Dr. M Tremblay, Department of Biochemistry, McGill University, Montreal, QC, Canada) only in the indicated cases. After transfection, cells were treated with vehicle (PBS), APAP (10 and 20 mM) or *tert*-butyl hydroquinone (*t*BHQ) (15 μM) for 16 h. Cells were lysed and assayed for luciferase activity with the dual luciferase assay system (Promega), according to the manufacturer's instructions. Relative light units were measured in a GloMax 96 microplate luminometer with dual injectors (Promega, Madison, WI, USA).

Homogenization and preparation of tissue extracts. Frozen livers were homogenized in 16 volumes (w/v) of ice-cold lysis buffer containing 50 mM Tris-HCl, 1% Triton X-100, 2 mM EGTA, 10 mM EDTA acid, 100 mM NaF, 1 mM $Na_4P_2O_7$, 2 mM Na_3VO_4, 100 μg/ml phenylmethylsulfonyl fluoride (PMSF), 1 μg/ml aprotinin, 1 μg/ml pepstatin A and 1 μg/ml leupeptin. Livers were homogenized in the same lysis buffer using the Brinkman PT 10/35 Polytron (American Laboratory Trading, Inc. East Lyme, CT, USA). Extracts were kept ice-cold at all times. Liver extracts were cleared by microcentrifugation at 40 000 × *g* for 20 min at 4 °C. The supernatant was aliquoted and stored at − 70 °C.

Protein determination. Protein determination was performed by the Bradford dye method, using the Bio-Rad reagent and BSA as the standard.

Immunoprecipitations and western blot. To obtain total cell lysates, cells from supernatants were collected by centrifugation at 2000 × *g* for 5 min at 4 °C. Attached cells were scraped off in ice-cold PBS, pelleted by centrifugation at 4000 × *g* for 10 min at 4 °C and resuspended in lysis buffer (25 mM HEPES, 2.5 nM EDTA, 0.1% Triton X-100, 1 mM PMSF and 5 μg/ml leupeptin). Cellular lysates were clarified by centrifugation at 12 000 × *g* for 10 min. After protein content determination, equal amounts of protein (600 μg–1 mg) were immunoprecipitated at 4 °C with the corresponding antibodies. The immune complexes were collected on agarose beads and submitted to western blot analysis. After SDS-PAGE, gels were transferred to Immobilon membranes and were blocked using 5% non-fat dried milk or 3% BSA in 10 mM Tris-HCl, 150 mM NaCl (pH 7.5) and incubated overnight with antibodies as indicated in 0.05% Tween-20, 10 mM Tris-HCl and 150 mM NaCl (pH 7.5). Immunoreactive bands were visualized using the ECL Western blotting protocol (Millipore).

Extraction of nuclear and cytosolic proteins. Cells and liver were resuspended at 4 °C in 10 mM HEPES-KOH (pH 7.9), 1.5 mM $MgCl_2$, 10 mM KCl, 0.5 mM DTT, 0.2 mM PMSF, 0.75 μg/ml leupeptin, 0.75 μg/ml aprotinin (Buffer A), allowed to swell on ice for 10 min, and then vortexed for 10 s. Samples were centrifuged and the supernatant containing the cytosolic fraction was stored at − 70 °C. The pellet was resuspended in cold buffer C (20 mM HEPES-KOH (pH 7.9), 25% glycerol, 420 mM NaCl, 1.5 mM $MgCl_2$, 0.2 mM EDTA, 0.5 mM DTT, 0.2 mM PMSF, 0.75 μg/ml leupeptin, 0.75 μg/ml aprotinin) and incubated on ice for 20 min for high salt extraction. Cellular debris was removed by centrifugation for 2 min at 4 °C, and the supernatant fraction was stored at − 70 °C.

Isolation of mitochondrial and cytosolic extracts. At the end of the culture time, cells were recovered by scrapping and collected by centrifugation at 2500 × *g* for 5 min at 4 °C. Mitochondrial and cytosolic extracts were obtained as described previously.[25]

Determination of GSH. The content of GSH was quantified by the fluorometric assay of Hissin and Hilf.[46]

Determination of GPx and GR enzymatic activities. Cells were collected in PBS and centrifuged at low speed (300 × *g*) for 5 min to pellet cells. Cell pellets were resuspended in 20 mM Tris containing 5 mM EDTA and 0.5 mM mercaptoethanol, submitted to ultrasound and centrifuged at 3000 × *g* for 15 min. Enzyme activities were measured in the supernatants as described.[47]

Measurement of intracellular ROS. For visualization and analysis of intracellular ROS by flow cytometry, the oxidation-sensitive DCFH-DA probe was used. Cells were detached by trypsinization and the cellular fluorescence intensity was measured after 30-min incubation with 5 μM DCFH-DA by using a FACScan flow cytometer (BD Biosciences, San José, CA, USA). For each analysis, 10 000 events were recorded.

Determination of protein carbonyl content. Protein oxidation of liver homogenates was measured as carbonyl groups' content according to the method of Richert *et al.*[48]

Determination of APA–protein adducts. Analysis of APAP covalently bound to proteins in liver was measured by initial protease treatment of liver homogenates, followed by high-performance liquid chromatography-electrochemical analysis for APAP-cysteine as described previously.[49]

Quantitative real-time PCR analysis and primer sequence. Total RNA was extracted with Trizol (Invitrogen) and reverse transcribed using a SuperScriptTM III First-Strand Synthesis System for qPCR following the manufacturer's indications (Invitrogen). qPCR was performed with an ABI 7900 sequence detector (Invitrogen) using the SyBr Green method and d(N)$_6$ random hexamer with the primers indicated in Supplementary Table 1. Primer-probe sets for mouse PTP1B, TNFα, IL6 and IL1β were purchased as predesigned TaqMan gene expression assays (Applied Biosystems, Life Technologies, Carlsbad, CA, USA).

Data analysis. Data are expressed as mean ± S.E.M. Comparisons between groups were made using one-way ANOVA. For qRT-PCR, a two-way ANOVA test followed by a Bonferroni's post-test was used. Differences were considered to be statistically significant at $P<0.05$. The data were analyzed with the SPSS (windows statistical package, version 9.0.1, SPSS Inc., Chicago, IL, USA).

Conflict of Interest

The authors declare no conflict of interest.

Acknowledgements. We acknowledge the following grant support: SAF2012-33283 (MINECO, Spain), Comunidad de Madrid S2010/BMD-2423, EFSD and Amylin Paul Langerhans Grant and Centro de Investigación Biomédica

en Red de Diabetes y Enfermedades Metabólicas Asociadas (CIBERDEM, ISCIII, Spain) (to AMV); SAF2012-38048 (MINECO, Spain) (to JM-P); PI09/0185 and Centro de Investigación Biomédica en Red de Enfermedades Hepáticas y Digestivas (CIBEREHD, ISCIII, Spain) (to JM); AGL2010-17579 (MINECO, Spain) (to LG); and SAF2010-17822 (MINECO, Spain) (to AC).

1. Rumack BH. Acetaminophen misconceptions. *Hepatology* 2004; **40**: 10–15.
2. Lee WM. Acetaminophen and the U.S. Acute Liver Failure Study Group: lowering the risks of hepatic failure. *Hepatology* 2004; **40**: 6–9.
3. Litovitz TL, Klein-Schwartz W, White S, Cobaugh DJ, Youniss J, Omslaer JC *et al.* 2000 Annual report of the American Association of Poison Control Centers Toxic Exposure Surveillance System. *Am J Emerg Med 2001* **19**: 337–395.
4. Lee WM. Acetaminophen toxicity: changing perceptions on a social/medical issue. *Hepatology* 2007; **46**: 966–970.
5. Kaplowitz N. Acetaminophen hepatoxicity: what do we know, what don't we know, and what do we do next? *Hepatology* 2004; **40**: 23–26.
6. Ramachandran R, Kakar S. Histological patterns in drug-induced liver disease. *J Clin Pathol* 2009; **62**: 481–492.
7. James LP, Mayeux PR, Hinson JA. Acetaminophen-induced hepatotoxicity. *Drug Metab Dispos* 2003; **31**: 1499–1506.
8. Jaeschke H, Bajt ML. Intracellular signaling mechanisms of acetaminophen-induced liver cell death. *Toxicol Sci* 2006; **89**: 31–41.
9. Han D, Shinohara M, Ybanez MD, Saberi B, Kaplowitz N. Signal transduction pathways involved in drug-induced liver injury. *Handb Exp Pharmacol* 2010; **196**: 267–310.
10. Thummel KE, Lee CA, Kunze KL, Nelson SD, Slattery JT. Oxidation of acetaminophen to *N*-acetyl-*p*-aminobenzoquinone imine by human CYP3A4. *Biochem Pharmacol* 1993; **45**: 1563–1569.
11. Newton JF, Hoefle D, Gemborys MW, Mudge GH, Hook JB. Metabolism and excretion of a glutathione conjugate of acetaminophen in the isolated perfused rat kidney. *J Pharmacol Exp Ther* 1986; **237**: 519–524.
12. Ghosh A, Sil PC. Protection of acetaminophen induced mitochondrial dysfunctions and hepatic necrosis via Akt-NF-kappaB pathway: role of a novel plant protein. *Chem Biol Interact* 2009; **177**: 96–106.
13. Reid AB, Kurten RC, McCullough SS, Brock RW, Hinson JA. Mechanisms of acetaminophen-induced hepatotoxicity: role of oxidative stress and mitochondrial permeability transition in freshly isolated mouse hepatocytes. *J Pharmacol Exp Ther* 2005; **312**: 509–516.
14. Jaeschke H, McGill MR, Ramachandran A. Oxidant stress, mitochondria, and cell death mechanisms in drug-induced liver injury: lessons learned from acetaminophen hepatotoxicity. *Drug Metab Rev* 2012; **44**: 88–106.
15. Enomoto A, Itoh K, Nagayoshi E, Haruta J, Kimura T, O'Connor T *et al.* High sensitivity of Nrf2 knockout mice to acetaminophen hepatotoxicity associated with decreased expression of ARE-regulated drug metabolizing enzymes and antioxidant genes. *Toxicol Sci* 2001; **59**: 169–177.
16. Tonks NK, Neel BG. Combinatorial control of the specificity of protein tyrosine phosphatases. *Curr Opin Cell Biol* 2001; **13**: 182–195.
17. Frangioni JV, Beahm PH, Shifrin V, Jost CA, Neel BG. The nontransmembrane tyrosine phosphatase PTP-1B localizes to the endoplasmic reticulum via its 35 amino acid C-terminal sequence. *Cell* 1992; **68**: 545–560.
18. Salmeen A, Andersen JN, Myers MP, Tonks NK, Barford D. Molecular basis for the dephosphorylation of the activation segment of the insulin receptor by protein tyrosine phosphatase 1B. *Mol Cell* 2000; **6**: 1401–1412.
19. Zabolotny JM, Bence-Hanulec KK, Stricker-Krongrad A, Haj F, Wang Y, Minokoshi Y *et al.* PTP1B regulates leptin signal transduction *in vivo*. *Dev Cell* 2002; **2**: 489–495.
20. Haj FG, Markova B, Klaman LD, Bohmer FD, Neel BG. Regulation of receptor tyrosine kinase signaling by protein tyrosine phosphatase-1B. *J Biol Chem* 2003; **278**: 739–744.
21. Sangwan V, Paliouras GN, Cheng A, Dube N, Tremblay ML, Park M. Protein-tyrosine phosphatase 1B deficiency protects against Fas-induced hepatic failure. *J Biol Chem* 2006; **281**: 221–228.
22. Buckley DA, Cheng A, Kiely PA, Tremblay ML, O'Connor R. Regulation of insulin-like growth factor type I (IGF-I) receptor kinase activity by protein tyrosine phosphatase 1B (PTP-1B) and enhanced IGF-I-mediated suppression of apoptosis and motility in PTP-1B-deficient fibroblasts. *Mol Cell Biol* 2002; **22**: 1998–2010.
23. Fabregat I, Herrera B, Fernandez M, Alvarez AM, Sanchez A, Roncero C *et al.* Epidermal growth factor impairs the cytochrome *C*/caspase-3 apoptotic pathway induced by transforming growth factor beta in rat fetal hepatocytes via a phosphoinositide 3-kinase-dependent pathway. *Hepatology* 2000; **32**: 528–535.
24. Valverde AM, Fabregat I, Burks DJ, White MF, Benito M. IRS-2 mediates the antiapoptotic effect of insulin in neonatal hepatocytes. *Hepatology* 2004; **40**: 1285–1294.
25. Gonzalez-Rodriguez A, Escribano O, Alba J, Rondinone CM, Benito M, Valverde AM. Levels of protein tyrosine phosphatase 1B determine susceptibility to apoptosis in serum-deprived hepatocytes. *J Cell Physiol* 2007; **212**: 76–88.
26. Kon K, Kim JS, Jaeschke H, Lemasters JJ. Mitochondrial permeability transition in acetaminophen-induced necrosis and apoptosis of cultured mouse hepatocytes. *Hepatology* 2004; **40**: 1170–1179.
27. Niture SK, Jain AK, Shelton PM, Jaiswal AK. Src subfamily kinases regulate nuclear export and degradation of transcription factor Nrf2 to switch off Nrf2-mediated antioxidant activation of cytoprotective gene expression. *J Biol Chem* 2011; **286**: 28821–28832.
28. Jain AK, Jaiswal AK. GSK-3beta acts upstream of Fyn kinase in regulation of nuclear export and degradation of NF-E2 related factor 2. *J Biol Chem* 2007; **282**: 16502–16510.
29. Zabolotny JM, Kim YB, Welsh LA, Kershaw EE, Neel BG, Kahn BB. Protein-tyrosine phosphatase 1B expression is induced by inflammation *in vivo*. *J Biol Chem* 2008; **283**: 14230–14241.
30. Sanderson SO, Smyrk TC. The use of protein tyrosine phosphatase 1B and insulin receptor immunostains to differentiate nonalcoholic from alcoholic steatohepatitis in liver biopsy specimens. *Am J Clin Pathol* 2005; **123**: 503–509.
31. Garcia-Monzon C, Lo Iacono O, Mayoral R, Gonzalez-Rodriguez A, Miquilena-Colina ME, Lozano-Rodriguez T *et al.* Hepatic insulin resistance is associated with increased apoptosis and fibrogenesis in nonalcoholic steatohepatitis and chronic hepatitis C. *J Hepatol* **54**: 142–152.
32. Bechmann LP, Jochum C, Kocabayoglu P, Sowa JP, Kassalik M, Gieseler RK *et al.* Cytokeratin 18-based modification of the MELD score improves prediction of spontaneous survival after acute liver injury. *J Hepatol* **53**: 639–647.
33. Antoine DJ, Jenkins RE, Dear JW, Williams DP, McGill MR, Sharpe MR *et al.* Molecular forms of HMGB1 and keratin-18 as mechanistic biomarkers for mode of cell death and prognosis during clinical acetaminophen hepatotoxicity. *J Hepatol May* **56**: 1070–1079.
34. Craig DG, Lee P, Pryde EA, Masterton GS, Hayes PC, Simpson KJ. Circulating apoptotic and necrotic cell death markers in patients with acute liver injury. *Liver Int* **31**: 1127–1136.
35. McGregor AH, More LJ, Simpson KJ, Harrison DJ. Liver death and regeneration in paracetamol toxicity. *Hum Exp Toxicol* 2003; **22**: 221–227.
36. Antoine DJ, Williams DP, Kipar A, Jenkins RE, Regan SL, Sathish JG *et al.* High-mobility group box-1 protein and keratin-18, circulating serum proteins informative of acetaminophen-induced necrosis and apoptosis *in vivo*. *Toxicol Sci* 2009; **112**: 521–531.
37. Tovar V, Alsinet C, Villanueva A, Hoshida Y, Chiang DY, Sole M *et al.* IGF activation in a molecular subclass of hepatocellular carcinoma and pre-clinical efficacy of IGF-1R blockage. *J Hepatol Apr* **52**: 550–559.
38. Vinayagamoorthi R, Bobby Z, Sridhar MG. Antioxidants preserve redox balance and inhibit c-Jun-N-terminal kinase pathway while improving insulin signaling in fat-fed rats: evidence for the role of oxidative stress on IRS-1 serine phosphorylation and insulin resistance. *J Endocrinol* 2008; **197**: 287–296.
39. Nieto-Vazquez I, Fernandez-Veledo S, de Alvaro C, Lorenzo M. Dual role of interleukin-6 in regulating insulin sensitivity in murine skeletal muscle. *Diabetes* 2008; **57**: 3211–3221.
40. Lu X, Malumbres R, Shields B, Jiang X, Sarosiek KA, Natkunam Y *et al.* PTP1B is a negative regulator of interleukin 4-induced STAT6 signaling. *Blood* 2008; **112**: 4098–4108.
41. Gonzalez-Rodriguez A, Mas Gutierrez JA, Sanz-Gonzalez S, Ros M, Burks DJ, Valverde AM. Inhibition of PTP1B restores IRS1-mediated hepatic insulin signaling in IRS2-deficient mice. *Diabetes* 2010; **59**: 588–599.
42. Pichard L, Raulet E, Fabre G, Ferrini JB, Ourlin JC, Maurel P. Human hepatocyte culture. *Methods Mol Biol* 2006; **320**: 283–293.
43. Gonzalez-Rodriguez A, Clampit JE, Escribano O, Benito M, Rondinone CM, Valverde AM. Developmental switch from prolonged insulin action to increased insulin sensitivity in protein tyrosine phosphatase 1B-deficient hepatocytes. *Endocrinology* 2007; **148**: 594–608.
44. Gonzalez-Rodriguez A, Mas-Gutierrez JA, Mirasierra M, Fernandez-Perez A, Lee YJ, Ko HJ *et al.* Essential role of protein tyrosine phosphatase 1B in obesity-induced inflammation and peripheral insulin resistance during aging. *Aging Cell* 2012; **11**: 284–296.
45. Welder AA Acosta D. (ed) *Enzyme Leakage As An Indicator of Cytotoxicity in Culture Cells*. Academic Press: New York, NY, USA, 1994, p 3.
46. Hissin PJ, Hilf R. A fluorometric method for determination of oxidized and reduced glutathione in tissues. *Anal Biochem* 1976; **74**: 214–226.
47. Rodriguez-Ramiro I, Martin MA, Ramos S, Bravo L, Goya L. Comparative effects of dietary flavanols on antioxidant defences and their response to oxidant-induced stress on Caco2 cells. *Eur J Nutr* **50**: 313–322.
48. Richert S, Wehr NB, Stadtman ER, Levine RL. Assessment of skin carbonyl content as a noninvasive measure of biological age. *Arch Biochem Biophys* 2002; **397**: 430–432.
49. Muldrew KL, James LP, Coop L, McCullough SS, Hendrickson HP, Hinson JA *et al.* Determination of acetaminophen–protein adducts in mouse liver and serum and human serum after hepatotoxic doses of acetaminophen using high-performance liquid chromatography with electrochemical detection. *Drug Metab Dispos* 2002; **30**: 446–451.

Supplementary Information accompanies this paper on Cell Death and Disease website (http://www.nature.com/cddis)